The Thesis Committee for David Philip Langefeld
certifies that this is the approved version of the following thesis:

Anchorage-Controlled Shear Capacity of Prestressed Concrete Bridge Girders

APPROVED BY
SUPERVISING COMMITTEE:

Oguzhan Bayrak, Supervisor

Wassim Ghannoum

Anchorage-Controlled Shear Capacity of Prestressed Concrete Bridge Girders

by

David Philip Langefeld, BS

Thesis

Presented to the Faculty of the Graduate School of
The University of Texas at Austin
in Partial Fulfillment
of the Requirements
for the Degree of

Master of Science in Engineering

The University of Texas at Austin
May 2012

ACKNOWLEDGEMENTS

I am especially thankful for the help of my advisor, Dr. Oguzhan Bayrak; for advising me through the highs and lows of graduate school and not giving up on me during the low points. I am grateful to him for assigning me to a prestressed concrete bridge girder project my first semester at The University of Texas at Austin and securing the necessary funding for me to transition onto an independent project. This research and corresponding thesis was made better because of Dr. Bayrak's technical expertise.

I am also especially grateful for the teaching and training I received from Alejandro Avendano and Catherine Hovell during my first year of graduate school. Both were always available when I had questions about coursework and research. After that first year, while I was fabricating and testing girders, Alejandro proved to be a great resource and was always accommodating all while finishing his dissertation. He taught me a great many things. Catherine was an especially useful resource during the job search. Lastly, special thanks to Dean Deschenes for answering my questions when Dr. Bayrak was out-of-town.

This research (and all other research at the Phil M. Ferguson Structural Engineering Laboratory) would not have been possible without the dedicated service of Andrew Valentine, Blake Stasney, Dennis Fillip, Eric Schell, Mike Wason, Barbara Howard, and Jessica Hanten. Special thanks go out to Andrew for the many hours of crane and forklift help and for having the patience to teach me how to weld. Finally, thanks, Andrew, for helping me when one set of hands simply was not enough to get the job done.

Thanks to all the students at FSEL who helped with my concrete pours and testing, specifically, Brian Hanson for being an immense help throughout the hottest summer in Texas history, Andy Moore for not being afraid to get dirty on the day of the pour, Kerry Kreitman for her excellent cylinder making abilities, Nancy Larson for always being able to spot the first crack during testing, and David Garber for helping me test in the evening when no one was around.

Anchorage-Controlled Shear Capacity of Prestressed Concrete Bridge Girders

David Philip Langefeld, MSE
The University of Texas at Austin, 2012

Supervisor: Oguzhan Bayrak

As part of the ongoing research on shear at the Phil M. Ferguson Structural Engineering Laboratory (FSEL) located at The University of Texas at Austin, the anchorage-controlled shear capacity of prestressed concrete bridge girders was in this research studied in two distinct ways, experimentally and analytically. The results of this research are an important step towards improving understanding of strand anchorage-related issues.

For the experimental program, two full-scale Tx46 prestressed concrete bridge girders were fabricated at FSEL. The Tx46 girders were topped with a concrete, composite deck. Both ends of the two girders were instrumented and tested. For the analytical program, a new Anchorage Evaluation Database (AEDB) was developed, by filtering and expanding the University of Texas Prestressed Concrete Shear Database (UTPCSDB), and then evaluated. The AEDB contained 72 shear tests, of which 25 were anchorage failures and 47 were shear failures.

The results and analysis from the experimental and analytical programs generated the following three main conclusions:

1. A reasonable percentage of debonding in Tx Girders does not have a marked impact on girder shear capacity calculated using the 2010 AASHTO LRFD General Procedure.
2. The AASHTO anchorage equation is conservative but not accurate. In other words, this equation cannot be used to accurately differentiate between a shear failure and an anchorage failure. In regards to conservativeness, anchorage

failures in AASHTO-type girders may lead to unconservative results with respect to the 2010 AASHTO LRFD General Procedure.

3. The 2010 AASHTO anchorage resistance model and its corresponding equation do not apply to Tx Girders. Because of the Tx Girders' wider bottom flange, cracks do not propagate across the strands as they do in AASHTO-type girders. This fact yields overly conservative results for Tx Girders with respect to AASHTO Equation 5.8.3.5-1.

In summary, this research uncovered the short-sided nature of the AASHTO anchorage design method. Given its short-comings, there is an obvious need for a validated, comprehensive, and rational approach to anchorage design that considers strength and serviceability. To appropriately develop this method, additional full-scale experimental testing is needed to expand the AEDB, as currently there are not enough tests to distinguish major, general trends and variables. Any future additional research would be expected to further validate and expand the significant findings that this research has produced and so take the next step toward safer, more-efficient bridge designs.

TABLE OF CONTENTS

LIST OF TABLES

LIST OF FIGURES

CHAPTER 1: INTRODUCTION

As part of the ongoing research on shear at the Phil M. Ferguson Structural Engineering Laboratory (FSEL) located at The University of Texas at Austin, the anchorage-controlled shear capacity of prestressed concrete bridge girders was studied in two distinct ways, experimentally and analytically, in this research. The experimental program focused on the impact of debonding on the anchorage of the prestressing strands. The analytical program focused on the adequacy of the American Association of State Highway and Transportation Officials (AASHTO) anchorage design procedures. The combined results of this research are an important step towards improving understanding of strand anchorage-related issues.

1.1 BACKGROUND

In a prestressed concrete bridge girder, the extreme fiber stresses—both when the prestressing force is transferred and under service loads—must be kept within the limits specified in the 2010 AASHTO LRFD Bridge Design Specifications (Figure 1-1). In Figure 1-1, "A" is the base configuration, which does not meet the stress limits. In order to stay within the stress limits, the designer has two options: reduce eccentricity or reduce the prestressing force. The first option, labeled "B" in Figure 1-1, involves a technique called harping, where end eccentricities are reduced by varying the strand profile in order to decrease end region stresses, but maximum eccentricity is maintained in places where moments caused by external loads will be greatest. Varying the strand profile involves the use of one or more hold-down points. Because hold-down points restrain highly stressed strands, harping poses dangers to fabrication workers due to the possibility of a strand's breaking or a hold-down point's failing. Also, harping can be difficult to achieve in members with sloped webs, such as Texas U-beams.

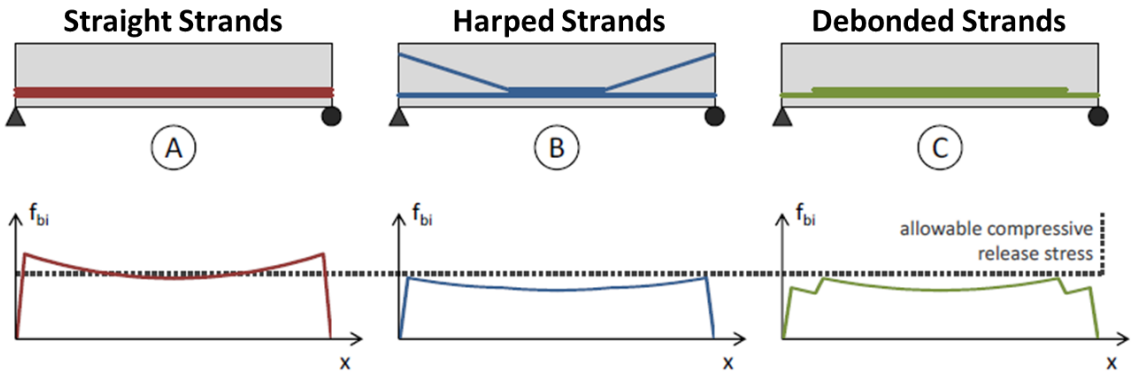

Figure 1-1: Techniques for End Region Stress Control; (A) Straight, (B) Harped, (C) Debonded

Debonding, the second option, labeled "C" in Figure 1-1, for staying within the AASHTO stress limits for prestressed concrete bridge girders, reduces the prestressing force in the end regions by coating or wrapping each strand to prevent force transfer into the concrete at the end region, thereby breaking the bond. (A strand that is not debonded is termed "fully-bonded".) One way to prevent such transfer is to place plastic sheathing (split or un-split) around the strand, taking special care to tape around both the length of the split sheathing and the end of all types of sheathing in order to prevent water and cement from migrating under the sleeve during casting and thereby forming unwanted bond. Debonding uses material more effectively and does not entail the dangers of harping. However, debonding reduces a girder's flexural and shear strengths in the end regions. The experimental program of this research focused on debonding because debonding results in the most-conducive conditions for an anchorage failure, which would facilitate meeting the objectives of the research.

1.2 OBJECTIVES

This research had a three primary and two secondary objectives. The primary objectives of this research were (i) to investigate the impact of debonding on the anchorage of the prestressing strands, (ii) to investigate the impact of debonding on the

girder's shear capacity, and (iii) to determine the accuracy and conservativeness of the current AAHSTO anchorage design method. The secondary objectives were (iv) to determine whether or not the assumed AAHSTO anchorage resistance model applies to modern prestressed concrete bridge girders, such as the recently developed Tx Girder, and (v) to determine what factors contribute to anchorage capacity.

1.3 SCOPE OF WORK

In order to meet the primary and secondary objectives, the scope of work was planned for both the experimental and analytical programs. First, available literature regarding anchorage-related issues and shear behavior of prestressed concrete bridge girders was reviewed. The review notably included a summary the University of Texas Prestressed Concrete Shear Database (UTPCSDB) that had previously assessed the accuracy and conservativeness of multiple shear design equations. Second, with knowledge in hand, two prestressed concrete bridge girders were designed to fail in anchorage. Strand diameter was varied because of its effect on transfer length. Third, the specimens were fabricated and instrumented so that the demand on the prestressing strand due to applied loads could be monitored. Finally, each end of each specimen was tested. In addition to the experimental work, an Anchorage Evaluation Database was formulated and analyzed as part of the research's analytical program.

1.4 OVERVIEW OF CHAPTER ORGANIZATION

This thesis is organized into six chapters. After this introductory Chapter 1, Chapter 2 presents discussion of the following: the shear strength of prestressed concrete bridge girders, the anchorage strength of the same, and select previous shear/anchorage-related research.

The experimental program is detailed in Chapter 3 and includes a discussion of: the design and fabrication of the girders and decks; the materials used in fabrication, including nominal and measured strengths; the instrumentation used during testing; and

the shear test setup and procedure. The preliminary analysis for each test is also presented in tabular and graphical form.

The results and analysis of the experimental program are detailed in Chapter 4, which includes a discussion of test summaries and outcomes, including photographs, plots, and crack maps; post-test ratio of demand-to-capacity; and data analysis and comparisons from testing.

The analytical program and associated conclusions are detailed in Chapter 5. The Anchorage Evaluation Database was developed to verify the conclusions drawn from the experimental program, determine behavioral differences between AASHTO-type girders and Tx Girders, determine what factors contribute to anchorage capacity, and determine the accuracy and conservativeness of the AASHTO anchorage design method.

Finally, Chapter 6 concludes this thesis with a summary of the findings and conclusions of this research. Some recommendations for future research are also included.

CHAPTER 2: BACKGROUND

As background for this research's experimental and analytical programs, this chapter discusses the shear strength of prestressed concrete bridge girders, the anchorage strength of the same, and select shear/anchorage related research.

2.1 OVERVIEW

First, in discussing the shear strength of prestressed concrete bridge girders, the results from a recent database evaluation of the shear design equations are reported, the chosen shear design equation is discussed in detail, and, because of the susceptibility of the modern I-girders to horizontal shear failures, information on horizontal shear is reported, including a summary of a recently proposed horizontal shear design method. Second, in discussing anchorage strength of prestressed concrete bridge girders, some background is presented regarding anchorage-related fundamentals and anchorage-related code provisions. Finally, selected previous research related to shear and anchorage is reported, especially as it pertains to debonding's influence on shear and flexural capacity.

2.2 SHEAR STRENGTH OF PRESTRESSED CONCRETE BRIDGE GIRDERS

Current knowledge of flexural behavior of prestressed concrete beams provides accurate estimations of a member's flexural strength and behavior, while shear behavior is veiled with much more uncertainty. Through work at the Phil M. Ferguson Structural Engineering Laboratory (FSEL) at The University of Texas at Austin, shear behavior has been extensively studied and better understood. Using The University of Texas Prestressed Concrete Shear Database (UTPCSDB), current shear design methods were previously checked for accuracy and conservatism. The methods based on Modified Compression Field Theory were found to be adequate, except when so-called nontraditional failure modes controlled failure. These nontraditional failure modes are horizontal shear and anchorage. Modern cross-sections with thin webs and wide bottom

flanges added more uncertainty to shear design because of their propensity to fail in horizontal shear. Recent work at FSEL on Texas U-Beams has investigated horizontal shear and proposed a new design method to more adequately predict horizontal shear capacity. This section details the database, the chosen shear design procedure, and the proposed horizontal shear design method.

2.2.1 The University of Texas Prestressed Concrete Shear Database

The UTPCSDB is a database of prestressed concrete beam shear tests collected from literature dated between 1954 and 2011, initially by Avendaño and Bayrak (2008) and then expanded by Nakamura (2011). As of this writing, there are a total of 1696 data points from studies conducted in the United States, Europe, and Japan. This database has been previously used to evaluate the accuracy of prestressed concrete shear strength equations.

Nakamura also reduced the database by applying three stages of filtering criteria. First, he reduced the full Collection Database (1696 data points) to the Filtered Database (1146 data points) by removing data points that met the following criteria:

- incomplete test information
- initial defects in the member
- moving loads
- no prestressing
- observed failure modes not consistent with a traditional shear failure

Next, the Evaluation Database-Level I (223 data points) was developed by including data points only when the following conditions were met:

- member depth greater than 12 in.
- made from conventional concrete with a 28-day strength greater than 4 ksi
- tested at a shear span-to-depth ratio greater than 2.0
- contained at least the minimum shear reinforcement per American Concrete Institute (2008) and AASHTO (2010) requirements

- simply supported beams (no segmental sections)
- prestressed or post-tensioned internally

The Evaluation Database-Level I was developed in order to evaluate the influence of various shear failure modes on the accuracy and conservativeness of the various existing design provisions. Nakamura categorized each of the data points as failing in one or more of the following seven ways: shear failure, flexural-shear failure, web-crushing failure, shear-compression failure, shear-tension failure, shear failure with signs of horizontal shear damage, and shear failure with signs of anchorage zone distress.

A brief description of each shear failure mode is helpful at this point. Of the seven listed above, the first, shear failure, is a general category. Nakamura used this designation when the literature itself was unclear as to precisely how the specimens failed. The other six possible failure modes are specific forms of shear failure (Figure 2-1). The first is flexure-shear. A flexure-shear failure is one where the specimen loses its shear carrying capacity after the widening of a flexure-shear crack. The second possible failure mode is web-crushing, which is typically seen in members with thin webs (I-beams, U-beams, etc.). The specimen loses shear carrying capacity after crushing of the diagonal concrete struts in the web. The third failure mode is shear compression. This mode is similar to web-crushing, except concrete crushes in other portions (such as the top flange) of the specimen in addition to the web. The fourth failure mode is shear tension, which occurs when the specimen loses shear carrying capacity after yielding or rupture of the shear reinforcement. The preceding four failure modes are traditional, well-understood shear failure modes, for which the design equations were written and calibrated. The fifth failure mode is horizontal shear. This failure mode involves sliding at the interface of the web and the bottom flange. Finally, the last failure mode is anchorage zone distress, which includes specimens that failed due to slip or a breakdown of the concrete-strand bond. These last two failure modes, horizontal shear and anchorage zone distress, are not as well understood. Examples of five of the six shear failure modes are shown in Figure

2-1. Anchorage zone distress is not included in Figure 2-1 because the characteristics of an anchorage failure are not easily discernible in a photograph.

Figure 2-1: Examples of Five Different Shear Failure Modes (Nakamura 2011)

The third reduction was termed the Evaluation Database-Level II (171 data points). This group contained only specimens that failed in a traditional shear failure mode (the first four modes described above).

Once the three filtrations were complete, Nakamura compared twelve shear design equations from multiple countries for accuracy and conservatism. The comparison was done by evaluating several statistics for each shear design equation using the variation in the shear strength ratio. The shear strength ratio is defined as the ratio of the measured shear capacity, V_{test}, to the calculated shear capacity, V_{calc}. (The reader may refer to Nakamura [2011] for more information and comparisons.) Of the twelve equations Nakamura compared, only three U.S. shear design equations are of interest for this research. The three equations are as follows: the 2008 ACI 318-08 Simplified Method, the 2008 ACI 318-08 Detailed Method, and the 2010 AASHTO LRFD General Procedure. Also, only his comparison using the Evaluation Database-Level I and the Evaluation Database-Level II are of interest here because these Evaluation databases accurately reflect the characteristics of today's prestressed concrete bridge girders.

The accuracy and conservatism of the three shear design equations were compared in terms of three statistical parameters of the shear strength ratio: the mean, the coefficient of variation (COV), and the percentage of unconservative cases. A mean shear strength ratio close to but greater than 1.0 is accurate and conservative. A low COV has a good level of precision (low scatter). A low percentage of unconservative cases is safe. The percentage of unconservative cases needs to be considered in conjunction with the mean, because, for example, a mean of 3.0 is safe but overly conservative.

The statistics for the shear strength ratio of the three shear design equations in the two databases are summarized in Table 2-1. In Table 2-1, the mean shear strength ratio is between 1.0 and 1.5 for all the equations except ACI 318-08 Simplified Method. Therefore, this method provides less accurate shear capacity estimations than the other two. The COVs in Table 2-1 are fairly similar. Nakamura's plots of the distribution of shear strength ratios illustrated that for a lower COV the distribution was more centrally

populated. Also of note is that the distribution for the Evaluation Database-Level I was less dense than the distribution for the Evaluation Database-Level II. Clearly, including tests with signs of horizontal shear and tests with signs of anchorage distress in the database sheds light on the limitation of the 2010 AASHTO LRFD General Procedure with respect to these two non-traditional shear failure modes.

Table 2-1: Shear Strength Ratio Statistics: Evaluation Database-Level I and Level II

	Evaluation Database-Level I (223 Tests)			Evaluation Database-Level II (171 Tests)		
	ACI 318-08 Simplified Method	ACI 318-08 Detailed Method	2010 AASHTO LRFD General Procedure	ACI 318-08 Simplified Method	ACI 318-08 Detailed Method	2010 AASHTO LRFD General Procedure
Minimum	0.86	0.73	0.62	0.98	0.82	0.94
Maximum	3.55	2.32	2.07	3.11	2.32	2.07
Mean	1.79	1.35	1.36	1.90	1.39	1.43
COV	0.29	0.22	0.22	0.23	0.21	0.18
Unconservative Cases	8	26	19	1	11	1
Unconservative %	3.6	11.7	8.5	0.6	6.4	0.6

As previously stated, the percentage of unconservative cases needs to be considered in conjunction with the mean. Nakamura set a percentage of unconservative tests less than or equal to 5.0% and a mean less than 1.5 as the criteria of evaluation. None of the three equations met these criteria in the Evaluation Database-Level I. Only the 2010 AASHTO LRFD General Procedure met these criteria in the Evaluation Database-Level II. These statistics were more proof that all three equations become more uncertain and less reliable when tests with signs of horizontal shear and tests with signs of anchorage distress are present.

In conclusion, of the twelve shear design equations that were evaluated, the 2010 AASHTO LRFD General Procedure has a low mean, low COV, and low percentage of unconservative cases. Therefore, this method provides the best estimation of shear capacity, though none of the three current U.S. shear design equations considered adequately estimates shear capacity in cases of horizontal shear and anchorage distress. Other recent research at The University of Texas at Austin has focused on predicting horizontal shear capacity (see below in Section 2.2.3), and this research focuses on predicting shear capacity in cases of anchorage distress. The next section details the 2010 AASHTO LRFD General Procedure used in this research.

2.2.2 AASHTO LRFD Bridge Design Specifications (General Procedure)

In the previous section, various shear design equations were evaluated. This evaluation showed the 2010 AASHTO LRFD General Procedure to be the most adequate method. As a result, all vertical shear capacity calculations in this research were done using this method. The 2010 AASHTO LRFD General Procedure, located in Section 5.8.3.4.2 of the AASHTO LRFD Bridge Design Specifications, was introduced into the AASHTO Specifications in 1994. The procedure is based on Modified Compression Field Theory (MCFT), which estimates the ability of diagonal cracks to transmit tension. This section details the calculations involved in using this method.

In the AASHTO LRFD specifications, the shear capacity is the total contribution from the concrete, the steel, and the vertical component of the prestressing force (if

harping/draping is present). A limit is placed on the shear capacity to prevent crushing of the concrete in the web prior to yielding of the shear reinforcement.

$$V_n = V_c + V_s + V_p \leq 0.25 f_c' b_v d_v + V_p \quad \text{Equation 2-1}$$

where:

V_n = nominal shear capacity (kips)

V_c = shear capacity provided by the concrete (kips)

V_s = shear capacity provided by shear reinforcement (kips)

V_p = component in the direction of the applied shear of the effective prestressing force (kips)

f_c' = compressive strength of concrete (ksi)

b_v = effective web width taken as the minimum web width within the depth d_v (in.)

d_v = effective shear depth (in.)

Concrete's contribution to shear capacity is given as the following:

$$V_c = 0.0316 \beta \sqrt{f'_c} b_v d_v \quad \text{Equation 2-2}$$

where:

β = factor estimating the ability of diagonally cracked concrete to transmit tension and shear

The β factor determines the ability of cracked concrete to transmit tension and shear. In successive prior versions of the AASHTO Specifications, β was first determined using graphs, then determined using tables, and now is calculated using a pair of equations. These equations, dependent on the amount of shear reinforcement, are as follows:

$$\beta = \frac{4.8}{1 + 750\varepsilon_x} \cdot \frac{51}{39 + s_{xc}} \; if \; A_v < A_{v,min} \quad \text{Equation 2-3}$$

$$\beta = \frac{4.8}{1 + 750\varepsilon_x} \; if \; A_v \geq A_{v,min} \quad \text{Equation 2-4}$$

Where the longitudinal strain, ε_x, the crack spacing parameter, s_{xe}, and the minimum area of shear reinforcement, $A_{v,min}$, are calculated using the following:

$$0 \leq \varepsilon_x = \frac{\frac{|M_u|}{d_v} + \frac{1}{2}N_u + |V_u - V_p| - A_{ps}f_{po}}{E_sA_s + E_pA_{ps}} \leq 0.006 \quad \text{Equation 2-5}$$

$$-0.0004 \leq \varepsilon_x = \frac{\frac{|M_u|}{d_v} + \frac{1}{2}N_u + |V_u - V_p| - A_{ps}f_{po}}{E_sA_s + E_pA_{ps} + E_cA_c} < 0 \quad \text{Equation 2-6}$$

$$A_{v,min} = 0.0316\sqrt{f'_c}\frac{b_v s}{f_y} \quad \text{Equation 2-7}$$

$$12 \leq s_{xe} = s_x \cdot \frac{1.38}{a_g + 0.63} \leq 80 \quad \text{Equation 2-8}$$

where:

M_u = factored moment, not to be taken less than $(V_u - V_p)d_v$ (kip-in)

N_u = factored axial force, taken as positive if tensile and negative if compressive (kips)

V_u = factored shear force (kips)

A_{ps} = area of prestressing steel on the flexural tension side of the member (in^2)

f_{po} = locked-in stress differential between prestressing strands and the surrounding concrete (ksi)

E_s = modulus of elasticity of non-prestressed longitudinal reinforcing bars (ksi)

A_s = area of non-prestressed steel on the flexural tension side of the member (in^2)

E_p = modulus of elasticity of prestressing tendons (ksi)

E_c = modulus of elasticity of concrete (ksi)

A_c = area of concrete on the flexural tension side of the member (in^2)

A_c = area of concrete on the flexural tension side of the member (in^2)

A_v = area of shear reinforcement within a distance s (in^2)

$A_{v,min}$ = minimum area of shear reinforcement within a distance s (in^2)

f_y = specified minimum yield strength of reinforcing bars (ksi)

s = spacing of stirrups (in.)

s_{xe} = crack spacing parameter (in.)

s_x = the lesser of either d_v or the maximum distance between layers of longitudinal crack control reinforcement, where the area of the reinforcement in each layer is not less than $0.003 b_v s_x$ (in.)

a_g = maximum aggregate size (in.)

Steel's contribution to shear capacity is given as follows:

$$V_s = \frac{A_v f_{yv} d_v (cot\theta + cot\alpha) sin\alpha}{s} \qquad \text{Equation 2-9}$$

where:

θ = angle of inclination of diagonal compressive stresses (°)

α = angle of inclination of transverse reinforcement to longitudinal axis (°)

The angle of diagonal compressive stresses (or cracks) from the horizontal is given as follows:

$$\theta = 29 + 3500\varepsilon_s \qquad \text{Equation 2-10}$$

Because the vertical shear capacity is dependent on an applied shear and moment, the shear capacity calculations are iterative, so the applied load causes a shear equal to V_n. Not surprisingly, despite undergoing simplifications before being incorporated into the AASHTO Specifications, the General Procedure is still complicated and challenging to master. Moreover, the General Procedure does not address horizontal shear, which has increasingly become a problem as girder cross-sections now have thinner webs and wider bottom flanges, as discussed in the next subsection.

2.2.3 Horizontal Shear

Optimizing prestressed concrete bridge girders for flexure creates sections with thin webs and wide bottom flanges. In recent years, research on prestressed concrete bridge girders has discovered an increase in horizontal shear failures at the interface of

the web and the bottom flange. As a result, in addition to vertical shear capacity, horizontal shear capacity, as related to the interface of the web and the bottom flange, was also calculated in this research. The calculations detailed in this subsection were developed as part of recent research at FSEL on prestressed concrete bridge girders.

Previous experimental research, specifically that by Hovell (2011), showed that horizontal shear failures follow a common failure pattern: a 45˚ crack passes from the load point to the interface of the web and bottom flange, and a horizontal crack extends all the way to the end of the beam. This failure pattern is illustrated in Figure 2-2, where the web slides relative to the bottom flange and the shear reinforcement kinks, both classic signs of horizontal shear. From the observation of a common failure pattern, a common point to measure demand was chosen. This point, called the ultimate evaluation point (UEP), is located at the intersection of the critical 45˚ crack and the interface of the web and the bottom flange. The location of the UEP is shown by the star in Figure 2-3 and defined as follows:

$$l_{UEP} = a + oh - \frac{l_{LP}}{2} - h + y_{crit} \qquad \text{Equation 2-11}$$

where:

l_{UEP} = distance from beam end to the UEP (in.)
a = shear span (in.)
oh = beam overhang, from centerline of bearing pad to beam end (in.)
l_{LP} = length of the load plate (in.)
h = total depth of the composite section (in.)
y_{crit} = height of critical interface, measured from the bottom (in.)

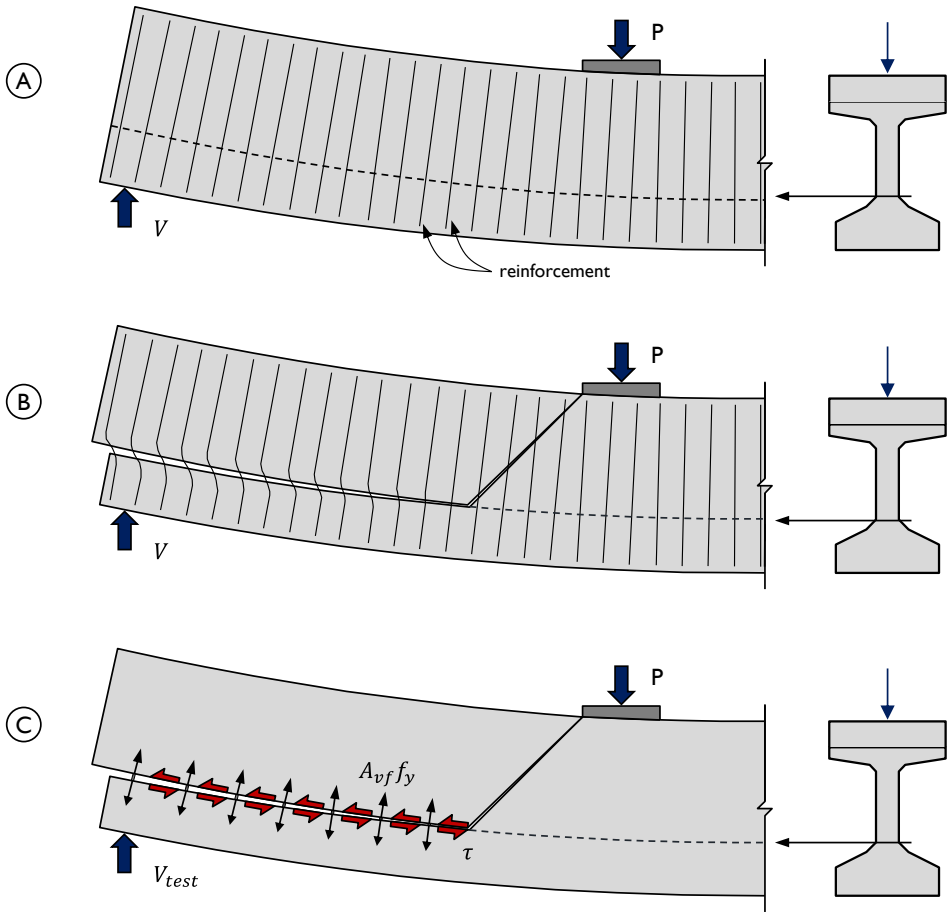

Figure 2-2: Flexure member (A) just prior to and (B) just after exceeding the horizontal shear capacity of the interface of the web and the bottom flange. (C) Free-body diagram drawn from the failed specimen (Hovell 2011)

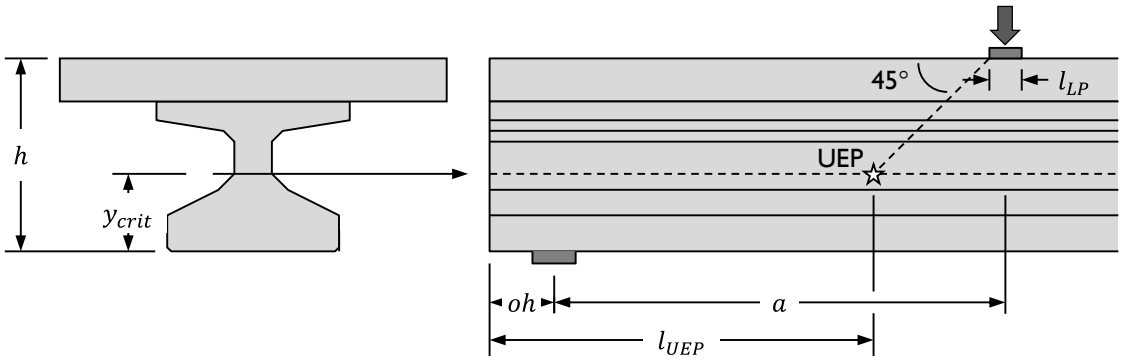

Figure 2-3: Location of Ultimate Evaluation Point (Hovell 2011)

To calculate the demand on the interface of the web and the bottom flange, the horizontal shear stress needed to be found. To find the best way of calculating horizontal shear stress, Hovell compared the results from a nonlinear method and an average approximation method. The nonlinear method is much more complex than the average approximation method. Table 2-2 contains the ratio of the nonlinear method to the average approximation method for the four beam types Hovell considered. A ratio close to 1.0 indicates that the average approximation method is sufficiently adequate.

Table 2-2: Comparison of Calculation Methods at Critical Interface (Hovell 2011)

Beam Type	Nonlinear / Average Shear Stress
Tx28	1.03
Tx46	1.10
4B28	1.08
TxU54	0.99

Since the ratio for each beam type is adequately close to 1.0, the average approximation method was chosen, given the difficulty of the nonlinear method. Thus, in this research the average horizontal shear stress due to applied loads, necessary for calculating interface demand, is found using an average vertical shear stress as follows:

$$v_{hs} = \frac{V_{applied}}{b_w d}$$ Equation 2-12

where:

v_{hs} = average horizontal shear stress caused by an applied load (ksi)

$V_{applied}$ = applied shear force on the section (kips)

b_w = width of the web at the interface of the web and the bottom flange (in.)

d = distance from extreme compression fiber to centroid of tensile reinforcement (in.)

Next, the horizontal shear stress due to applied loads is converted to a force, given as follows:

$$V_{u_{hs}} = v_{hs} b_w l_{crit}$$ Equation 2-13

where:

$V_{u_{hs}}$ = horizontal shear demand (kips)

l_{crit} = length of demand (in.)

The length, l_{crit}, takes into account the overhang beyond the bearing pad.

$$l_{crit} = l_{UEP} - oh \qquad \text{Equation 2-14}$$

The preceding equations would suggest that calculating the horizontal shear demand is quite easy. Once Hovell developed an equation for the horizontal shear demand, she carried on by developing an equation to adequately estimate a girder's horizontal shear capacity.

Hovell developed a calculation for horizontal shear capacity based on an existing concept called shear-friction. The shear-friction equation in the 2010 AASHTO LRFD specifications applies to any horizontal interface (when it comes to bridge girders, mainly the interface between the top flange and the deck). This equation has three terms: cohesion, friction due to clamping force, and friction due to loads. The equation is as follows:

$$V_{ni} = cA_{cv} + \mu\left(A_{vf}f_y + P_c\right) \qquad \text{Equation 2-15}$$

where:

V_{ni} = nominal shear resistance of the interface plane (kips)

c = cohesion factor , equal to 0.4 for monolithically-placed concrete (ksi)

A_{cv} = area of concrete considered to be engaged in interface shear transfer (in^2)

A_{vf} = area of interface shear reinforcement crossing the shear plane (in^2)

f_y = specified yield strength of reinforcement, limited to 60 (ksi)

P_c = permanent net compressive force normal to the shear plane (kips)

Since the AASHTO equation was intended for the interface of the top flange and the deck, Hovell adapted it for the purpose of calculating horizontal shear capacity at the interface of the web and the bottom flange.

Hovell's recommended equation for horizontal shear capacity at the interface of the web and bottom flange is different from the shear-friction equation in several ways. First, the term from the net compressive force is replaced by a prestressing transfer term, which accounts for the bursting reinforcement within the transfer length. This reinforcement is designed to carry a bursting stress of 4% of the prestressing force. This bursting demand reduces the reinforcement's ability to resist horizontal shear stresses. The second difference is an added factor for reflecting the beam shape and/or reinforcement detailing. This factor is 1.0 for I-beams relevant to this research. Hovell's horizontal shear capacity equation is as follows:

$$V_{ni} = k_d\left[cA_{cv} + \mu(A_{vf}f_y - 0.04P_{PS})\right] \qquad \text{Equation 2-16}$$

where:

V_{ni} = nominal shear resistance of the interface plane (kips)

k_d = beam shape/reinforcement detailing factor, equal to 1.0 for I-Beams

c = cohesion coefficient, equal to 0.4 (ksi)

A_{cv} = area of concrete considered to be engaged in interface shear transfer (in^2)

μ = friction coefficient, equal to 1.4

A_{vf} = area of interface shear reinforcement crossing the shear plane within the area A_{cv} (in.)

f_y = specified yield strength of reinforcement, limited to 60 (ksi)

P_{ps} = force of prestressing transferred to the beam within the region of interest (kips)

The coefficients c and μ are defined following Article 5.8.4.3 in the 2010 AASHTO LRFD specifications. For beams whose concrete is placed monolithically, such as I-beams, c and μ equal 0.40 ksi and 1.4, respectively.

The AASHTO capacity equation on which Hovell's equation is based has two limit states that place a maximum on how much horizontal shear force the interface can carry, and those two limit states still apply to Hovell's equation. The first limits horizontal shear force to a percentage of the concrete compressive strength, and the

second places an absolute limit on the horizontal shear force. The limit states are as follows:

$$V_{ni} \leq K_1 f_c' A_{cv} \qquad \text{Equation 2-17}$$

and

$$V_{ni} \leq K_2 A_{cv} \qquad \text{Equation 2-18}$$

where:

K_1 = For normal-weight monolithic concrete, 0.25

K_2 = For normal-weight monolithic concrete, 1.5 (ksi)

Only concrete placed monolithically is relevant to this research.

The horizontal shear capacity must be calculated at several points between the end of the beam and the ultimate evaluation point in order to reflect changes in prestressing, shear reinforcement, and geometry.

To verify the method described above, Hovell analyzed a new filtered subset of the UTPCSDB's Evaluation Database-Level I. This subset, called the Horizontal Shear Evaluation Database (HSEDB), contained tests that both showed signs of horizontal shear damage and did not show signs of horizontal shear damage. This analysis was done so that the horizontal design procedure could be evaluated for accuracy and conservatism both when horizontal shear was present and when it was not present. The horizontal and vertical shear ratios were calculated for each test. In each case, the shear ratio was defined as the ratio of the shear demand, HS_{test} and V_{test}, respectively, to the estimated shear capacity, HS_n and V_n, respectively.

Hovell plotted together the horizontal shear ratio and the vertical shear ratio from the 2010 AASHTO LRFD General Procedure (Figure 2-4). Horizontal shear is on the vertical axis, and vertical shear is on the horizontal axis. On the vertical axis, a ratio greater than 1.0 indicates both that the horizontal shear demand is greater than the capacity and that horizontal shear damage is expected. If Hovell's design method is adequate, tests that showed signs of horizontal shear distress will fall, as they do fall, in

the upper two quadrants, and tests that showed no signs of horizontal shear distress will fall, as they do generally fall, in the lower two quadrants.

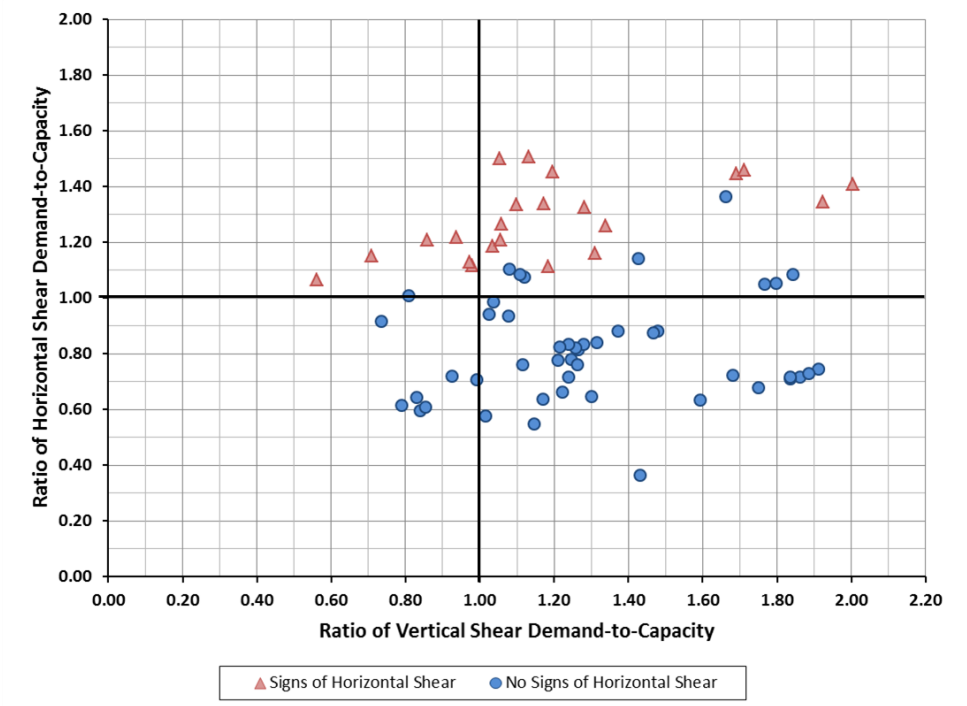

Figure 2-4: Vertical and Horizontal Shear Strength Ratios (Hovell 2011)

Hovell also statistically compared her method using the HSEDB. The mean, COV, and accuracy for her equation as applied to cases with and without horizontal shear damage are reported in Table 2-3. The method was considered acceptable if over-conservative (that is, it expected horizontal shear damage that was not seen) but not unconservative (that is, it expected adequate horizontal shear strength that was not present). The method proved to be conservative because the mean is above 1.0 for tests with signs of horizontal shear and less than 1.0 for tests without signs of horizontal shear. The method is also precise (low scatter) because the COV is low for both. The method is accurate because it perfectly predicted each case of horizontal shear.

Table 2-3: Summary of Horizontal Shear Calculation Method (Hovell 2011)

Without Horizontal Shear Distress		With Horizontal Shear Distress
0.81	**Mean**	1.27
0.23	**COV**	0.12
38/47	**Accuracy**	22/22

The foregoing evaluation makes clear that Hovell's method is an adequate predictor of horizontal shear. Thus, her method was used in this research to estimate the horizontal shear capacity.

2.3 ANCHORAGE STRENGTH OF PRESTRESSED CONCRETE BRIDGE GIRDERS

Hovell's method is proven to reduce the previously-discussed uncertainty that traditional equations left regarding horizontal shear, and this research is focused on reducing the uncertainty regarding anchorage-related failures. The results from the UTPCSDB discussed in Section 2.2.1 showed that anchorage-related failures are difficult to predict using traditional shear design methods. To better understand anchorage-related failures, this section presents four anchorage-related fundamentals and details anchorage-related code provisions.

2.3.1 Anchorage-Related Fundamentals

Prior to detailing the anchorage capacity equation, several fundamental aspects related to anchorage are covered as background. This subsection details four aspects: transfer and development length, bond mechanism review, debonding's effect on shear, and shear's effect on tension in longitudinal reinforcement.

2.3.1.1 Transfer and Development Length

The first anchorage-related fundamental pertains to transfer and development length. The transfer length is the distance required to transfer the full prestressing force from the strand to the concrete. The point where the transfer length begins differs for fully-bonded and debonded strands. For a fully-bonded strand, transfer length is the

distance from the free end of the strand to the point where the prestressing force is fully effective. For a debonded strand, transfer length is the distance from the termination of debonding to the point where the prestressing force is fully effective. The prestressing force is transferred to the concrete through bond that prevents the strand from slipping relative to the concrete. Such bond stresses assumedly increase linearly over the transfer length and are constant once the prestressing force is fully effective. For a girder with debonded strands, there are multiple strand transfer lengths along the girder length. Older codes included transfer length in the shear provisions, which demonstrates transfer length's importance to shear strength; Russell, et al. (1993).

The development length, or flexural bond length, is the distance required to anchor the strand as it experiences additional tension from external loads acting on a girder, enabling the strand to resist strand slip relative to the concrete. Bond stresses increase in order to maintain equilibrium, as discussed below. If, for example, a girder fails in flexure (concrete crushes or strand ruptures), the available bond length must have been greater than or equal to the development length. If, however, the strand slips and fails in bond, the available bond length must have been less than the development length. "Flexural bond length" has been the historical term used to explain bond stresses that resist external loads, but this term is a misnomer because the stress need not be limited to flexure.

2.3.1.2 Bond Mechanism Review

Transfer and development length are directly related to the bond mechanism, the second anchorage-related fundamental treated here. As mentioned, internal forces must be in equilibrium; bond always makes up the difference between the compression in the concrete and the tension in the strand. When bond cannot make up the difference, anchorage is lost. This difference between the strain in the concrete and the strand is called the strain differential ($\Delta\varepsilon_p$), without which a girder would not be considered prestressed concrete. A good understanding of bond is necessary in order to know how

debonding will affect a girder's strength. The following paragraphs give a qualitative sense of the fundamentals of bond.

Bond is actually the combination of three mechanisms. The first mechanism of bond is adhesion, or the "glue" that forms between strand and concrete. Adhesion prevents the movement of the strand relative to the concrete until a certain stress level is reached. After such limit is reached, and the strand slips even a minute amount, adhesion provides zero resistance and is replaced by the other bond mechanisms discussed below. Adhesion is of little concern, because, at release, the strand draws-in to the beam several tenths of an inch. Because of this draw-in, this researcher holds that adhesion does not contribute to the transfer or development bond.

The second mechanism of bond is Hoyer's Effect, named for E. Hoyer, who performed early research on anchorage mechanisms; Hoyer and Friedrich (1939). Hoyer's Effect is the wedging of the strand against the hardened concrete due to Poisson's ratio. When a strand is tensioned, its diameter decreases. In a prestressed concrete bridge girder, the concrete is placed while the strands are tensioned. At release, the strands try to regain their initial diameter, but the surrounding hardened concrete restrains their lateral movement. This lateral restraint (N) creates slip resistance from friction ($f = \mu N$). Throughout the length of a girder, moment and shear due to external loads create additional tension in the strand, causing the strands' diameter to decrease and likewise decreasing the wedging action. As stated before, if, for example, a girder fails in flexure (concrete crushes or strand ruptures), the restraint provided by Hoyer's Effect must have been enough to prevent an anchorage failure.

The final bond mechanism is mechanical interlock, which results from cement paste filling the narrow crevices (interstices) of the strands. When concrete cracks, the strands react against the ridges in the concrete, creating high bond-stresses in the area around a crack. In order for mechanical interlock to be effective, the strand must have torsional restraint. Various researchers disagree how much torsional restraint is available (Russell, et al. [1993]).

In summary, Hoyer's Effect and mechanical interlock provide most of the bond between the strands and the concrete. Knowing the three bond mechanisms is theoretical background, but the general code equations for transfer length and development length are empirical; the general equations do not explicitly account for the three bond mechanisms individually.

2.3.1.3 The Effect of Debonding on Shear Strength

The third anchorage-related fundamental is debonding's effect on shear strength. Precompression caused by prestressing increases the shear that causes cracking. Such shear cracking results from stresses due to applied loads' exceeding concrete's inclined (principle) tensile strength. If a girder's effective prestressing force is less, due to the breaking of the bond, then its crack resistance is also less. When crack resistance decreases due to debonding, less external load is required to form a web-shear crack or flexure-shear crack in the end-regions.

When a web-shear crack or flexure-shear crack forms in or near a strand's transfer length and/or development length, the strand will slip a small amount and carry more tension by engaging increased bond stresses on both sides of the crack. In addition to that tension, still more tension must be carried in the strand after cracking. Once a web-shear crack or flexure-shear crack forms and the strand slips, the effective prestressing force is less, reducing the load required to form additional cracks. As the external load increases, additional tension, both from slippage and from shear demand, eventually becomes too great, and an anchorage failure occurs. While this type of failure can occur in girders with fully-bonded strands, the presence of debonded strands should make this type of failure more likely to occur at lower loads.

This anchorage failure can be explained by examining a crack's effect on bond. When a crack forms, tension that was initially shared by the strand and the concrete is then carried only by the strand. In this case, Hoyer's Effect has been lost because external loads placed enough tension on the strands. Once Hoyer's Effect is gone, torsional

restraint is also lost, and mechanical interlock ceases to prevent the strand from slipping. Anchorage failure is imminent in this state. Research has shown anchorage failures to be sudden and explosive (Russell, et al. 1993; Shahawy and Cai 2001).

The preceding discussion makes clear that care must be taken to limit strand tension from external loads so as to prevent an anchorage failure. Moreover, cracking induces high bond stresses and corresponding high tension in the strand, so the ways to prevent anchorage failures are either to prevent cracking within the development length or to provide sufficient anchorage that ensures the strand can carry additional tension caused by cracking.

2.3.1.4 The Effect of Shear on Tension in Longitudinal Reinforcement

The fourth anchorage-related fundamental is shear's effect on tension in longitudinal reinforcement. A truss model, Figure 2-5, is an excellent conceptual model to show the forces that exist in a diagonally cracked concrete beam. In the truss model, the top chord represents the compression block (strut), and the bottom chord represents the longitudinal tensile reinforcement (tie). The vertical ties represent the shear reinforcement, and the diagonal struts represent the inclined compressive forces between the inclined cracks. At each truss joint along the bottom chord, the diagonal strut increases the amount of tension that the longitudinal reinforcement is required to carry. The increase in tension in the longitudinal reinforcement is illustrated in Figure 2-6. The presence of diagonal cracking causes increases the demand on the longitudinal reinforcement. This increase in demand is important for anchorage in beams tested in shear. With basic knowledge in hand regarding anchorage, the AASHTO code equations are now covered.

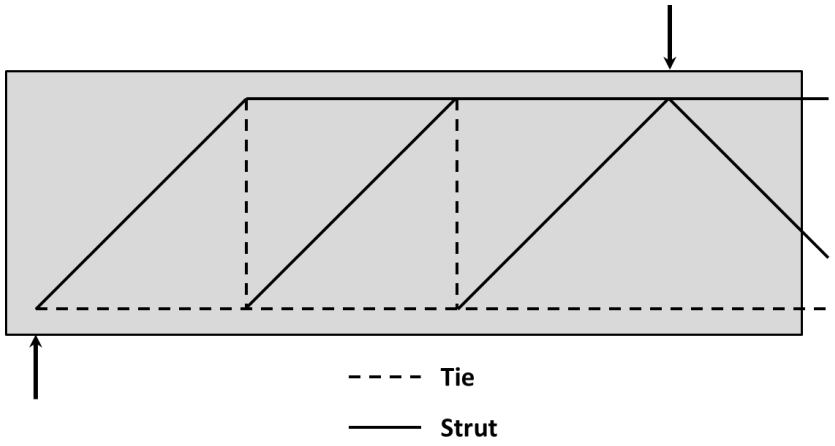

Figure 2-5: Truss Model for Shear Cracked Beam

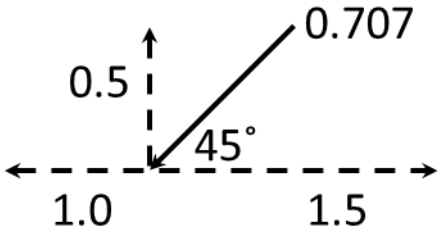

Figure 2-6: Increase in Tensile Force in Longitudinal Reinforcement from Diagonal Cracking

2.3.2 2010 AASHTO LRFD Bridge Design Specifications (Anchorage Design)

Just as the 2010 AASHTO LRFD Bridge Design Specifications were used for the shear design, so also these specifications are used for the anchorage-related design. This section provides details regarding the anchorage resistance model and the associated design equation, as well as the transfer and development length equations, in order to account for the partial development in the end-regions.

2.3.2.1 Anchorage

This section details the 2010 AASHTO anchorage equation. When a beam carries shear, its longitudinal reinforcement, after the onset of cracking, carries additional tension. This additional tension depends on both the angle of the diagonal struts (demand increases as θ decreases) and the magnitude of V_c (demand increases as V_c increases). These mechanics were the basis for the anchorage provisions located in section 5.8.3.5 of the 2010 AASHTO LRFD Bridge Design Specifications.

The resistance model, illustrated by a free-body diagram in Figure 2-7, assumes the critical condition to be a shear crack crossing the longitudinal reinforcement at the front of the bearing pad, where the strands are not fully developed. The model also makes several simplifications. The aggregate interlock force, V_{agg}, is assumed to have negligible moment about Point O, and the change in distance between V_n and V_p is assumed to be negligible, though this change in distance may not, in fact, always be negligible.

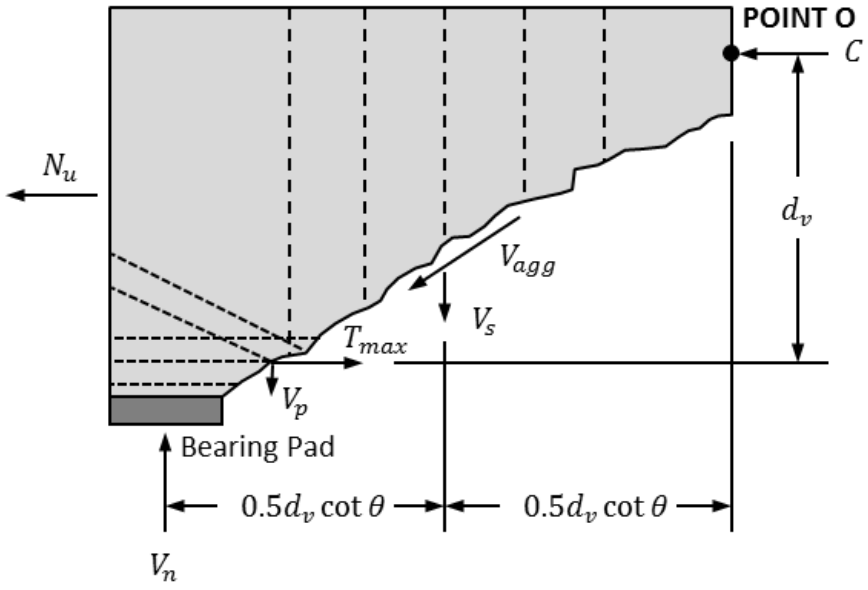

Figure 2-7: Anchorage Free-Body Diagram
Forces Assumed in Resistance Model Caused By Moment and Shear

The anchorage equation (AASHTO Equation 5.8.3.5-1) is found by taking the moment about Point O. When evaluating the anchorage equation at the bearing pad, the moment and the axial force are both taken as zero. The anchorage capacity and demand are as follows:

$$T_n \geq T_{max} \qquad \text{Equation 2-19}$$

$$A_{ps}f_{ps} + A_s f_y \geq \frac{|M_u|}{\varphi_f d_v} + 0.5\frac{N_u}{\varphi_c} + \left(\left|\frac{V_u}{\varphi_v} - V_p\right| - 0.5V_s\right)cot\theta \qquad \text{Equation 2-20}$$

where:

T_n = tensile capacity of the longitudinal reinforcement on the flexural tension side of the member (kips)

T_{max} = maximum tensile demand on longitudinal reinforcement (kips)

A_{ps} = area of bonded prestressing strands (in^2)

f_{ps} = maximum average stress in prestressing strands at a particular section (ksi)

A_s = area of bonded longitudinal mild reinforcement (in^2)

f_y = yield stress of mild reinforcement (ksi)

M_u = moment at the section (kip-in)

N_u = axial force, taken as positive if tensile (kips)

d_v = effective shear depth (in.)

V_u = shear at the section (kips)

$\varphi_f, \varphi_c, \varphi_v$ = resistance factors

V_p = component in the direction of the applied shear of the effective prestressing force (kips)

V_s = shear resistance provided by the transverse reinforcement found using AASHTO LRFD 2010 General Procedure (kips)

θ = angle of inclination of diagonal compressive stresses, found using AASHTO LRFD 2010 General Procedure (°)

Both this equation and the resistance model from which it is derived are significant for attempting to calculate anchorage capacity, but consideration must also be given to other factors, such as transfer and development length, which are discussed next.

2.3.2.2 Transfer Length and Development Length

In the 2010 AASHTO LRFD anchorage resistance model just discussed, a critical shear crack forms at the front of the bearing pad, where the strands are not fully developed. Because of the partial development of the strands, the transfer and development length equations are critical for accurate capacity calculations. This sub-subsection details the 2010 AASHTO LRFD transfer and development length equations. To determine the shear or flexural capacity of a prestressed concrete bridge girder, the engineer must consider the gradual stress increase in the strands within the transfer and development lengths. In the transfer length, the code assumes the stress in the strands varies linearly from zero to the effective stress after losses. Between the end of the transfer length and the end of the development length, the code assumes the stress in the strands increases linearly from the effect stress after losses up to the stress at the nominal flexural resistance of the girder.

Section 5.11.4 of the 2010 AASHTO LRFD specifies transfer length and development length. A simplified transfer length is typically taken as a distance equal to 60 times the strand diameter. A more accurate transfer and development length is given as the following:

$$l_d \geq \kappa \left(f_{ps} - \frac{2}{3} f_{pe} \right) d_b \qquad \text{Equation 2-21}$$

where:

l_d = development length (in.)

κ = modification factor
for members with depth ≤ 24 in. = 1.0
for members with depth > 24 in. = 1.6
for members with debonding = 2.0

f_{ps} = average stress in prestressing steel at the time for which the nominal resistance of the member is required (ksi)

f_{pe} = effective stress in the prestressing steel after losses (ksi)

d_b = nominal strand diameter (in.)

When a portion of the strands are debonded, the maximum force that can be developed is reduced in the end region; refer to the example in Figure 2-6. The blue curve is for a specimen with 10 fully-bonded 0.5 in. diameter strands. The effective prestressing force is transferred linearly over 30 in. The red curve is for a specimen with 8 fully-bonded and 2 debonded (for 5 ft) 0.5 in. diameter strands. The red curve has two distinct transfer lengths: one for the fully-bonded strands and one for the debonded strands. As a result, fewer fully-bonded strands are transferring force, so the initial slope is shallower. Finally, the total transfer length for the debonded specimen is 5 ft longer than for the fully-bonded specimen. Here, the effect of debonding on the transfer length (and thus development length) is obvious.

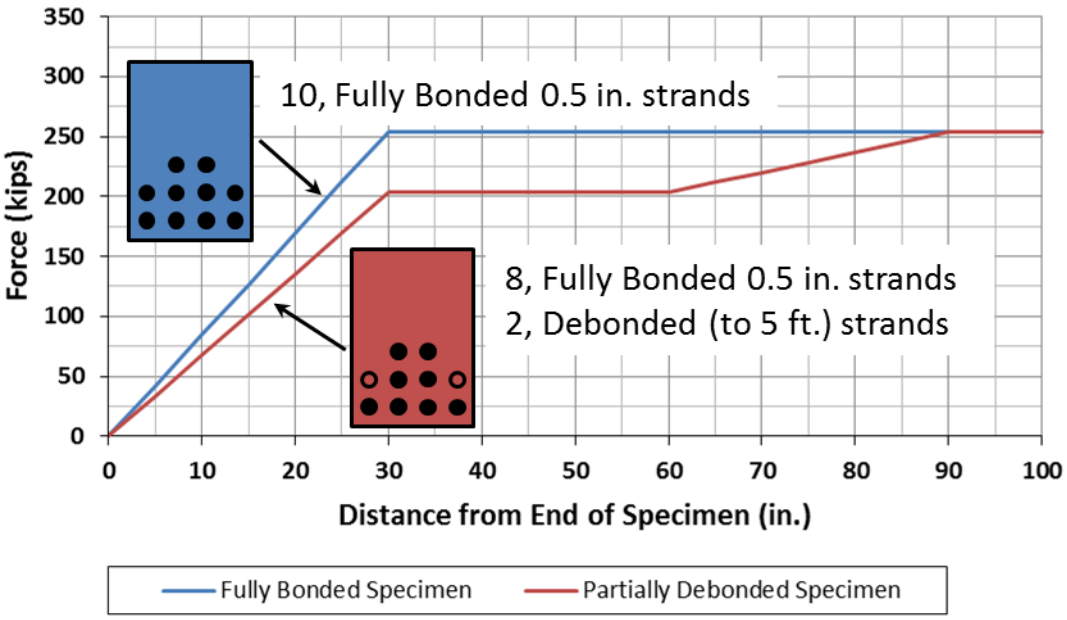

Figure 2-8: Example for Idealized Transfer Length

2.4 SELECT SHEAR/ANCHORAGE RELATED RESEARCH

Having demonstrated both that the 2010 AASHTO LRFD General Procedure provides the best shear estimation and that the same General Procedure does not accurately estimate horizontal shear and anchorage capacities, and having detailed

anchorage-related fundamentals and code provisions, summaries of selected shear/anchorage related research can now be presented. Thus, the following section describes previous research related to anchorage and debonding's influence on shear or flexural capacity. Significantly more previous research was studied and reviewed before the formation of the Anchorage Evaluation Database in Chapter 5. Nearly all of this previous research was performed on the standard AASHTO cross sections and so provides good comparison for this research on newer I-girders. In addition to providing background for anchorage and shear research, this previous research was important for a comparison to the experimental and analytical results. Summaries of four key studies follow in chronological order.

2.4.1 Abdalla, Ramirez, and Lee (1993)

In 1993, Abdalla, Ramirez, and Lee published their study of ten, full-scale, simply supported specimens under a single concentrated load. Eight specimens were AASHTO Type I prestressed concrete bridge girders built with a 48 in. by 4 in. concrete, composite deck that overlapped the girder by 0.5 in. The other two specimens were Indiana State Type CB-27 box girders also built with a concrete, composite deck. (Only the AASHTO Type I comparison results are relevant for this research.) The goal of their research was to investigate the effects of strand debonding on the flexure and shear behavior of prestressed concrete bridge girders. Consequently, half of their beams had varying percentages of debonded prestressing strands, while the other half contained no debonded strands. The behavior of the beams with debonded prestressing strands was compared to the behavior of the beams without debonded strands. The strand patterns are drawn in Figure 2-9. The specimen and test details are listed in Table 2-4; note that the sets in Table 2-4 refer to two beams identical except for the debonding. All strands were 0.5 in. diameter, Grade 270, low relaxation. All shear reinforcement was two legs of Grade 60 #3 U-bars spaced at 4 in.

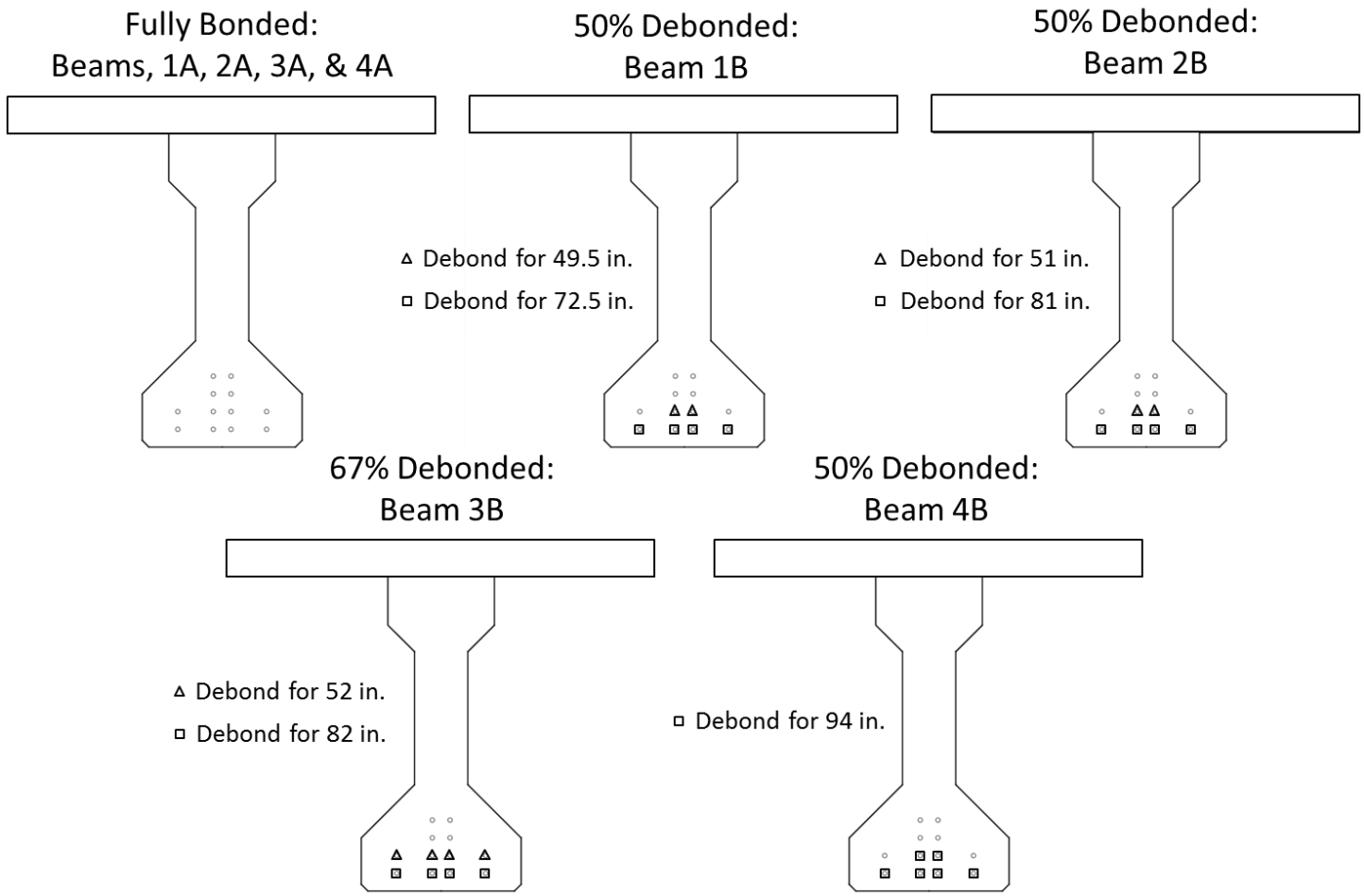

Figure 2-9: Strand Patterns (adapted Abdalla, et al. 1993)

Table 2-4: Specimen and Test Details (Abdalla, et al. 1993)

Set	Beam	Span in.	a in.	a/d	# Fully Bonded	# Debonded	Distance in.	Failure Mode
1	A	210	90	3.33	12	0	--	Deck Splitting
	B	210	90	3.33	6	2, 4	49.5, 72.5	
2	A	210	90	3.33	12	0	--	Anchorage
	B	210	90	3.33	6	2, 4	51, 81	
3	A	210	90	3.33	12	0	--	Anchorage
	B	210	90	3.33	4	4, 4	52, 82	
4	A	288	144	5.33	12	0	--	Flexure
	B	288	144	5.33	6	6	94	

The results of Abdalla, et al.'s experimental testing of AASHTO Type I prestressed concrete bridge girders show that anchorage failures can occur following the assumed AASHTO resistance model. Both girders in sets 2 and 3 failed in anchorage because shear cracks propagated into the bottom flange within or near the transfer length. Maximum slip of the fully-bonded strands in the debonded beams ranged from 0.1 in. to 0.5 in. Following strand slip, the cracks widened and the strain in the shear reinforcement increased. Eventually some of the shear reinforcement yielded. Both girders in set 4 failed in flexure, so the embedment length must have been enough to prevent cracks from propagating into the bottom flange. (Set 1 failed in the deck, due to improper detailing of the transverse reinforcement, which was corrected in the other sets.)

Abdalla, et al.'s research shows that cracking within the bottom flange in the transfer length causes an anchorage failure. Their research supports the applicability of the assumed AASHTO anchorage resistance model, but they did not calculate anchorage demand and capacity and so do not address the accuracy of the AASHTO anchorage equation.

2.4.2 Russell, Burns, and ZumBrunnen (1994)

In 1994, Russell, Burns, and ZumBrunnen published their results from flexural tests performed on prestressed concrete beam specimens made with debonded strands.

They developed a new failure prediction model that anticipated strand anchorage failures based on the prediction of cracking in regions of the transfer length of debonded strands. In the end, they found good agreement between their prediction model and test results. The paragraphs that follow here discuss separately both their model and their test results.

Russell, et al.'s anchorage failure prediction model was developed in a simple and straightforward manner: cracking through the transfer length of pretensioned strands will cause the prestressing strands to fail in anchorage. Such cracking through the transfer length is only exacerbated by debonding, which decreases a beam's resistance to both flexural cracking and web shear cracking in the end-regions of a beam. (The influence of cracking on bond was presented in Section 2.3.1.3.) Russell, et al. stated that because cracking in the concrete could be predicted reliably, anchorage failure of the prestressing strands could also be predicted.

In order to predict cracking reliably, they drew logical conclusions from existing mechanics, including the impact of debonding on cracking. The impact of debonding is shown in Figure 2-10, where applied moment is compared to the beam's cracking moment, M_{cr}. Here, M_{cr} is defined as the applied moment that causes flexural cracking in the bottom tension fiber of the cross section; it is calculated based on a bottom fiber tensile stress equal to the modulus of rupture, $7.5\sqrt{f'_c}$. The cracking moment, M_{cr}, is a property of the beam and is dependent on both the cross-sectional properties and the beam's effective prestressing force. Flexural cracking can be expected wherever the applied moment exceeds the cracking moment and occurs primarily in the regions of the largest applied moment, near the load point. As load increases, the region of flexural cracking expands as the region where the applied moment exceeds M_{cr} expands. In a beam with fully bonded strands, only one region of flexural cracking would be expected. However, in beams with debonded strands, flexural cracking can occur in the debonded/transfer length, toward the end-regions of the beam.

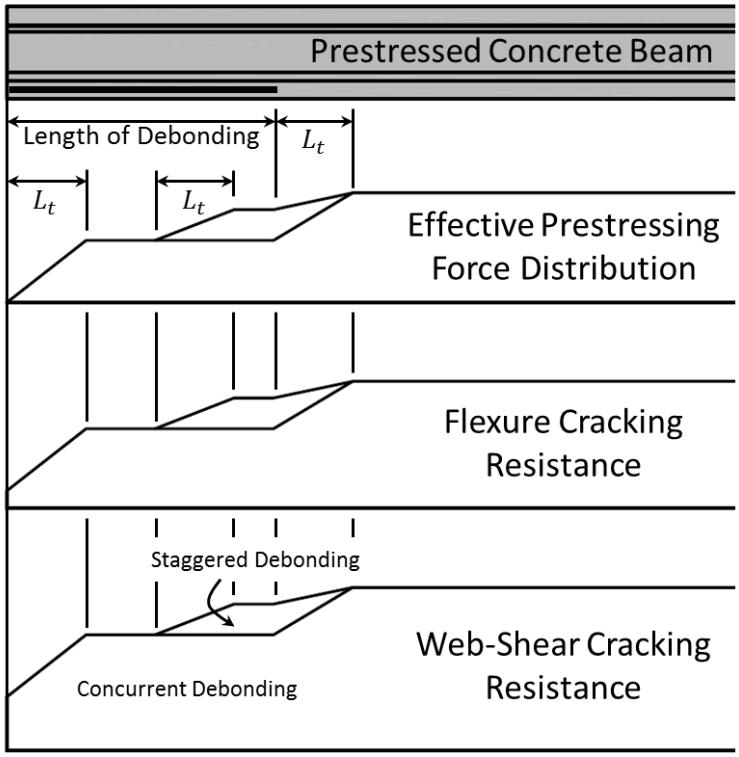

Figure 2-10: Debonding's Influence on Flexure and Shear Cracking (Russell, et al. 1994)

Figure 2-10 also illustrates the theoretical difference in behavior between a beam with concurrent debonding and a beam with staggered debonding. Concurrent debonding means that the debonded length is the same for all debonded strands. Staggered debonding means there is variation in the debonded length, in other words, the termination of debonding varies for each strand. Russell, et al. theorized that staggered debonding would have the effect of gradually increasing the effective prestressing force through the debonded regions, thus improving the beam's resistance to cracking. Staggered debonding would then minimize cracking in the debonded/transfer length.

Russell, et al.'s anchorage failure prediction model involved plotting the embedment length versus the debonded length. To prevent an anchorage failure from flexure in the case of concurrent debonding, the applied moment needed to pass through

two points: the termination of debonding and the point of maximum applied moment. The line that connects those two points relates the minimum embedment length, L_e, to the debonded length, L_b. (Russell, et al. defined embedment length as the distance from the termination of debonding to the load point.) This line is drawn in Figure 2-11.

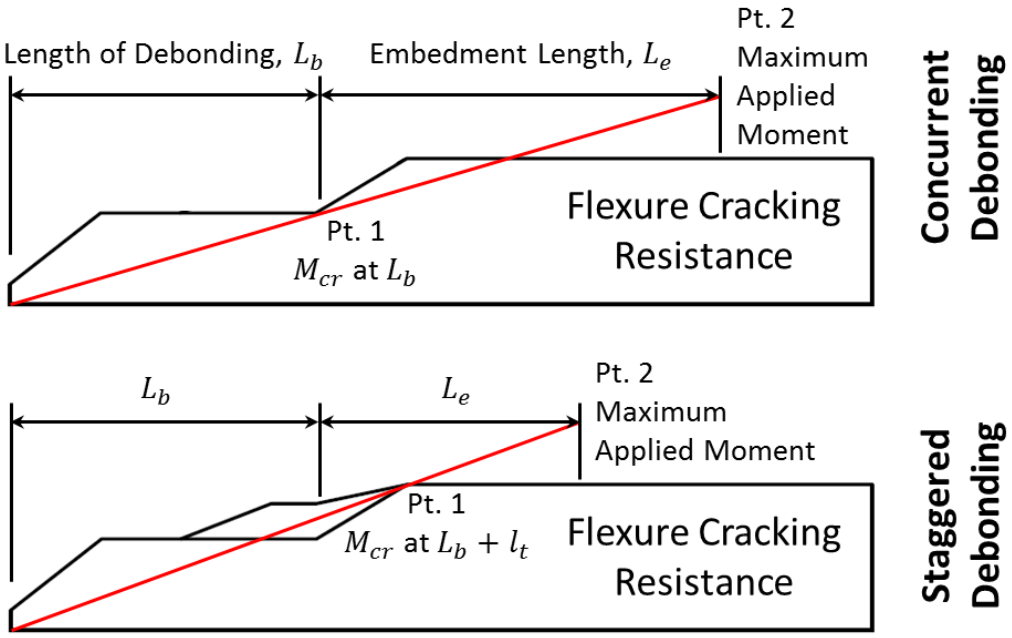

Figure 2-11: Generating the Anchorage Failure Prediction Model (Moment) (adapted Russell, et al. 1994)

To plot the relationship, L_e must become a function of L_b. This function was created using similar triangles and solving for L_e:

$$\frac{M_{cr}(at\ L_b)}{L_b} = \frac{M_{ult}(at\ load\ point)}{L_b + L_e} \qquad \text{Equation 2-22}$$

$$L_b = \frac{M_{cr}L_e}{M_{ult} - M_{cr}} \qquad \text{Equation 2-23}$$

For staggered debonding, the only change is an additional transfer length, l_t.

$$\frac{M_{cr}(at\ L_b + l_t)}{L_b + l_t} = \frac{M_{ult}(at\ load\ point)}{L_b + L_e} \qquad \text{Equation 2-24}$$

$$L_b = \frac{M_n l_t - M_{cr} L_e}{M_{cr} - M_{ult}} \qquad \text{Equation 2-25}$$

Just as they did for moment (Figure 2-10), Russell, et al. determined the beam's resistance to web-shear cracking, V_{cw}, along the length and plotted a similar line for shear, again relating the embedment length and the debonded length. Here, V_{cw} is defined as the applied shear that causes diagonal cracking in the web. The web-shear cracking resistance is a property of the beam and is dependent on the cross-sectional properties and the effective compression at the centroid of the section from prestressing. To prevent cracking in the transfer length, the applied shear had to be equal to the beam's resistance to web-shear cracking in the first debonded region, as drawn in Figure 2-12.

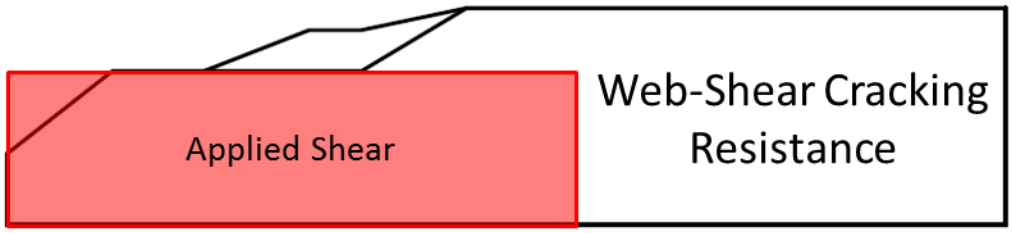

Figure 2-12: Generating the Anchorage Failure Prediction Model (Shear) (adapted Russell, et al. 1994)

Then, using principles of shear, an equation relating L_b to L_e was generated as follows:

$$L_b + L_e = \frac{M_{ult}}{V_n} \qquad \text{Equation 2-26}$$

$$L_b = \frac{M_{ult}}{V_n} - L_e \qquad \text{Equation 2-27}$$

Ascertaining the foregoing line for shear completed the necessary steps for the anchorage failure prediction model.

The resulting equations for the anchorage failure prediction model are plotted in Figure 2-13, based on the capacities for the specimens Russell, et al. tested. Several important observations should be noted from the plot. First, the embedment length necessary to prevent bond failures depends on the length of debonding. Second, to ensure strand anchorage, longer debonded lengths required greater embedment lengths. Third, the differences between concurrent and staggered debonding patterns is clear: in order to prevent anchorage failures, a concurrent debonding pattern requires more strand embedment than a staggered debonding pattern.

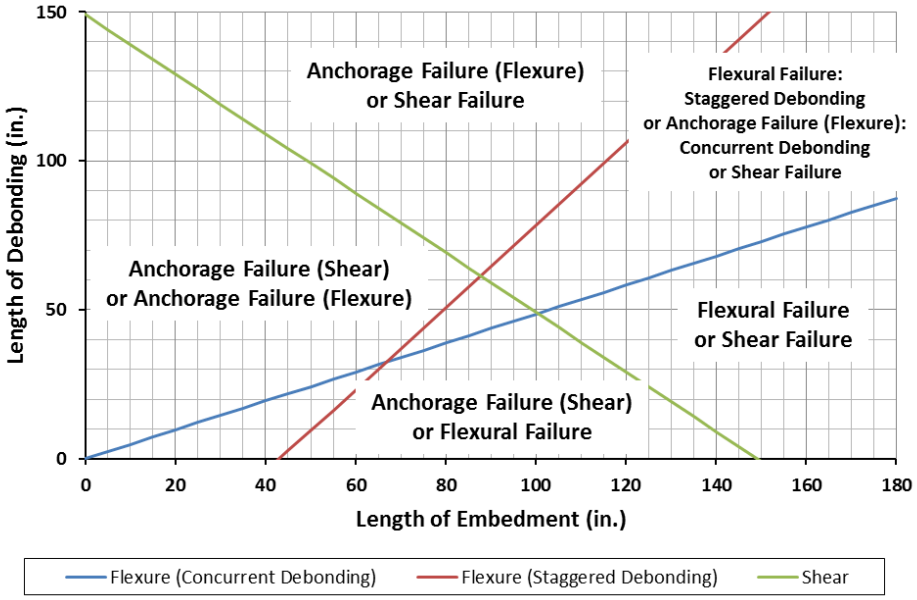

Figure 2-13: Anchorage Failure Prediction Model (adapted Russell, et al. 1994)

In order to verify the preceding anchorage failure prediction model, Russell, et al. fabricated 40 ft long beams and conducted flexural tests (not every beam or test is relevant to this research). The shear reinforcement was the same for each test. Also, no confinement or special anchorage details were used. Each beam contained eight 0.5 in. diameter strands. The debonding schedule is given in Table 2-5. In two of the beams, four

strands were debonded for 36 in. In three of the beams, four strands were debonded for 78 in. This latter debonding distance was chosen because this length offered the greatest range of possible outcomes. The embedment lengths were also chosen so that bond failures, shear failures, or flexural failures for either concurrent or staggered debonding patterns could be obtained. Table 2-6 contains a summary of test results relevant to this research.

Table 2-5: Specimen Details and Debonding Schedule (adapted Russell, et al. 1994)

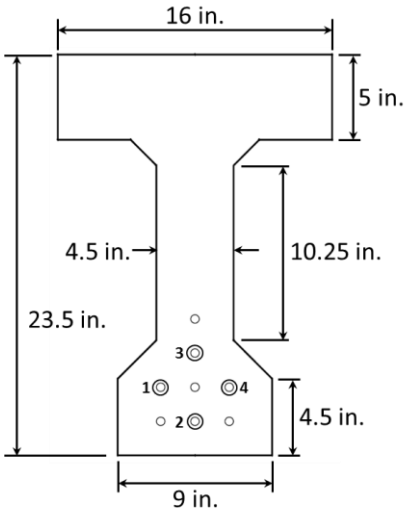

Debonding Schedule					
Beam	S or C	Strand (in.)			
		1	2	3	4
1	S	18	36	36	18
3	S	39	78	78	39
4	S	39	78	78	39
5	C	78	78	78	78

Table 2-6: Summary of Tests (Russell, et al. 1994)

Test	Debonded Length	Embedment Length	P_{test}	M_{test}	M_{test}/M_n	Failure Mode
	in.	in.	kips	kip-in		
1A	36S	84	69.58	5358	0.98	Anchorage
3A	78S	80	81.16	5590	0.93	Anchorage
3B	78S	108	52.24	5851	0.97	Flexure/Anchorage
4A	78S	120	88.00	5104	0.85	Anchorage
4B	78S	100	93.60	5738	0.95	Anchorage
5A	78C	120	95.97	5622	0.94	Anchorage
5B	78C	150	93.29	5778	0.96	Flexure

Before discussing the results, Russell, et al. needed to define what constituted a flexural failure and an anchorage failure. They defined a flexural failure as crushing of the top flange concrete or yielding of the strands. This type of failure had to involve large deflections and occur after reaching the nominal moment capacity. They defined an anchorage failure as slip of multiple strands before the nominal moment capacity was reached. The anchorage failures were often sudden and violent.

Numerous tests failed in anchorage. In all but one instance of flexural failure, little strand slip was observed, and little to no cracking in the transfer length was observed. In one borderline case, a flexural failure occurred with significant strand slip. This particular test shows that a shorter embedment length would have resulted in an anchorage failure as the model predicted. The anchorage failures contained cracking in the transfer length. After testing, the results were plotted on the bond failure prediction model graph (Figure 2-14 for concurrent debonding and Figure 2-15 for staggered debonding). These results showed good agreement with the model for both concurrent and staggered debonding. Because of its promising initial results, although verified by limited testing, Russell, et al.'s new method is investigated further using the results of this research (Section 4.3.1). The only other seeming issue with their method, though they do not discuss it, is that the failure regions overlap.

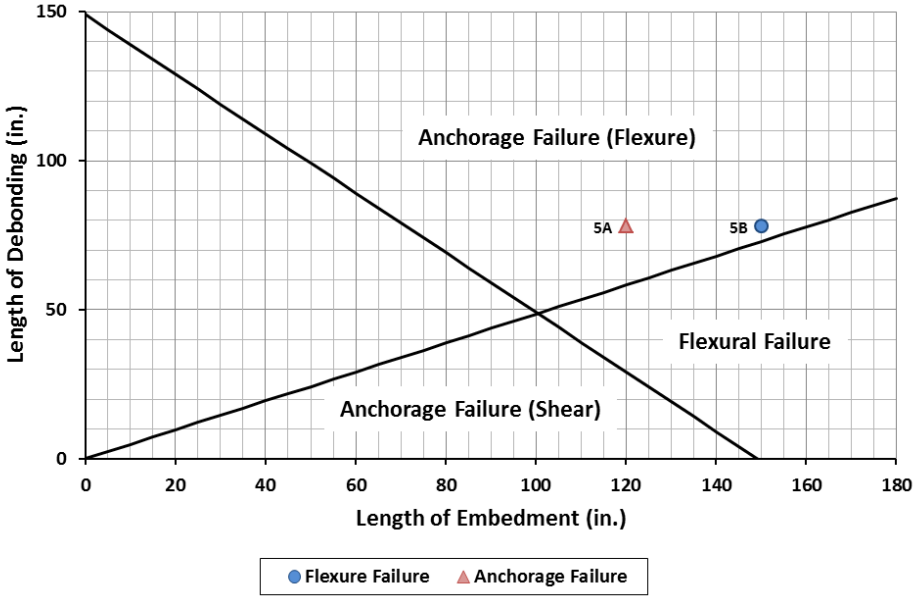

Figure 2-14: Plotted Test Results - Concurrent Debonding (adapted Russell, et al. 1994)

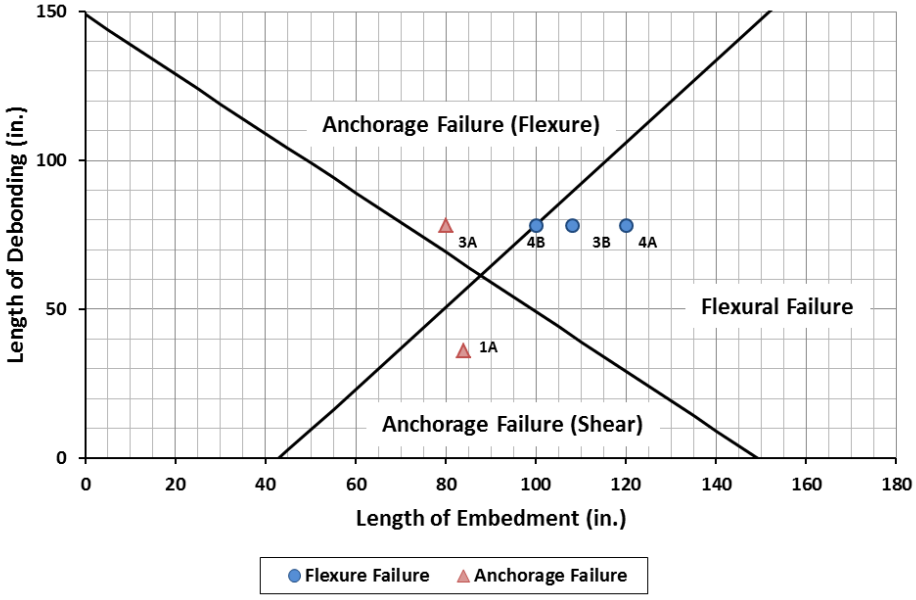

Figure 2-15: Plotted Test Results - Staggered Debonding (adapted Russell, et al. 1994)

2.4.3 Shahawy (2001)

In 2001, Shahawy published his study evaluating proposals for the development length of prestressing strands. Using the results from a test program on piles and AASHTO Type II girders, he observed a direct interaction between shear and anchorage occurring at the ends of prestressed concrete members. Shahawy concluded by offering a new approach for development length for members with a depth of 24 in. or greater; his new approach included terms for both flexure and shear. Only his shear testing of AASHTO Type II prestressed concrete bridge girders and its results are relevant to this research and so presented in what follows.

All the AASHTO Type II girders were fully bonded and contained the required shear reinforcement as specified in the 1999 AASHTO Standard Specifications for Highway Bridges. He divided his tests into three groups for three different strand diameters: the "A" group contained 0.5 in. diameter strand, the "B" group contained 0.5 in. special diameter strand, and the "C" group contained 0.6 in. diameter strand. Figure 2-16 illustrates his strand patterns, and Table 2-7 contains a summary of each of his tests.

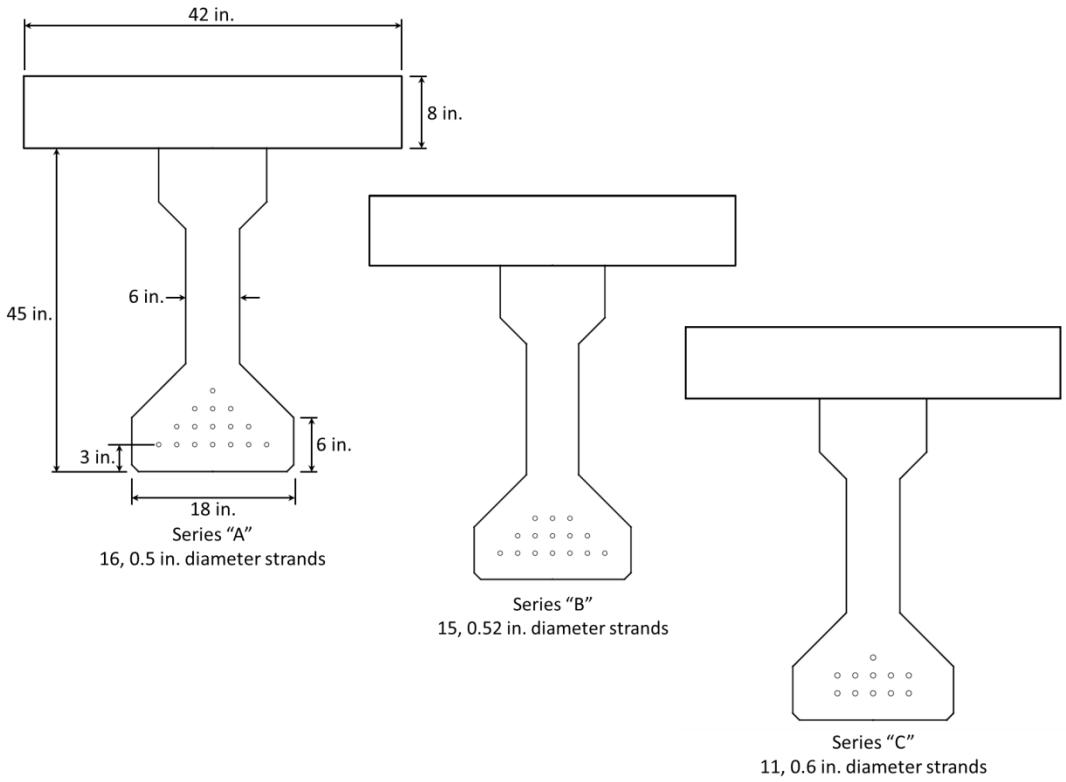

Figure 2-16: Strand Patterns for Each Group (adapted Shahawy 2001)

Table 2-7: Summary of Each Test (Shahawy 2001)

Girder	End	Span	Shear Span	a/d	Failure Mode
		in.	in.		
A0-00	N	480	85	2.1	Shear/Anchorage
	S	324	85	2.1	Shear
A1-00	N	480	102	2.5	Shear/Anchorage
	S	378	124	3.1	Flexure/Anchorage
A3-00	N	480	102	2.5	Shear/Anchorage
	S	378	124	3.1	Shear/Anchorage
A4-00	N	480	85	2.5	Flexure/Anchorage
	S	424	85	3.1	Shear/Anchorage
B0-00	N	480	102	1.5	Shear/Anchorage/Flexure
	S	378	124	1.3	Shear/Flexure
B1-00	N	240	60	1.5	Shear/Anchorage
	S	222	54	1.3	Shear/Anchorage
C0-00	N	336	142	3.5	Flexure
	S	480	132	3.2	Flexure
C1-00	N	480	142	3.5	Flexure
	S	378	132	3.2	Flexure

Most of Shahawy's tests failed in an anchorage-related manner. The typical anchorage failure mechanism involved initial slip at, or shortly after, the appearance of the first shear crack. More strands slipped as more cracking developed. Once all of the strands slipped, the girders were unable to carry additional load. His crack maps for specimen A3-00 are redrawn in Figure 2-17. As can be seen, many cracks propagated into the bottom flange, crossing the strands. This failure mechanism is the same that the AASHTO anchorage resistance model predicts, suggesting that the model is well-founded for AASHTO-type girders.

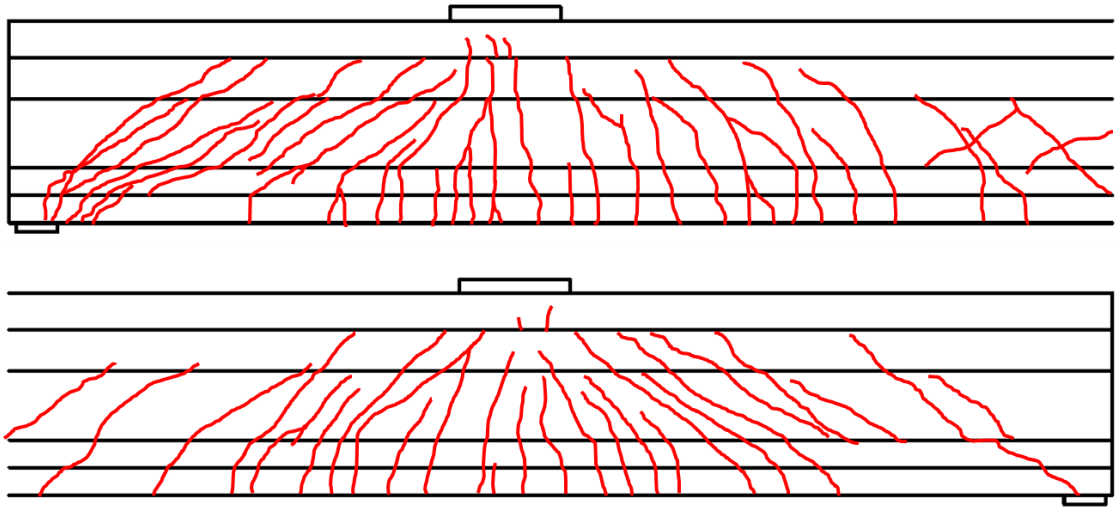

Figure 2-17: Specimen A3-00 Crack Maps North, Top, and South, Bottom (adapted Shahawy 2001)

Shahawy made several plots to analyze his results. On one such plot, the ratio of the moment at first slip to the nominal moment capacity was graphed against the ratio of the embedment length to the strand diameter. This plot showed that nearly all anchorage related failures fell below a ratio of 1.0, which means that slip was occurring before the girders were reaching their capacity.

Though development length was Shahawy's primary concern, the importance of his study for this research is not the findings related to development length but those related to the manner of the girders' failing in anchorage. Numerous shear cracks propagated into the bottom flange, crossing the strands, and the strands slipped. Shahawy's research shows that the assumed anchorage resistance model is well-founded with respect to AASHTO-type prestressed concrete bridge girders. Moreover, that an anchorage failure occurred in girders without debonding can logically lead to the conclusion that the same specimens with debonding would have failed at much lower applied loads. As with Abdalla, et al.'s work, a drawback of Shahawy's study is that he

did not calculate anchorage demand and capacity and so does not address the accuracy of the AASHTO equation.

2.4.4 Hamilton, Llanos, and Ross (2009) & Ross, Ansley, and Hamilton (2011)

In 2009, Hamilton, Llanos, and Ross published the initial results of a testing program of in-service prestressed concrete bridge girders, and, in 2011, Ross, Ansley, and Hamilton published the final results of the same project. Since the two publications deal with the same data, the following discussion treats them as one study. Among others, the in-service prestressed concrete bridge girders the researchers tested included AASHTO Type III and AASHTO Type IV, which are the only girders of interest to this research.

Four AASHTO Type III girders were salvaged from a 30-year-old bridge in Florida, each with a deck and end diaphragm, and a strand pattern as drawn in Figure 2-18. These girders were tested in three-point bending with shear span-to-depth ratios varying between 1.2 and 5.4. For shear span-to-depth ratios less than 3.0, a flexure-shear crack formed near the support, causing the strands to slip, and a distinct loss of stiffness was observed in the girder. After this initial slip, the vertical and horizontal mild reinforcement engaged and provided some reserve capacity. Eventually, however, even this reinforcement either yielded or failed in anchorage. Figure 2-19 contains a photograph of the failure crack and a free-body diagram showing the mild reinforcements' contribution.

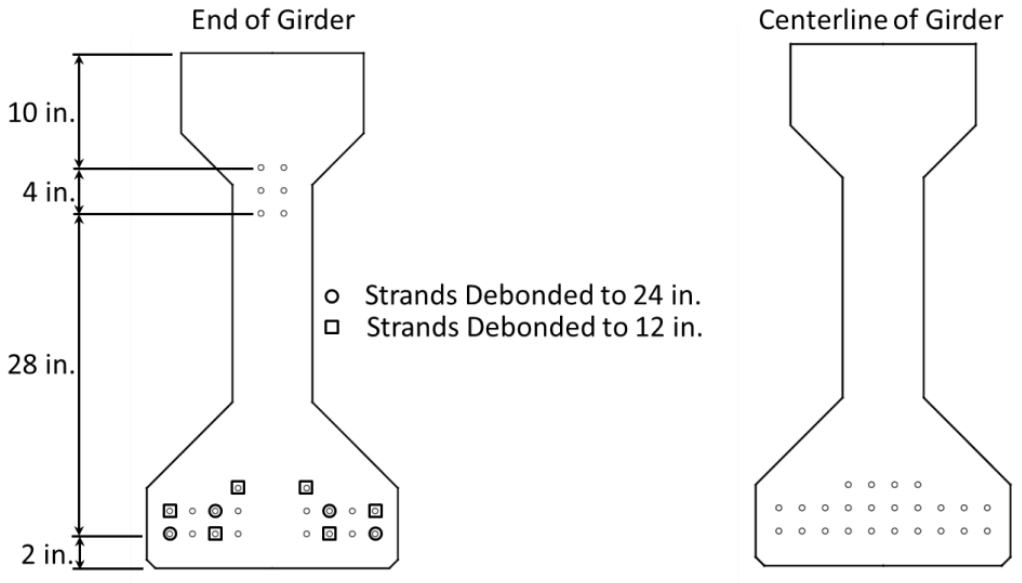

Figure 2-18: AASHTO Type III Strand Pattern (adapted Ross, et al. 2011)

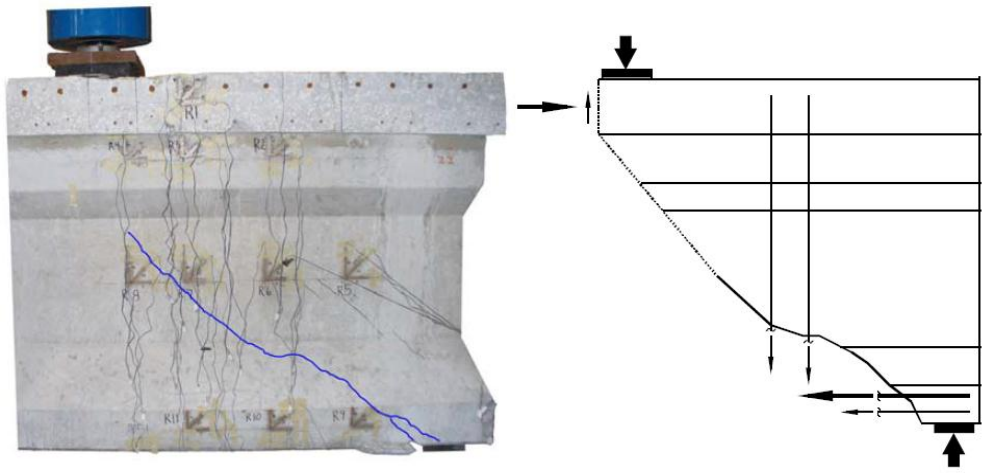

Figure 2-19: Typical Failure and Free-Body Diagram (Hamilton, et al. 2009)

The measured shear capacity of these same four Type III girders was compared to the shear capacity as calculated by four different methods: the 2010 AASHTO LRFD General Procedure, strut-and-tie modeling, the 2008 ACI Detailed Method, and a modified version of the 2010 AASHTO LRFD anchorage equation. Before using the

anchorage equation, Ross, et al. modified the equation in three ways. First, the harped strands were included separately from the straight strands, taking into account the change in distance from T. Second, the angle of inclination, θ_m, was taken as the angle between the longitudinal axis of the girder and a line between the load point and the support. Third, the actual distribution of the transverse reinforcement was accounted for by x_s, which was the distance from the load point to the resultant of V_s. Figure 2-20 contains their free-body diagram for the modified anchorage calculation. The AASHTO anchorage equation was rearranged with the modifications so that the shear capacity, V_{nER}, could be calculated as follows:

$$V_{nER} = \frac{T}{cot\theta_m} + \frac{Hd_h}{d_p cot\theta_m} + \frac{V_s x_s}{d_p cot\theta_m} + \frac{V_p d_h}{d_p} \qquad \text{Equation 2-28}$$

where:

V_{nER} = nominal shear capacity of the end region (kips)

T = capacity of prestressing and mild reinforcement, accounting for development length (kips)

θ_m = angle between the longitudinal axis of the girder and a line between the support and load point (˚)

H = capacity of harped strands, accounting for development length (kips)

d_h = depth of harped strands at intersection with inclined section boundary (in.)

d_p = depth of straight strands and mild reinforcement (in.)

V_s = capacity of shear reinforcement (kips)

x_s = distance from load point to resultant V_s (in.)

V_p = vertical component of effective prestressing force (kips)

Table 2-8 contains the results from all the calculations, which show that the best ratios were generated by the modified anchorage equation, meaning it was the best predictor of the shear capacity of the beam end-region. Note that the results from the strut-and-tie analysis are highly dependent on the researchers' model. The strut-and-tie model was not checked as part of this review.

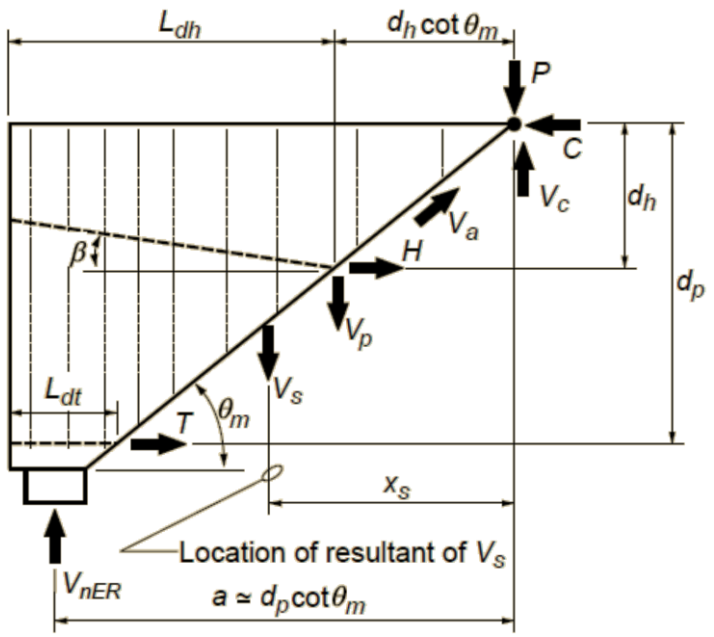

Figure 2-20: Free-Body Diagram for Modified Anchorage Equation (Ross, et al. 2011)

Table 2-8: Comparison of Calculated Shear Capacity and Measured Shear Capacity (Ross, et al. 2011)

a/d	V_{test}	Strut-and-Tie Modeling		ACI Detailed		AASHTO General Procedure		Modified Anchorage Equation	
		V_n	$\frac{V_{test}}{V_n}$	V_n	$\frac{V_{test}}{V_n}$	V_n	$\frac{V_{test}}{V_n}$	V_n	$\frac{V_{test}}{V_n}$
1.2	344	159	2.16	268	1.28	211	1.63	252	1.37
2.1	255	108	2.36	243	1.05	231	1.10	255	1.00
3.1	207	NA	NA	227	0.91	193	1.07	222	0.93
4.2	180	NA	NA	181	0.99	181	0.99	NA	NA
4.2	198	NA	NA	181	1.09	181	1.09	NA	NA
5.4	158	NA	NA	160	0.99	167	0.95	NA	NA

Their study of the in-service AASHTO Type III girders further proves that the assumed anchorage resistance model applies to AASHTO-type prestressed concrete bridge girders. Their study used a modified AASHTO anchorage equation to calculate

shear demand and capacity, as limited by anchorage, and the modified equation accurately predicts the shear capacity of the end region.

The AASHTO Type IV girders were fabricated to replicate existing bridge girders in Florida. When tested in shear, these Type IV girders displayed a splitting failure of the bottom flange. Hamilton, et al. concluded that the presence of an unusual debonding pattern caused the splitting failure. The fully bonded strands were located at the outside of the flange, and the debonded strands were located under the web. This debonding pattern created an offset between the longitudinal ties and the strut in the web. A simple strut-and-tie model of the end region of the beam illustrates how the unintended transverse tensile force formed above the bearing pad (Figure 2-21). This study of the Type IV girders highlights the importance of debonding pattern. Unique, undesirable failure modes can occur when the wrong strands are debonded. As a results, the design of the girders for the experimental program of this research avoided putting debonded strands under the web.

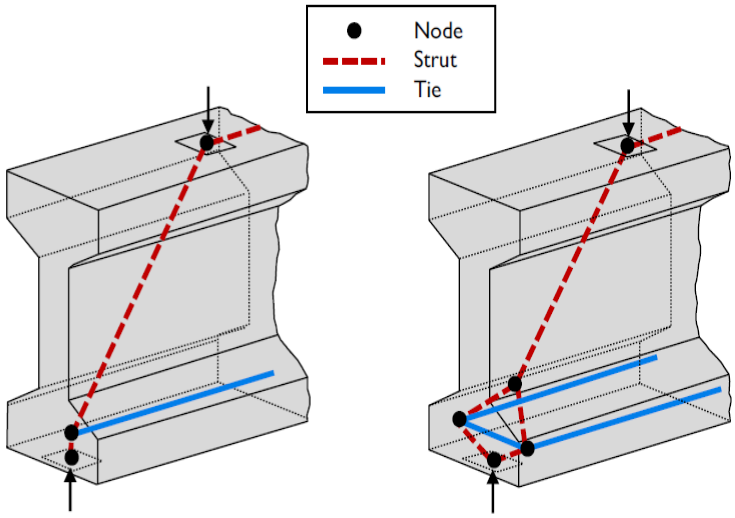

Figure 2-21: Strut-and-Tie Model for Beam with Fully Bonded Tendons (Left) and Beam with No Bonded Strands under the Web (Right) (Hamilton, et al. 2009)

This study of Type III and Type IV girders provides further proof that the assumed anchorage resistance model applies to AASHTO Type III prestressed concrete bridge girders. Also, for these few tests, the modified AASHTO anchorage equation appears to accurately predict the shear capacity of the end-region.

2.5 SUMMARY

Theoretical background and highlights of previous research are important for this research's experimental and analytical programs. Most significantly, analysis of the data in the UTPCSDB indicates that, of the various shear design methods, the 2010 AASHTO LRFD General Procedure gives the best results for traditional modes of vertical shear failure but not for both horizontal shear failure or anchorage failure. Hovell's method based on shear friction reliably predicts horizontal shear failure, and the 2010 AASHTO resistance model and a corresponding derived equation are currently used to predict anchorage failure. So, the questions are left whether that current method for predicting anchorage failure is adequate, and, if not, what can be done to improve that method. Previous studies pertaining to that method of predicting anchorage failure suggest the anchorage resistance model is well founded, at least on AASHTO-type girders, and at least one study suggests the equation is accurate in such cases, as well. Another question that has not been addressed in previous studies is whether the 2010 AASHTO anchorage resistance model and its corresponding equation are adequate in cases of modern I-girders. Answering that question is one of the goals of this research, but before an answer can be attempted, the details of the experimental program—including information about specimen design and fabrication, instrumentation, and test setup—must be given, as they are in Chapter 3 that follows next.

CHAPTER 3: EXPERIMENTAL PROGRAM

The Phil M. Ferguson Structural Engineering Laboratory (FSEL) at The University of Texas at Austin continues its groundbreaking research on shear, most recently explaining one of two nontraditional shear failures, namely, horizontal shear. This research investigated the other, anchorage, specifically anchorage failure in prestressed concrete bridge girders fabricated with a reasonable percentage of debonded strands.

3.1 OVERVIEW

With theoretical background and highlights of previous research relevant to this research's experimental and analytical program addressed in Chapter 2, this chapter, Chapter 3 of this thesis, discusses the experimental program: the design and fabrication of the test specimens, girders and decks; the materials used in fabrication, including their nominal and measured strengths; the instrumentation used for data collection during testing; the shear test setup and procedure; and the preliminary analysis.

3.2 DESIGN AND FABRICATION OF TEST SPECIMENS

The first aspect of the experimental program this chapter covers is the design and fabrication of the research's test specimens: girders and decks. Two, thirty-foot-long prestressed concrete bridge girders were fabricated at FSEL. Both were designed to have a high likelihood of failing in anchorage. A concrete, composite deck was added to each girder. The girder plus the concrete deck had a combined weight of approximately 43 kips. An I-girder was chosen due to its simplicity in fabrication, testing, and analysis. An I-girder was also appropriate because of this research's objective of studying a more modern cross-section, in contrast to an AASHTO-type I-girder. A brief history of the modern I-girder in Texas is next.

Within the last ten years, the Texas Department of Transportation (TxDOT) has developed a new family of prestressed concrete I-girders in order to take full advantage of high-strength concrete and larger diameter strands (Avendano 2008). These I-girders, called Tx Girders, have been flexurally optimized so they have a thin web relative to a wide bottom flange. The Texas beams can be larger and accommodate more prestressing strands because of modern high-strength concrete. The section properties and cross sections are located in Table 3-1 and Figure 3-1, where the member depth in inches corresponds to the TxDOT designation for the beam. The middle cross-section shown is 46 in. deep and so designated Tx46. That more modern, Tx46 cross section was chosen, in keeping with the objectives of this research. Details on the fabrication of the experimental program's two beams follow.

Table 3-1: Tx Girder Section Properties

Girder Type	Depth	y_t	y_b	Area	I_x	I_y	Weight
	in.	in.	in.	in^2	in^4	in^4	plf
Tx28	28	15.02	12.98	585	52772	40559	610
Tx46	46	25.90	20.10	761	198089	46478	793
Tx70	70	38.09	31.91	966	628747	57579	1006

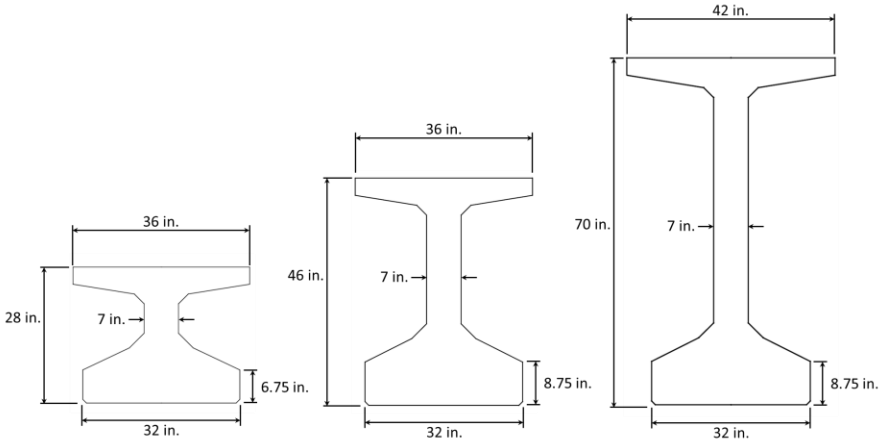

Figure 3-1: Tx Girder Cross-Sections

3.2.1 Girder Design

Both girders for this research's experimental program were designed according to the AASHTO LRFD Bridge Design Specifications (2007, with consideration of the 2008, 2009, and 2010 Interim Revisions). Fabrication of all specimens took place in FSEL, located on the J.J. Pickle Research Campus of The University of Texas at Austin.

In order to meet the primary objectives of this research, the girder specimens were designed to fail in anchorage. With that intent, the design called for debonding 35 percent of the strands for 6 ft. The addition of debonding reduces the tensile force that can be developed in the longitudinal reinforcement, and thus the addition of debonding also reduces the applied load required to exceed the longitudinal reinforcement's anchorage capacity and thus fail. Since no data were available to determine the ratio of the average measured failure load to the calculated failure load, an anchorage failure was assumed to occur when the ratio of T_{max} to T_n equaled 1.0.

That lack of data and the assumption it produced influenced the design of the girders. To provide a buffer, the design of the girders left enough reserve capacity to avoid all other failure modes (i.e., flexure, shear, and horizontal shear) under the demand from the load that would cause an anchorage failure. This designed buffer was necessary because of the lack of anchorage data noted above. In other words, an anchorage failure could occur when the ratio of T_{max} to T_n equaled something greater than 1.0. Further design details relative to the three failure modes to be avoided follow.

The girders' flexural design included maximizing the eccentricity of the prestressing strands for maximum flexural capacity. The strand patterns for the two specimens are drawn in Figure 3-2. The design methods for estimating the flexural capacity of a prestressed concrete member are well understood. A flexural failure is expected to occur when the ratio of M_u to M_n equals about 1.0. The addition of a concrete, composite deck increased the girders' flexural capacity by 70% and 30%, respectively.

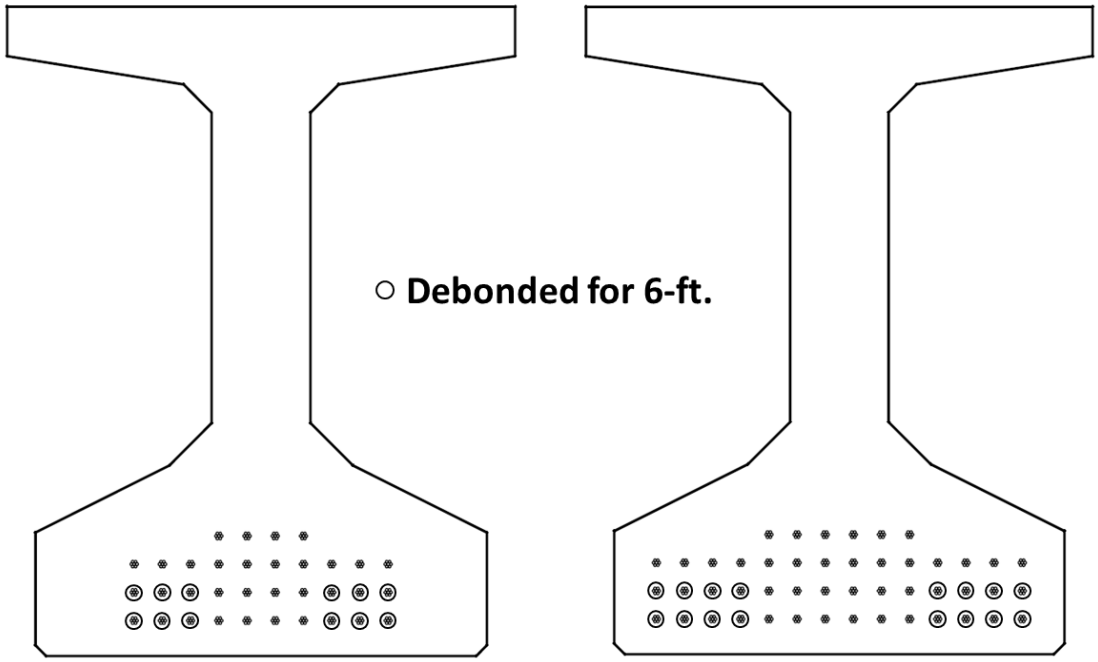

Figure 3-2: Strand Patterns

The girders' vertical shear design was done using the 2010 AASHTO LRFD General Procedure discussed in Section 2.2.2. The reinforcement followed TxDOT's standard shear reinforcement detail. The UTPCSDB analysis discussed in Section 2.2.1 has shown that a traditional shear failure is expected to occur when the ratio of V_u to V_n equals about 1.40. The impact of debonding on the shear strength was checked. Debonding decreased the girders' shear capacity at $a/2$ by 1.6% and 1.2%, respectively for the two specimens. The addition of the concrete, composite deck reduces f_{pc} and increases d_v. The large difference in the width of the deck compared to the width of the web meant that the girders' shear capacities increased by 20% and 18%, respectively. The shear reinforcement details are given in Appendix B.

The girders' horizontal shear design used the method presented in Section 2.2.3, which discuss the Horizontal Shear Evaluation Database (HSEDB). The HSEDB showed that a horizontal shear failure is expected to occur when the ratio of HS_u to HS_n equals

about 1.30. Preliminary analysis of the two specimens is presented below in Section 3.5. Next, the process of fabricating the girders is detailed and illustrated.

3.2.2 Girder Fabrication

The two Tx Girders for this research's experimental program were fabricated in-house, as opposed to being fabricated in a commercial precast plant. The high-precision, high-capacity prestressing bed at FSEL, shown in Figure 3-3, can carry up to 3200 kips of prestressing force. All strands are stressed simultaneously (gang-stressing) through a set of 4 hydraulic rams that push a 12 in. thick steel bulkhead, as shown in Figure 3-4. Worth noting is that a gradual release of strands by retracting hydraulic rams establishes a safe working environment as opposed to torch cutting.

Figure 3-3: Prestressing Bed at FSEL (O'Callaghan 2007)

Figure 3-4: Gang-Stressing Operations

Fabrication started with the installation of prestressing strands. First, each strand was run through the dead and live bulkheads. Once all the strands were in place, both the dead and live ends received chucks. Then, using a mono-strand jack, each strand was tensioned to about 2500 psi (less than 1 kip/strand) in order to remove the slack. Two top strands were added and also pulled to 2500 psi. The two top strands served as construction strands only and were never fully-stressed. The next step in fabrication was the installation of the internal instrumentation: strain gauges on select strands and the vibrating wire gauges. (More information about instrumentation is presented below in Section 3.4). Once the internal instrumentation was installed, the shear, bursting, and confinement reinforcement was tied in place following the TxDOT standard.

Once the specimen was ready for concrete placement, the casting operation was scheduled. In the morning on the day of concrete placement, strands were gang-stressed to a jacking stress of around 202.5 ksi. The total prestressing force was 1487 kips for both specimens. During stressing operations, the stress in the strands was monitored using the

strain gauges, the displacement/elongation was checked using linear voltage differential transducers, and the force was measured using pressure transducers.

Concrete placement, illustrated in Figure 3-5, took place later in the day. The concrete was placed using a 1 yd^3 bucket and consolidated using external and internal vibrators. After all concrete was placed, and while it was still in the plastic state, anchors were installed into the concrete for deck fabrication, as illustrated in Figure 3-6. (More information regarding the deck fabrication is provided below in Section 3.2.5.) The specimens were covered with plastic to prevent moisture and heat loss.

Figure 3-5: Placing Concrete for Tx46

Figure 3-6: Sample Deck Anchor and Installing Deck Anchors

The side forms were removed, and the strands were gradually released, once concrete strength reached the minimum strength required to satisfy AASHTO stress limits. After release, the strands were cut and the beam was moved into the testing position.

3.2.3 Temperature Match Curing

At commercial precast plants, a match curing system is used during the fabrication of the specimens to ensure that the concrete strength of the specimen and their concrete cylinders match. This system ensures that release will be done at the optimum time. At FSEL, a match curing system is also used. During the fabrication of each girder for this research, twenty concrete cylinders were made and match cured. Two temperature sensors, called thermocouples, were placed 8 ft from each end of the beam and 4 in. above the bottom. A third thermocouple was installed outside the beam for measurement of the ambient temperature. During concrete placement and in the following hours, the main computer controller system, shown in Figure 3-7, monitored temperature data. This controller also monitored the temperature of the attached concrete cylinders and adjusted their temperatures to match the incoming temperatures from the thermocouples. Figure 3-8 contains the match curing time-temperature plots for each beam's internal and ambient temperatures.

Figure 3-7: Match Curing System at FSEL

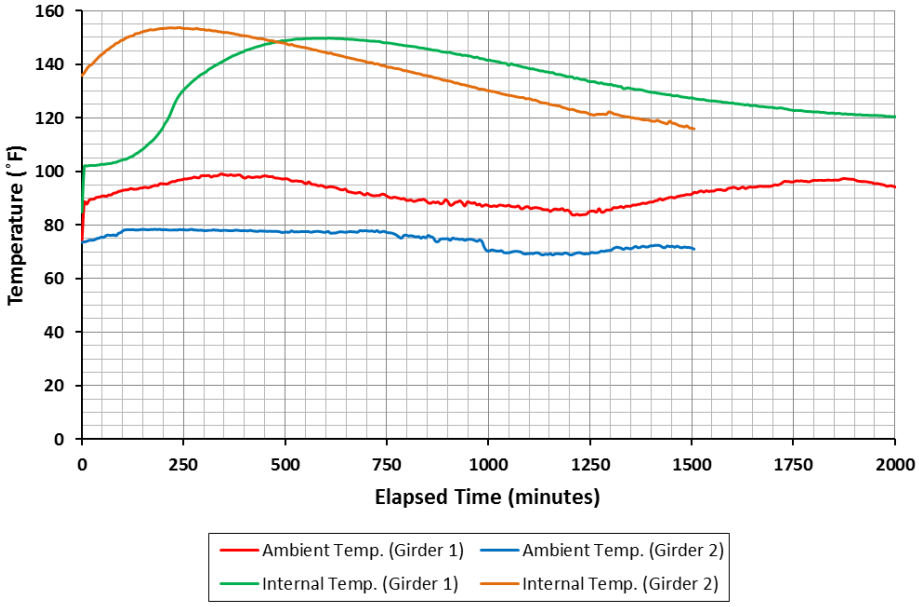

Figure 3-8: Match Curing Time-Temperature Plots

3.2.4 Deck Design

After each specimen was moved to the test setup, a concrete, composite deck was added to each specimen. The addition of a deck changes the location of the centroid and thus reduces f_{pc} but increases d_v. The deck was reinforced with four sheets of Grade 70 welded wire (7 x 6 – D19.7 x D19.7 with a width of 69 in., no side overhangs, and 187 in. long). The longitudinal lap splice between sheets was 18 in. Figure 3-9 illustrates reinforcement size and spacing for the composite deck.

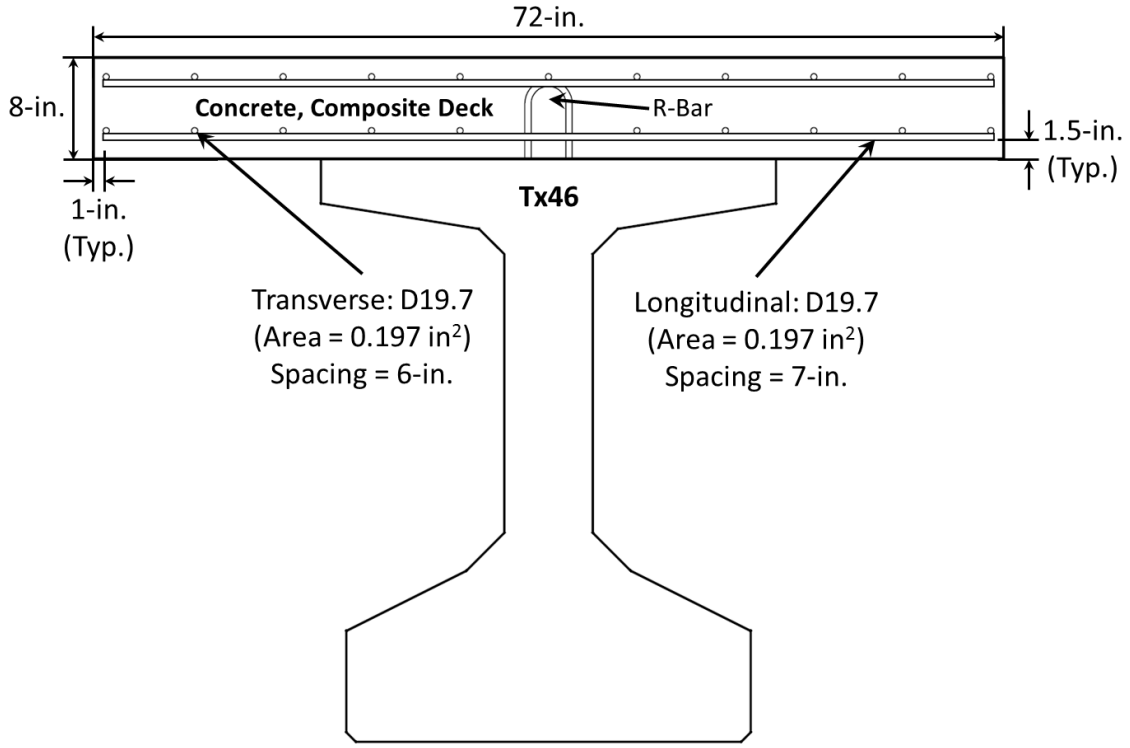

Figure 3-9: Concrete, Composite Deck Design

3.2.5 Deck Fabrication

To fabricate the composite deck, platforms with plywood sheathing and dimensional lumber joists were built and supported on bridge overhang brackets. The overhang brackets were hung using a coil rod threaded through the embedded anchors that were placed in the girder at the time of fabrication. Side forms and end forms were

installed on top of the wood platforms. Figure 3-10 illustrates the fabrication setup. Concrete was placed using a 1 yd^3 bucket and consolidated using internal vibrators. Figure 3-11 illustrates concrete placement. The deck cured at least one week before shear testing began. In order for test results to be analyzed, the actual, not the assumed, properties of the materials used in the foregoing fabrications needed to be determined. The following section discusses the specifications and actual properties of the materials used in the fabrication of the specimens for this research.

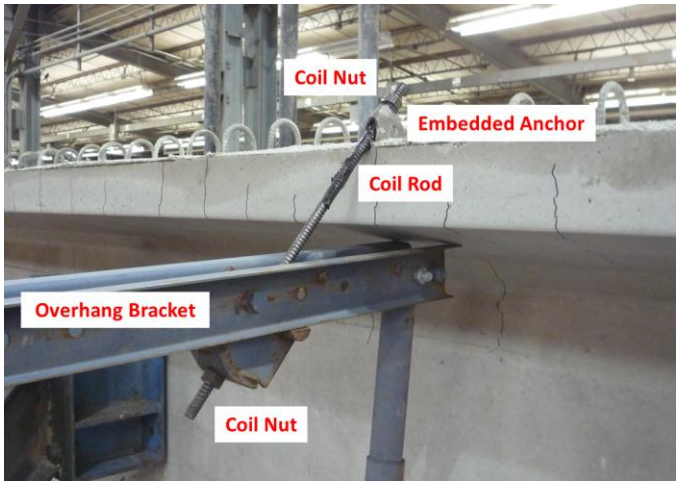

Figure 3-10: Deck Fabrication Setup

Figure 3-11: Placing Concrete for Deck

3.3 MATERIAL SPECIFICATIONS AND PROPERTIES

Prior to conducting large-scale testing, samples of the materials used in fabricating the specimens for the large-scale testing were themselves tested in order to determine certain engineering properties. The following subsections detail the results of this small-scale testing for the girder concrete, deck concrete, girder prestressing strands, and girder shear reinforcement.

3.3.1 Girder Concrete Specifications, Mixtures, and Strengths

Concrete for the Tx Girders was obtained from Coreslab Structures Texas, Inc. in Cedar Park, TX. Type III cement was specified, as was a compressive strength of 6.5 ksi after 16 hours and a slump of 7 in. The mix designs for the girders are in Table 3-2, and concrete strengths for the girders are listed in Table 3-3 (both tables follow Section 3.3.2, as they also contain data relevant to it).

3.3.2 Deck Concrete Specifications, Mixtures, and Strengths

The concrete for the deck was obtained from Texas Concrete in Round Rock, TX, and was specified to be around 10 ksi at 28 days and have a slump of 6 in. The mix designs for the decks are also in Table 3-2, and concrete strengths for the decks are also listed in Table 3-3.

Table 3-2: Concrete Mix Designs

Materials		Details	Quantity				Units
			Girder 1	Girder 2	Deck 1	Deck 2	
Slump		--	8.75	6.0	10.5	7.0	in.
Cementitious Materials		Type III Cement	591.1	592.4	--	--	lb/yd^3
		Type F Fly Ash	198.1	211.6	--	--	lb/yd^3
		Type I Cement	--	--	590.0	592.0	lb/yd^3
		Type C Fly Ash	--	--	205.0	200.0	lb/yd^3
Coarse Aggregate		Unknown Unknown	1376.0 --	1408.0 --	-- 1733.3	-- 1720.0	lb/yd^3
Fine Aggregate		Unknown Unknown	1557.3 --	1434.7 --	-- 710.0	-- 1416.3	lb/yd^3
Water		--	248.7	264.1	177.3	178.0	lb/yd^3
w/cm ratio		--	0.32	0.33	0.22	0.22	--
Admixtures	HRWR	Sika Viscocrete 2110	299	322	284	284	oz.
	Retarder	Sika Plastiment	246	249	94	94	

Table 3-3: Concrete Compressive Strengths from Cylinder Testing

	Girder 1	Girder 2	Deck 1	Deck 2	Units
Avg. Release Strength	5600	7500	--	--	psi
Avg. Test 1 Strength	5800	11200	7400	12300	psi
Avg. Test 2 Strength	5800	11200	7800	12300	psi

3.3.3 Prestressing Strand Properties

Girder prestressing strands for both specimens were low-relaxation but differed in strand diameter; the diameter was 0.6 in. and 0.5 in., respectively. All strand had a 270 ksi nominal ultimate strength. Two-samples from each spool of strand were tested by loading from 0 ksi to 202.5 ksi, and the stress-strain curves given in Figure 3-12 were generated. From the stress-strain curves, the average modulus was found to be 29300 ksi and 28000 ksi for the 0.6 in. and 0.5 in. strand, respectively. For more accurate results, these moduli were used in all calculations. The strength of the strand was taken as the nominal value.

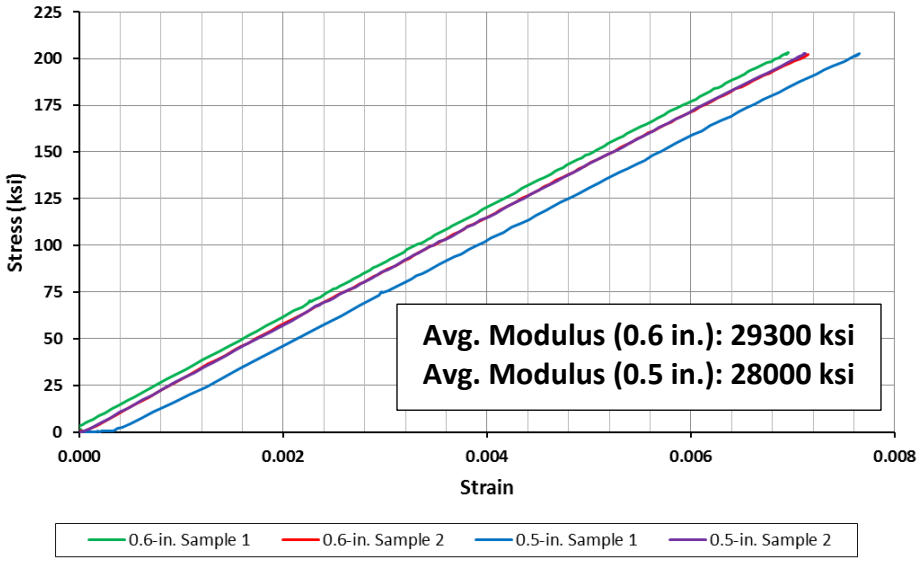

Figure 3-12: Stress-Strain Plot for 0.5 in. and 0.6 in. Diameter Prestressing Strand

3.3.4 Shear Reinforcement Properties

Girder shear reinforcement consisted of both conventional Grade 60 No. 4 deformed reinforcing bars (R-Bars) throughout the length for shear and Grade 60 No. 6 deformed reinforcing bars (S-Bars) in the end region for bursting and shear. All the reinforcement for both specimens was shipped together, so strengths are not reported for individual girders. The samples were tested using an extensometer to determine strain, though it was removed near fracture to keep it from being damaged. Figure 3-13 shows the stress-strain curves for rebar samples, though the ultimate strength is not reflected, due to the extensometer's removal. The ultimate load was recorded by the testing machine. Table 3-4 lists measured yield stresses and ultimate stresses.

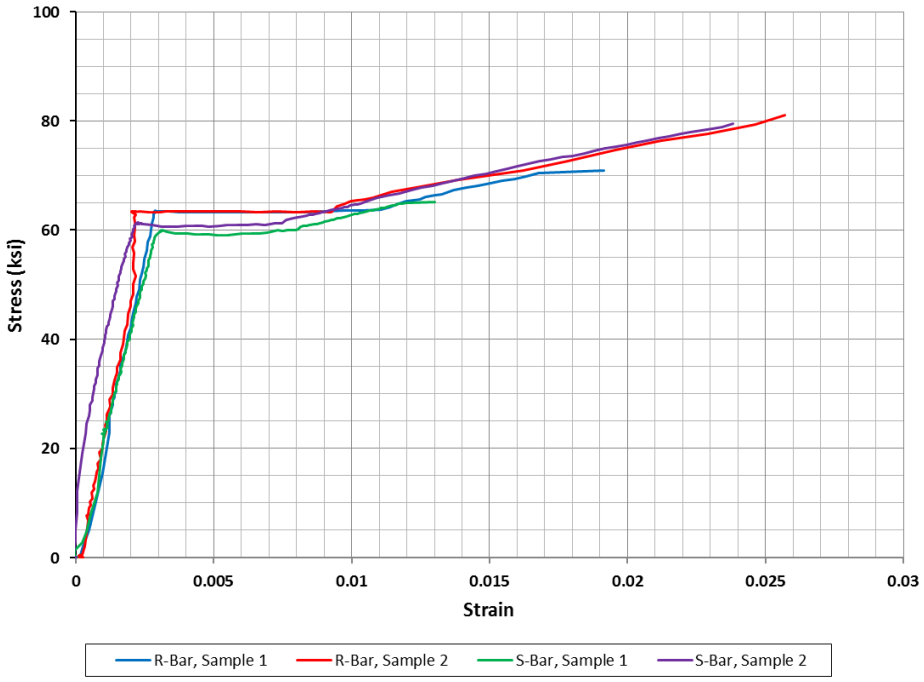

Figure 3-13: Stress-Strain Plot for Shear Reinforcement

Table 3-4: Summary of Measured Properties of Shear Reinforcement

	R-Bar, Sample 1	R-Bar, Sample 2	S-Bar, Sample 1	S-Bar, Sample 2	Units
Yield Stress	63.3	63.4	60.1	62.3	ksi
Ultimate Stress	100.2	100.1	102.3	101.9	ksi

3.4 INSTRUMENTATION FOR DATA DURING TESTING

As is evident from the preceding section, instrumentation was vital to this experimental program because anchorage failures are difficult to determine from visual inspection alone. The following instrumentation was placed inside and outside the specimens to collect the listed data during testing: strain gauges for stress in the prestressing strands, vibrating wire gauges for stress in the prestressing strands, linear voltage differential transducers for strand slip, linear voltage differential transducers for deflection, and load cell for load.

3.4.1 Strain Gauges for Stress in the Prestressing Strands

Strain gauges were installed on the bottom layer of prestressing strands to measure stress during gang-stressing and testing, though the gauges actually measure the difference in resistance, which is used to calculate strain, which is then, in turn, used to calculate stress. In case the strain gauges influenced the bond of the strands with the concrete, strain gauges were only included on one end of each specimen. This practice provided a behavioral comparison between the end with strain gauges and the end without strain gauges. Figure 3-14 illustrates the location of the strain gauges for each specimen. Relevant especially in Chapter 4's presentations of results, an identification system for each strain gauge was devised: <row # - column # - distance from the end face of the beam>.

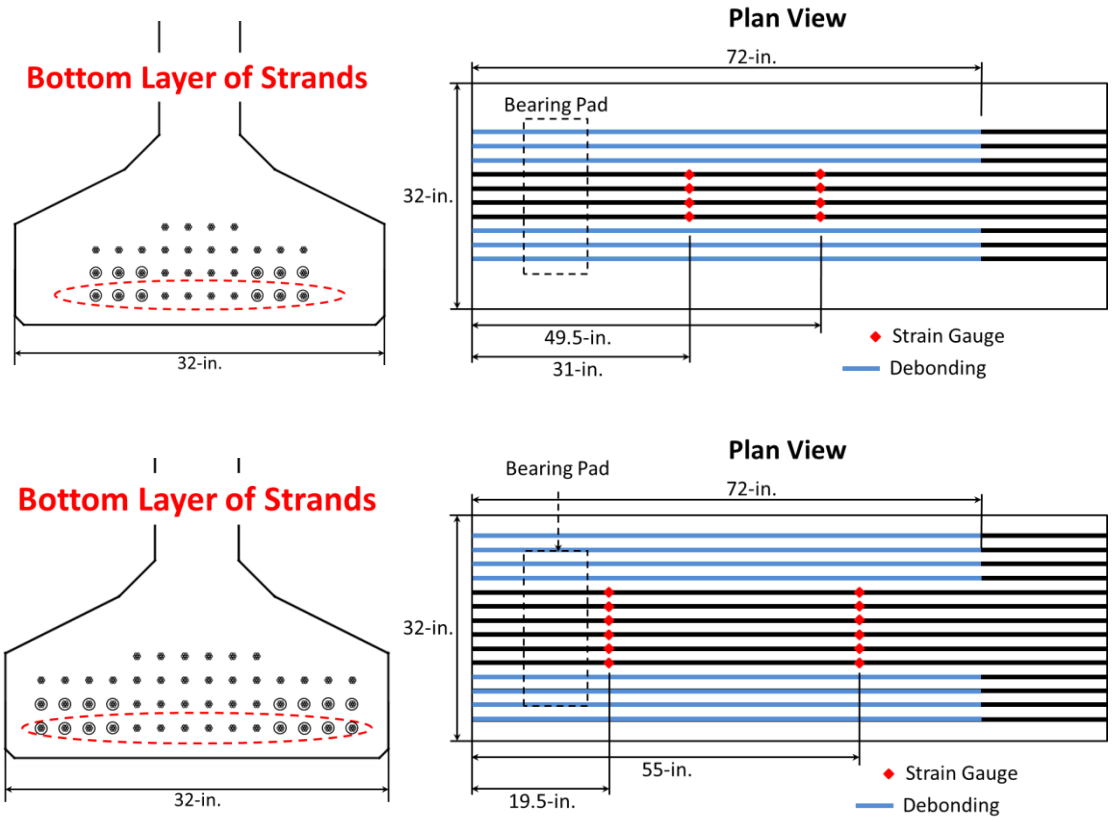

Figure 3-14: Strain Gauge Locations for Both Specimens

3.4.2 Vibrating Wire Gauges for Stress in the Prestressing Strands

In part for comparison, three vibrating wire strain gauges were installed in the second specimen. These gauges also served both to measure losses from release to the time of testing and to measure demand on the strands from external loads during testing. Vibrating wire gauges have a magnetic coil that excites a tensioned wire. The gauge indicates strain by measuring the change in frequency of the wire. As the applied strain increases, the resonant frequency of the wire increases. The wire is excited by a coil close to the wire. The gauges also account for temperature because that affects the frequency. For this specimen, temperature was fairly constant at the time readings were taken. Three gauges were installed at the centroid of the prestressing strands: at midspan and 5 ft from both ends. Figure 3-15 gives a photo of one gauge and the location of the vibrating wire gauges in both cross-section and plan.

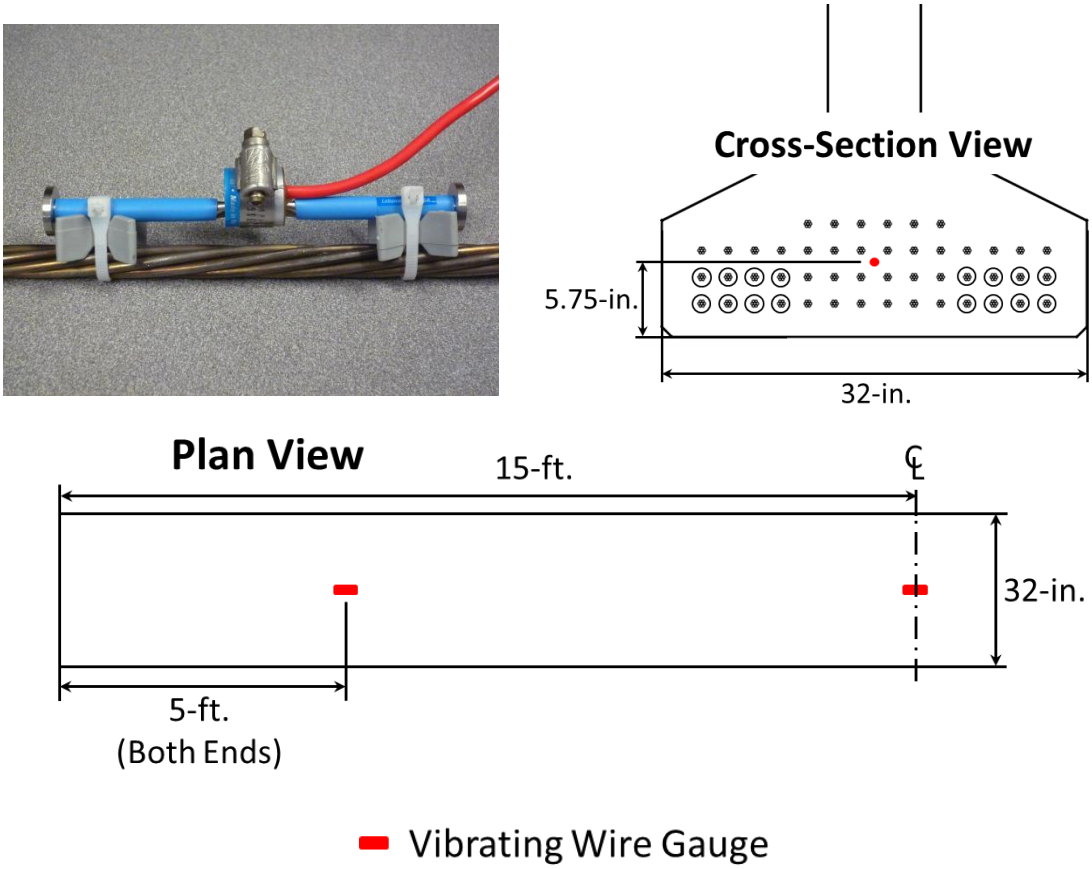

Figure 3-15: Vibrating Wire Gauges

3.4.3 Linear Voltage Differential Transducers for Strand Slip

Linear voltage differential transducers (LVDTs) were used to measure strand slip. Monitoring strand slip is the best way to identify anchorage failures, because, if anchorage is lost, the strand will slip into the beam. Slip was measured using a series of LVDTs attached to the strands where indicated in Figure 3-16. Relevant especially in Chapter 4's presentations of results, an identification system for each strand slip gauge was devised: <row # - column #>.

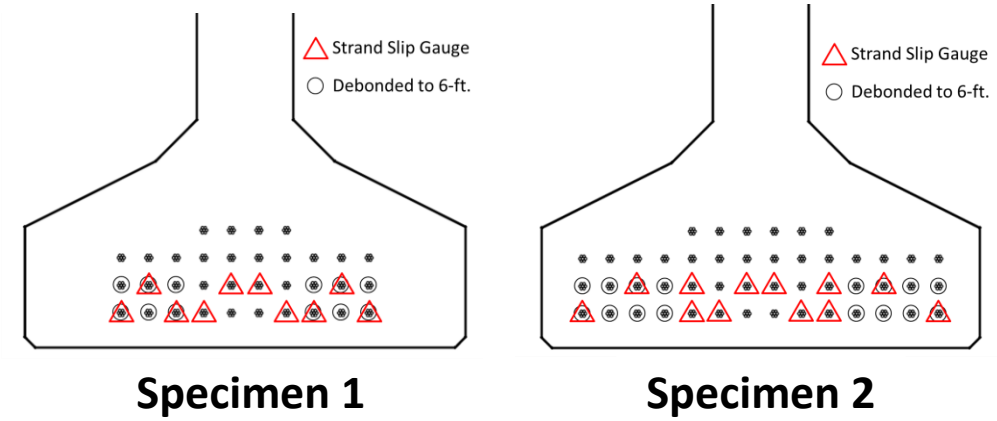

Figure 3-16: Strands Monitored for Slip

3.4.4 Linear Voltage Differential Transducers for Deflection

Three other LVDTs were used to measure deflection during testing. Two were positioned at the center of the two bearing pads, and the third was centered under the load point. Torsion of the specimens was not expected, so only one side of the specimen was monitored. The effective deflection under the load was obtained by subtracting the two deflection measurements at the supports (i.e., the rigid body movements were filtered out).

3.4.5 Load Cell for Load

A 1000 kip load cell was placed between the hydraulic ram and the deck, centered over the web, in order to measure the applied load during testing. Figure 3-17 shows the load cell in position. Using the effective deflection mentioned in the preceding section and the applied load data, the load-deflection plots were obtained and are presented in Chapter 4. All the foregoing instrumentation for data collection during testing were critical as the tests themselves were conducted according to the procedure that follows below in Section 3.6.2. First, discussion of preliminary analysis of the test specimens is relevant because the results of the preliminary analysis are necessary to know what to expect in the testing itself.

Figure 3-17: 1,000,000 lb Load Cell

3.5 TEST SPECIMENS – PRELIMINARY ANALYSIS

Prior to testing any of the specimens, preliminary analysis of the failure mode capacities, the anticipated demands at anchorage failure, and the anchorage failure expectations was conducted. This section details these preliminary analyses. The four tests are identified as follows: 1-0.6-N, 1-0.6-S, 2-0.5-N, and 2-0.5-S, where "1" or "2" is the first or second specimen, "0.6" or "0.5" indicates the strand diameter, and "N" or "S" indicates the end being tested.

Using the material properties and methods detailed above in Section 3.3, the capacities of each failure mode were calculated: anchorage, vertical shear, horizontal shear, and flexure. The anchorage capacity was calculated at 19.5 in. from the end of the beam, just in front of the bearing pad. The vertical shear capacity was calculated at half of the shear span, which varied between tests but was around 6 ft from the end of the beam. The horizontal shear capacity was calculated at multiple points along the beam up to the ultimate evaluation point, which also varied between tests. Finally, the flexural

capacity was calculated at two points, the termination of debonding (6 ft) and under the load. The capacities are listed in Table 3-5.

Table 3-5: Test Capacities

Test ID	T_n kips	V_n kips	HS_n kips	M_n kip-ft	M_n kip-ft
1-0.6-N	427.3	440.6	679.6	4944.5	7688.2
1-0.6-S	427.3	440.6	633.2	4944.5	7688.2
1-0.5-N	528.3	492.9	644.1	4928.9	7464.2
1-0.5-S	528.3	492.9	644.1	4928.9	7464.2
	19.5 in.	$a/2$	UEP	6 ft	a

In addition to the capacities, the applied load at which an anchorage failure was expected to occur ($T_{max}/T_n = 1.00$) was found. The demand due to that applied load was then calculated for all the failure modes: shear, horizontal shear, and flexure; the pre-test demands are in Table 3-6. For each of those same failure modes at that same applied load, the ratio of demand-to-capacity was then found; the pre-test ratios are in

Table 3-7. After finding the ratios, a histogram, Figure 3-18, was made to illustrate the amount of additional capacity if an anchorage failure were not to occur at a ratio of 1.00.

Table 3-6: Pre-Test Demands at Expected Failure Load

Test ID	T_u kips	V_u kips	HS_u kips	M_u kip-ft	M_u kip-ft	$P_{applied}$ kips
1-0.6-N	427.0	348.1	545.1	1844.4	3138.8	522.0
1-0.6-S	427.0	341.4	498.7	1722.7	3216.1	612.9
1-0.5-N	527.7	388.3	568.1	1956.9	3657.1	698.4
1-0.5-S	528.7	388.7	568.8	1959.1	3661.4	699.2
	19.5 in.	$a/2$	UEP	6 ft	a	a

Table 3-7: Pre-Test Ratio of Demand-to-Capacity at Expected Failure Load

Test ID	T_u kips	V_u kips	HS_u kips	M_u kip-ft	M_u kip-ft	$P_{applied}$ kips
1-0.6-N	1.00	0.79	0.80	0.37	0.41	522.0
1-0.6-S	1.00	0.77	0.79	0.35	0.42	612.9
1-0.5-N	1.00	0.79	0.88	0.40	0.49	698.4
1-0.5-S	1.00	0.79	0.88	0.40	0.49	699.2
	19.5 in.	$a/2$	UEP	6 ft	a	a

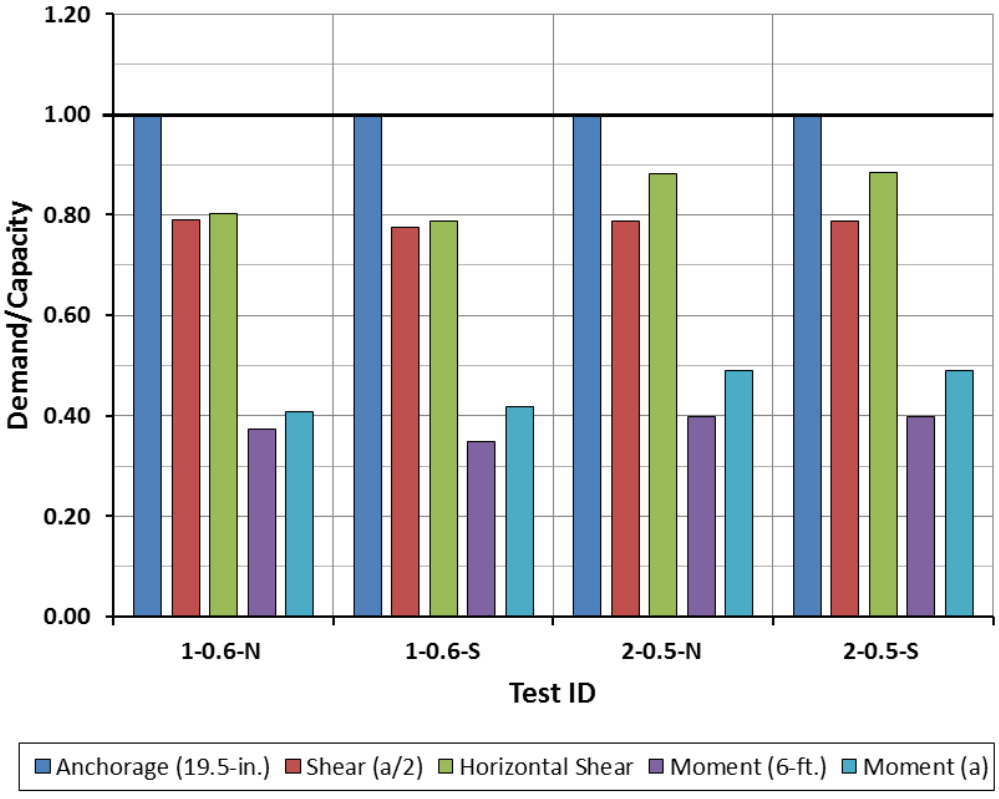

Figure 3-18: Pre-Test Histogram

As stated earlier, each specimen was designed to fail in anchorage. From the above histogram, if the specimen did not fail in anchorage, the next most likely failure mode was shear or horizontal shear. The demand on the longitudinal reinforcement at 95% of the shear and horizontal shear capacity was calculated and compared to the longitudinal reinforcements' anchorage capacity. This comparison, given in Table 3-8 demonstrates that if the anchorage equation is correct, an anchorage failure (and thus strand slip) should occur before a shear or horizontal shear failure. With the preliminary analysis complete, the shear testing commenced.

Table 3-8: Anchorage Failure Expectations

Test ID	T_n kips	$0.95V_n$ kips	T_{max} kips	$\frac{T_{max}}{T_n}$	$0.95HS_n$ kips	T_{max} kips	$\frac{T_{max}}{T_n}$
1-0.6-N	427.3	418.6	936.9	**2.19**	645.6	751.2	**1.76**
1-0.6-S	427.3	418.6	976.9	**2.29**	601.5	413.8	**0.97**
2-0.5-N	528.3	468.3	967.0	**1.83**	611.9	592.1	**1.12**
2-0.5-S	528.3	468.3	967.0	**1.83**	611.9	592.1	**1.12**

3.6 SHEAR TESTING

All of the experimental objectives depended on shear testing, the procedure for which is described in this section. Both specimens were tested in shear. The shear tests were conducted by loading through the web of the girder using a 2000 kip hydraulic ram that reacted on a steel spreader beam, which in turn transferred load to two smaller steel beams, photographed in Figure 3-19 and schematically diagramed in Figure 3-20. The smaller steel beams transferred load to six 3.5 in. diameter rods bolted to the underside of the strong floor. The test frame was designed to resist an applied load of 4000 kips. Each specimen was tested twice, once on each end. After the first test, the specimen was turned around in the test setup. The following subsections detail the shear testing setup and procedure.

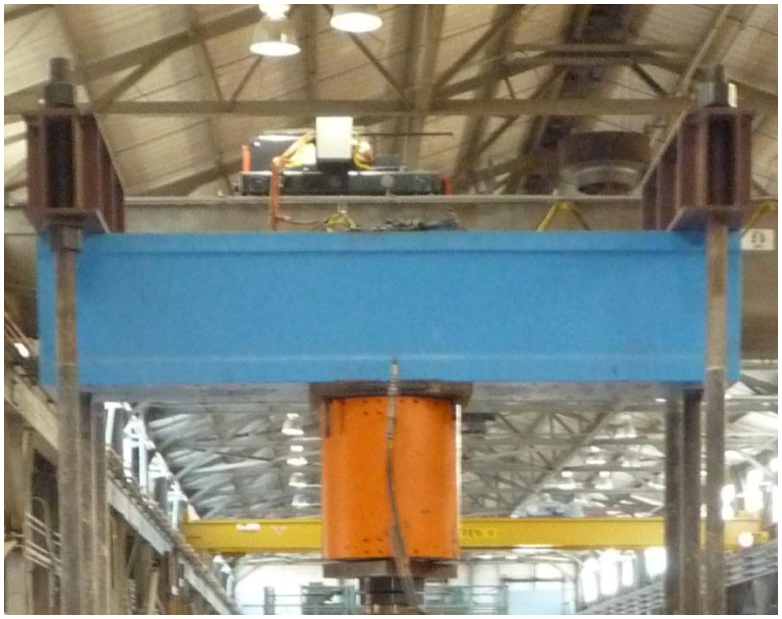

Figure 3-19: Load Reaction Frame

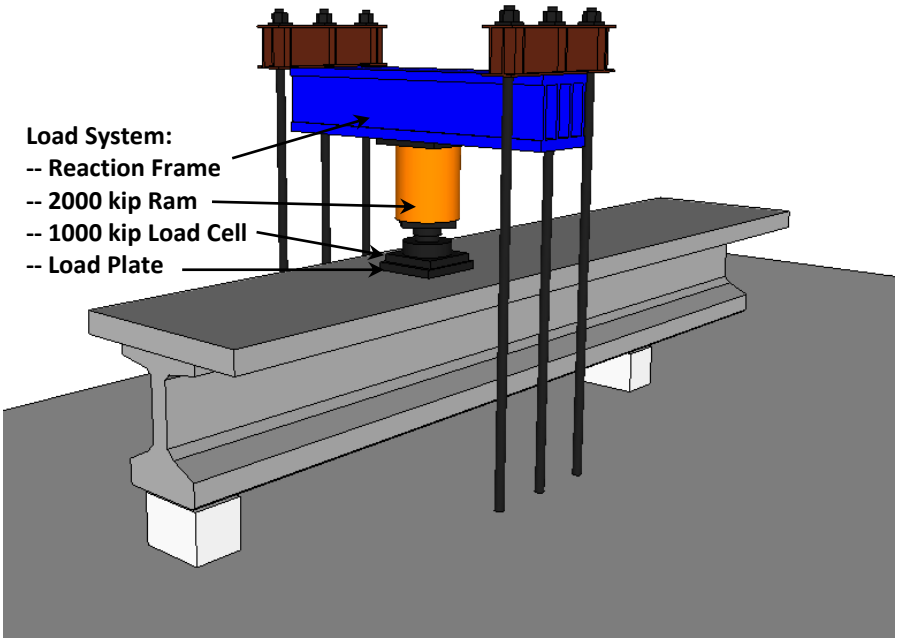

Figure 3-20: Rendering of Reaction Frame

3.6.1 Shear Testing Setup

For this shear testing, various considerations dictated how the beam was positioned. The specimen being tested was supported on two composite, elastomeric bearing pads (9 in. long, 21 in. wide, and 2.5 in. thick), positioned differently depending on the end of the beam and other parameters of the test. The centerline of the bearing pad on the end of consideration (Overhang 1) was located one foot from the end of the specimen. The location of the centerline of the other bearing pad measured from the end of the beam (Overhang 2) varied. The shear span was defined as the distance from the centerline of the bearing pad on the end of consideration to the center of the load point, and back span was defined as the span less the shear span. The various measurements to define the test configuration are illustrated in Figure 3-21, and their values are given in Table 3-9. Table 3-9 also indicates the shear span-to-depth ratio, which was chosen to avoid both deep beam behavior and a flexure-dominated test. Using the UTPCSDB, a shear span-to-depth ratio around 2.5 was found to be adequate for shear testing (Nakamura 2011). With the shear testing set-up described, attention can be given to the shear testing procedure.

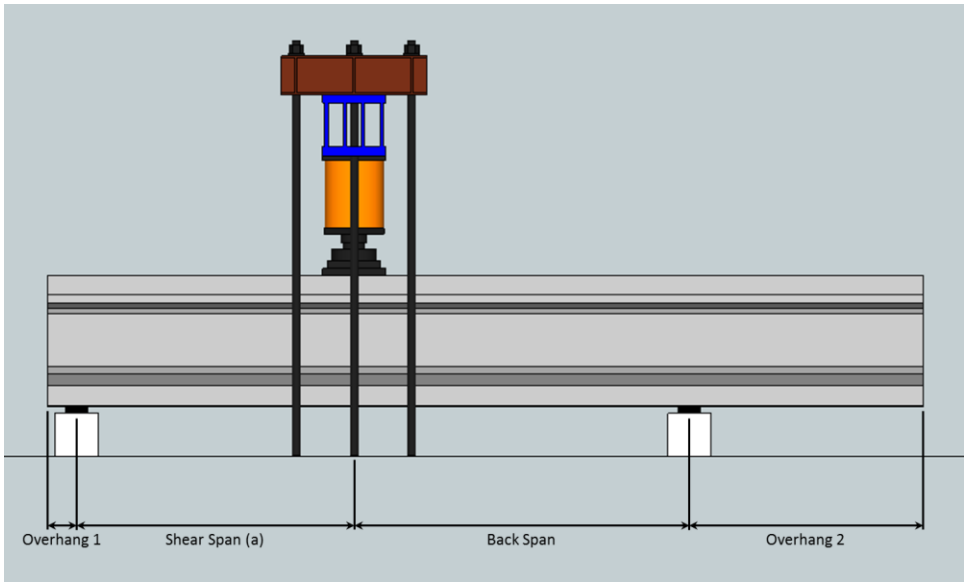

Figure 3-21: Test Configuration Definitions

Table 3-9: Shear Testing Configurations

	1-0.6-N	1-0.6-S	2-0.5-N	2-0.5-S	
Overhang 1	1	1	1	1	ft
Shear Span	10	9.5	9.5	9.5	ft
Back Span	18	11.5	11.5	11.5	ft
Overhang 2	1	8	8	8	ft
d_v	43.40	43.40	43.43	43.43	in.
a/d	2.76	2.63	2.62	2.62	--

3.6.2 Shear Testing Procedure

This section reviews what procedure was followed during testing. Before the first test of each specimen started, initial bursting cracks were marked. In the case of the second test on the same specimen, cracks formed during the first test were documented before starting the second test. To start the tests, the specimens were loaded monotonically to 100 kips. Subsequently, load was added in increments of 50 kips; however, in the vicinity of the load causing web-shear cracking and flexure-shear cracking, load was added in increments of 25 kips to allow for close inspection of the specimen. Once the specimens lost stiffness based on the slope of the load-deflection curve, failure was considered to be imminent, and the specimens were loaded to failure. Failure was defined as a drop of approximately 30% of the load being carried. Data from the instrumentation were monitored and recorded every second during the tests. In addition to those data the instrumentation were collecting, several occurrences of the testing needed to be recorded by hand: the web-shear cracking load, the flexure-shear cracking load, the width of the cracks, and the failure mode (web crushing, bond slip, horizontal shear, etc.).

3.7 SUMMARY

The experimental program is one half of this research and was designed to accomplish four objectives: (i) to investigate the impact of debonding on the anchorage of the prestressing strands, (ii) to investigate the impact of debonding on the girder's shear capacity, (iii) to determine whether or not the assumed anchorage resistance model applied to modern prestressed concrete bridge girders, and (iv) to determine what factors contribute to anchorage capacity. To accomplish the objectives, two Tx46s with concrete, composite decks were designed to fail in anchorage and fabricated at FSEL. The girders were instrumented for data collection and this data was used to analyze the results of the shear testing that culminated the experimental program of this research. Those results are presented next in Chapter 4.

CHAPTER 4: EXPERIMENTAL RESULTS & ANALYSIS

The details of the experimental program were presented in Chapter 3. This chapter, Chapter 4, discusses the results and analysis of the experimental program. The first section briefly reviews the experimental program. The second section gives the results of each test with a summary of the outcome and discussion using crack maps, plots, and photographs. The third section presents the analysis of specific aspects of the data. Together, the results and analysis of the experimental program begin to answer several questions regarding the current method for predicting anchorage failure and work toward a better understanding of anchorage-related issues in concert with the analytical program in Chapter 5.

4.1 EXPERIMENTAL PROGRAM SUMMARY

As discussed in Chapter 3, two full-scale Tx46 prestressed concrete bridge girders were fabricated at the Phil M. Ferguson Structural Engineering Laboratory. The 30 ft long Tx46 girders were topped with a concrete, composite deck that was 8 in. thick and 6 ft wide. Both ends of the two girders were instrumented and tested. The first two tests (1-0.6-N and 1-0.6-S) were conducted on the Tx46 with 0.6 in. diameter prestressing strand. The second two tests (2-0.5-N and 2-0.5-S) were conducted on the Tx46 with 0.5 in. diameter prestressing strand. The test configurations, including the shear spans and the shear span-to-depth ratios, were summarized in Section 3.6.1. Throughout testing, data from the instrumentation (Section 3.4) were monitored and recorded. During testing, the prestressed concrete bridge girders were loaded to failure, defined as a drop of approximately 30% of the peak load.

Crack mapping for each test was important for visually communicating the failure progression during testing. Prior to testing, bursting cracks formed during release of the prestressing were marked and documented. Cracks formed during testing were mapped in increments to show the progression of crack formation. For the second test on the same

specimen, the cracks from the previous shear test were marked and documented, and, at the conclusion of the second test, all cracks were marked and documented.

4.2 EXPERIMENTAL PROGRAM TESTING RESULTS

The results of the four shear tests are summarized in the first four of the following five subsections; each gives the results with a summary of the outcome and discussion using crack maps, plots, and photographs. The plots show the data recorded from the instrumentation (load-deflection, strand slip, and demand on the prestressing strands). The final subsection summarizes the post-test demand at the maximum applied load for each failure mode (this is a direct comparison of the preliminary analysis presented in Section 3.5).

4.2.1 Test 1-0.6-N

Test 1-0.6-N had a shear span of 10 ft (a/d = 2.76). The first web-shear cracking in the end region occurred at an applied load of 250 kips (V = 161 kips). At an applied load of 600 kips (V = 386 kips), a flexure-shear crack formed on both sides of the girder 6 ft from the end of the beam. Flexure-shear cracks are expected to occur in regions where moment is semi-large, and these flexure-shear cracks formed exactly where expected. After surpassing by 200 kips the applied load expected to cause an anchorage failure, localized spalling and crushing occurred in the flanges over the bearing pad because a few confinement reinforcing bars wandered during the girder's concrete placement. Loading continued, until at an applied load of 865 kips (V = 569 kips), the region near the flexure-shear cracks began forming a plastic hinge. The loading was stopped to prevent significant damage from affecting the second test on that specimen. The hinging is demonstrated in the flattening of the load-deflection curve above about 800 kips (Figure 4-1). Even with some crushing and spalling in the flange over the bearing pad, this test failed at a load significantly higher than that which was expected to cause an anchorage failure (P = 522.0 kips). The data from the instrumentation associated

with this test was not affected by the damage from the crushing and spalling of the flange over the bearing pad.

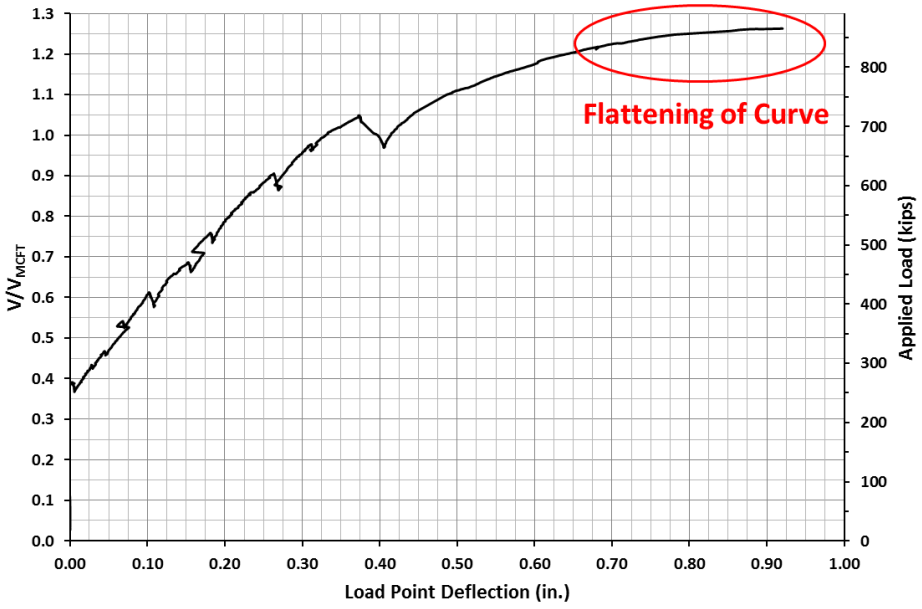

Figure 4-1: Load-Deflection Curve for Test 1-0.6-N

Because test 1-0.6-N was the first on this specimen, only bursting cracks were present at the start of the test. Those cracks and the cracks formed during testing are mapped in Figure 4-2. Cracks drawn in black represent bursting cracks formed at prestress transfer, and cracks drawn in red represent cracks formed during the testing of the north end of the specimen. Solid red colored portions represent areas of concrete crushing and/or spalling. Of particular note is that minimal cracking in the bottom flange in front of the bearing pad was observed.

Each crack map contains specific information for that increment of loading. For example, at an applied load of 400 kips, the cracks formed on the east and the west sides of the beam, as well as the cracks formed on the north end face of the beam, are drawn. At this load stage, the applied shear (V) is given, along with the ratio of the applied shear to the shear capacity, using the 2010 AASHTO LRFD General Procedure (V_{MCFT}). The maximum crack width on the east and the west side is given at this load stage as well.

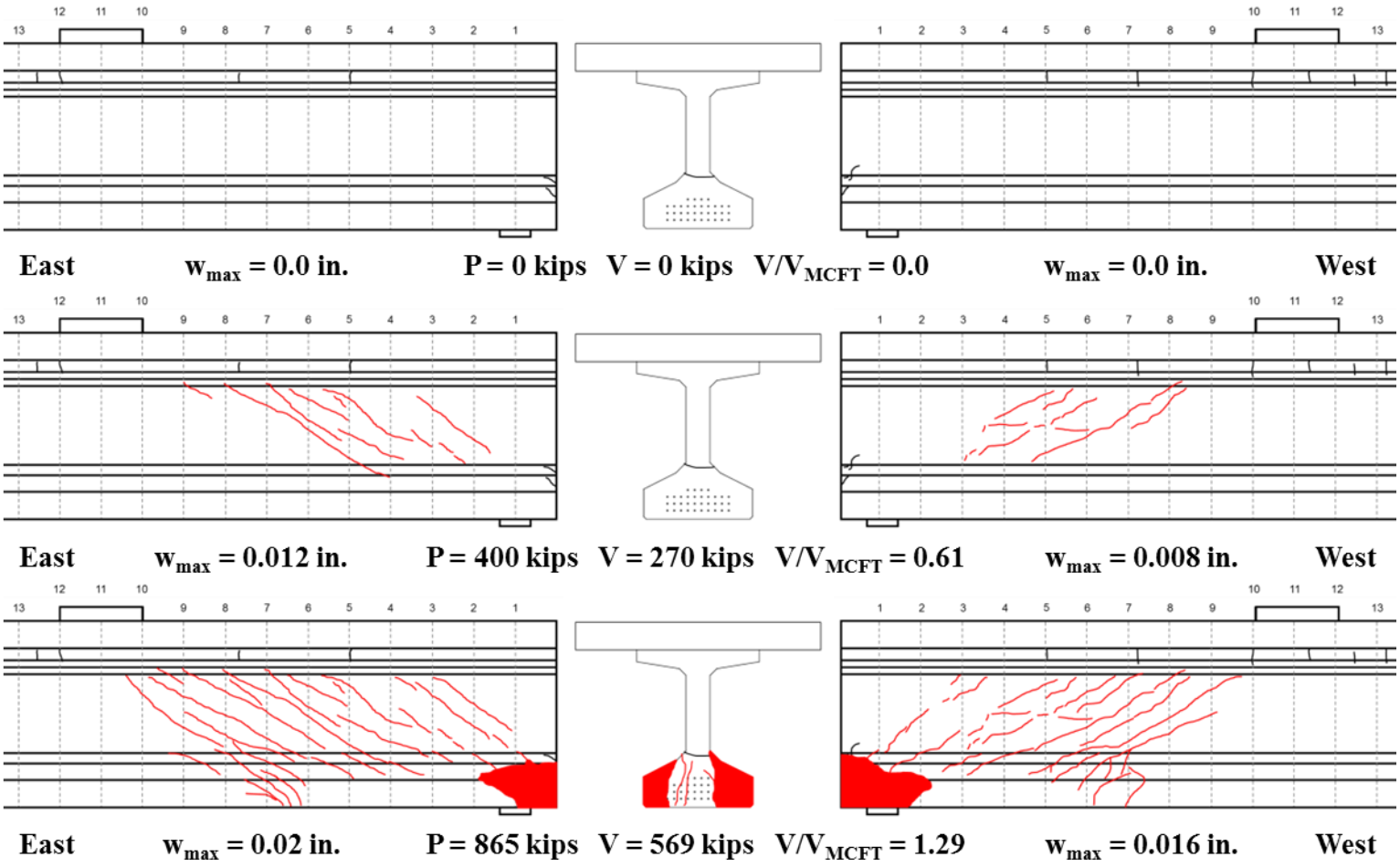

Figure 4-2: Crack Maps for Test 1-0.6-N

Because anchorage failures are difficult to identify visually, strands were monitored for slip during all testing. Strand slip for the fully-bonded strands in rows one and two is plotted in Figure 4-3. These slip values are quite small; no appreciable strand slip was observed.

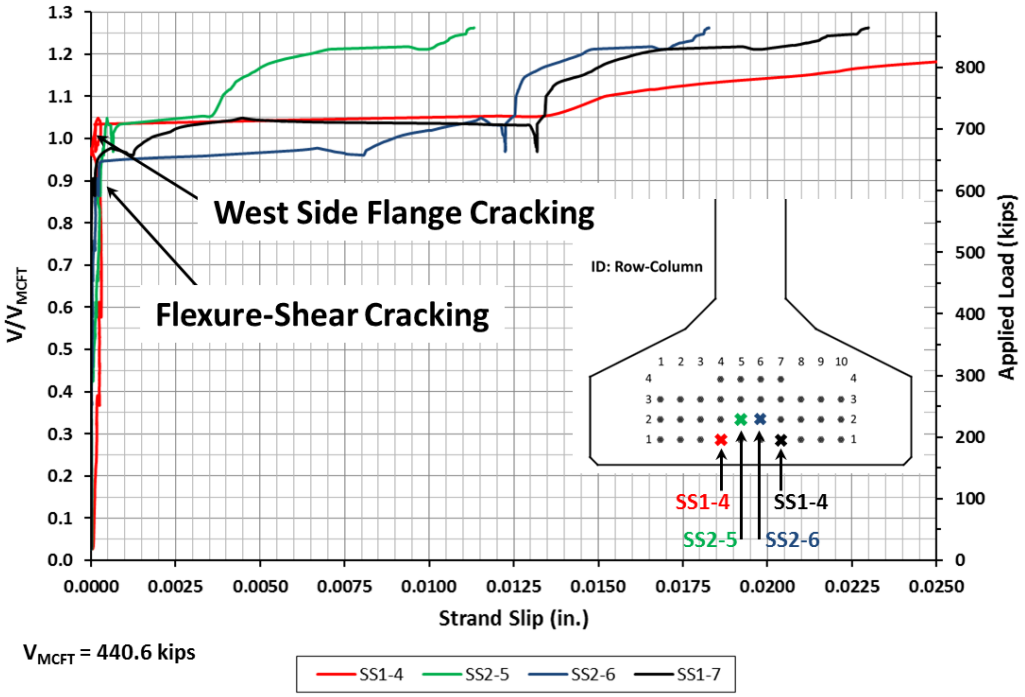

Figure 4-3: Strand Slip Plot for Test 1-0.6-N

The strain in the strands due to applied load was monitored during test 1-0.6-N (and test 2-0.5-N). Figure 4-4 and Figure 4-5 plot the strain in the fully-bonded strands 31 in. and 49.5 in. from the end of the beam. These strains, all quite small for this test, are used in Section 4.3 for analysis.

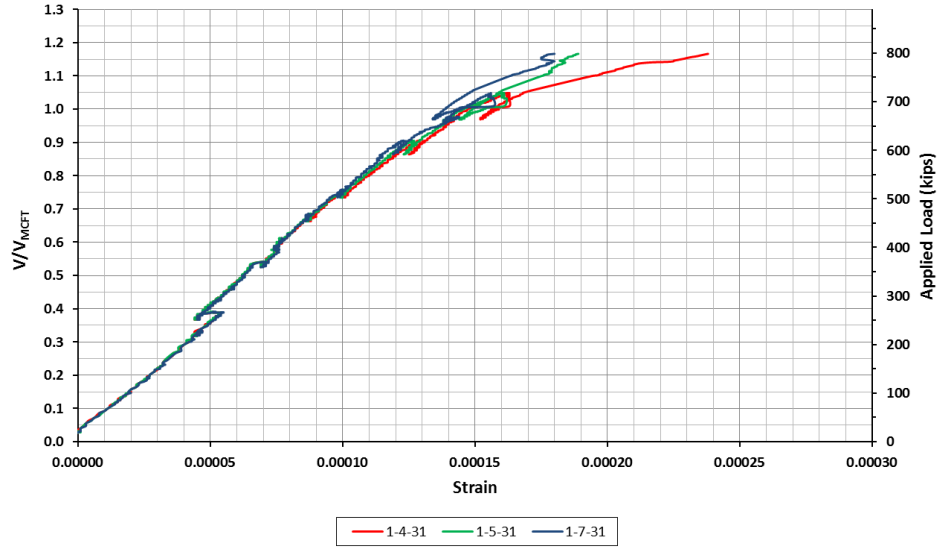

Figure 4-4: Strand Strain Due to Applied Load - 31 in. Series (Test 1-0.6-N)

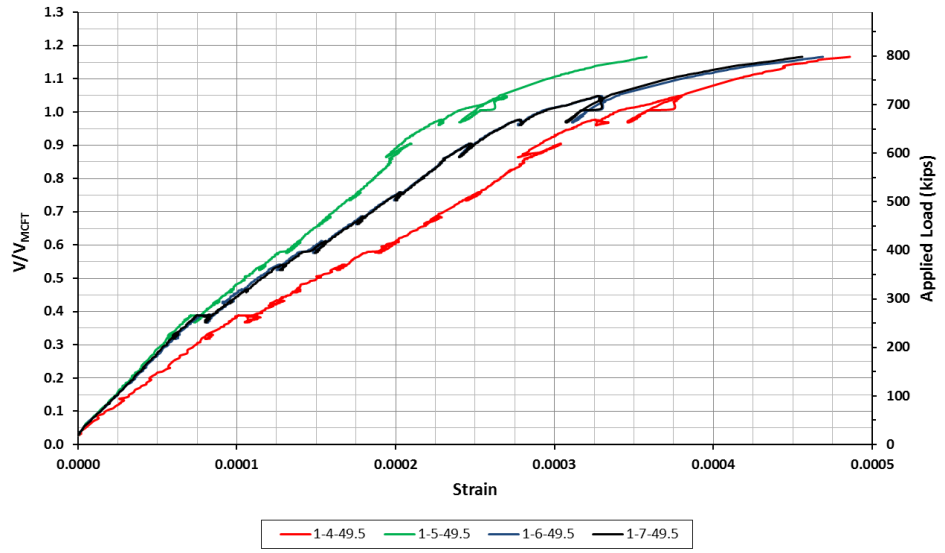

Figure 4-5: Strand Strain Due to Applied Load - 49.5 in. Series (Test 1-0.6-N)

Test 1-0.6-N failed in the formation of a plastic hinge. The strand slip and strand strain measurements indicate that the demand on the strands was minimal, despite the maximum applied load's greatly exceeding the applied load that was expected to cause an anchorage failure. Compared to the results of the AASHTO-type girders presented in

Chapter 2, the Tx46s experienced minimal crack propagation into the bottom flange. The damage from test 1-0.6-N was positioned such that it did not affect the south end test, the results of which are summarized in the next subsection, including a different failure mode.

4.2.2 Test 1-0.6-S

Test 1-0.6-S had a shear span of 9.5 ft (a/d = 2.63). The first web-shear cracking in the end region occurred at an applied load of 175 kips (V = 96 kips). At an applied load of 675 kips (V = 370 kips), a flexure-shear crack formed on both sides of the girder 6 ft from the end of the beam. As loading continued, additional web-shear and flexure-shear cracks formed. At an applied load of 900 kips (V = 493 kips), signs of horizontal shear were observed and can be seen in the photograph in Figure 4-6. Loading continued until the girder failed in horizontal shear at an applied load of 967 kips (V = 535 kips). The major failure cracks are highlighted in Figure 4-7. The load-deflection curve is plotted in Figure 4-8.

Figure 4-6: Signs of Horizontal Shear (Test 1-0.6-S) at 900 kips

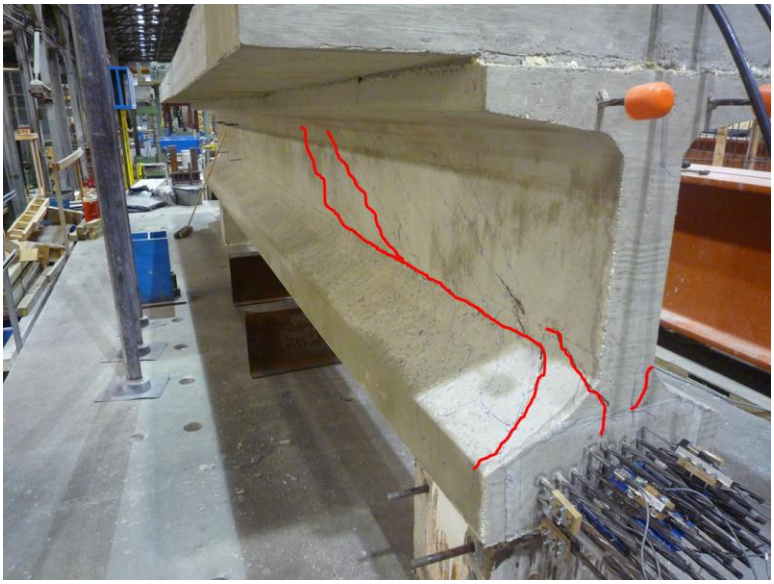

Figure 4-7: Horizontal Shear Failure (Test 1-0.6-S)

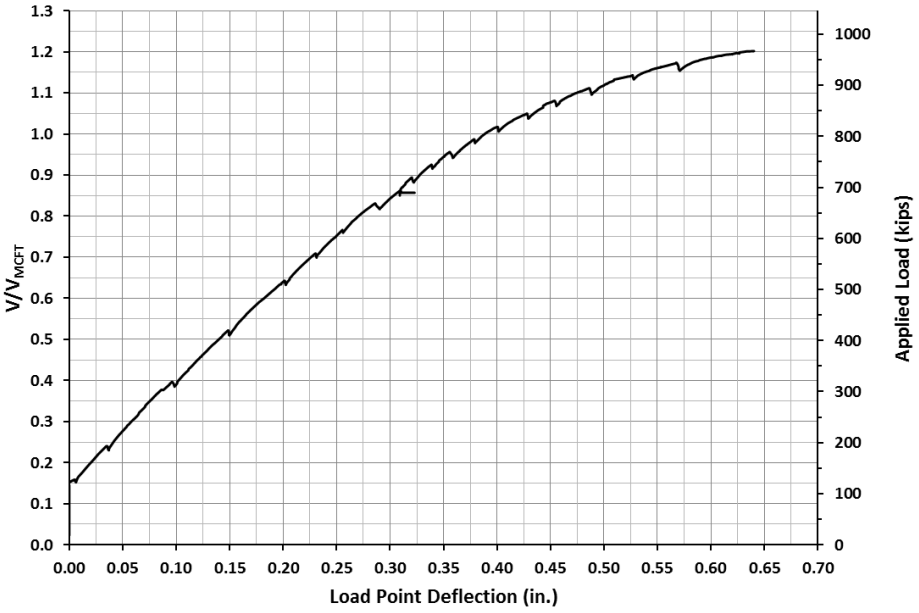

Figure 4-8: Load-Deflection Curve for Test 1-0.6-S

The shear span crack maps for test 1-0.6-S are located in Figure 4-9. Cracks drawn in blue represent cracks formed during the testing of the south end.

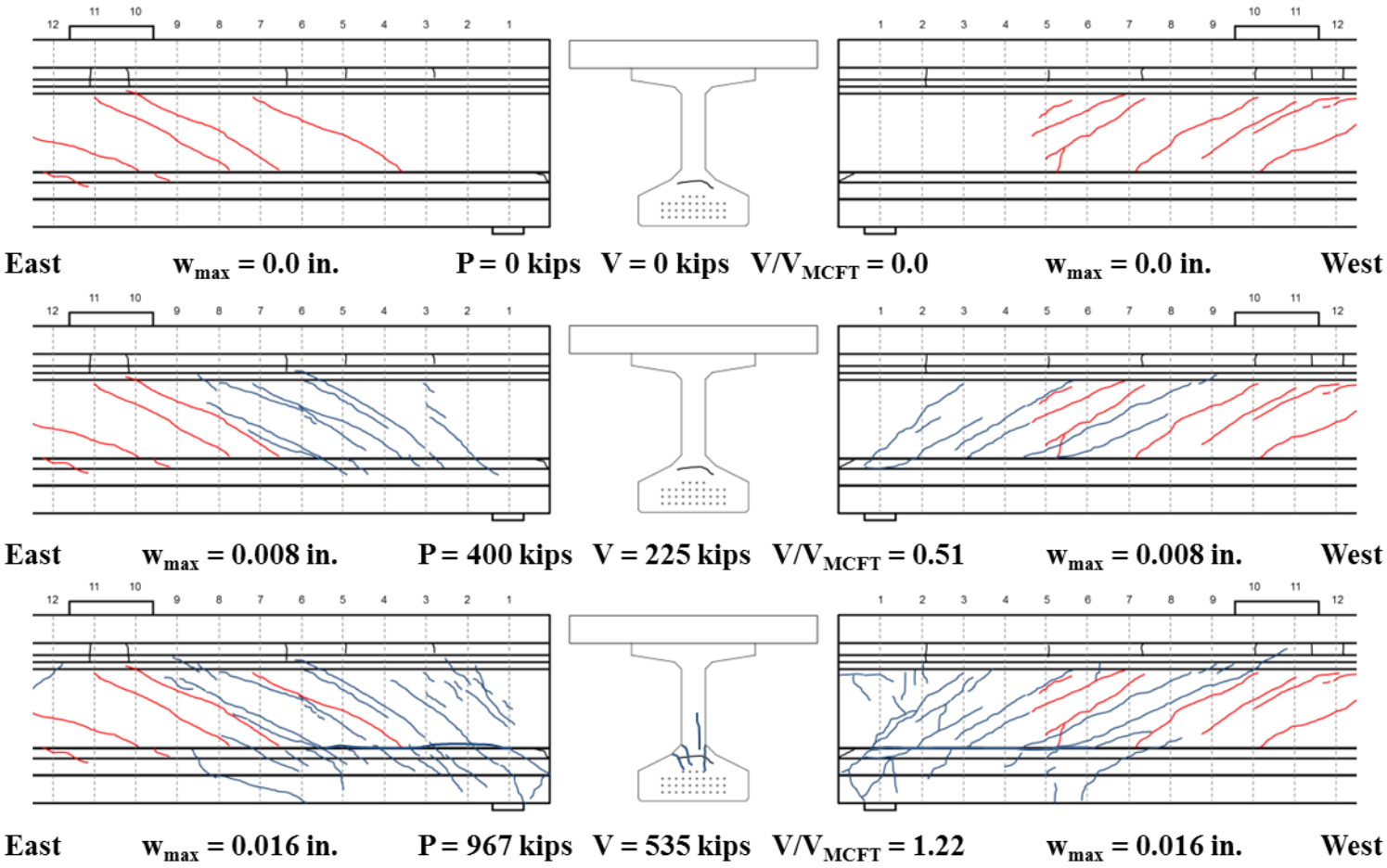

Figure 4-9: Crack Maps for Test 1-0.6-S

Strand slip was again monitored, and the slip values for the fully-bonded strands in rows one and two are plotted in Figure 4-10. These slip values are again quite small; no appreciable strand slip was observed.

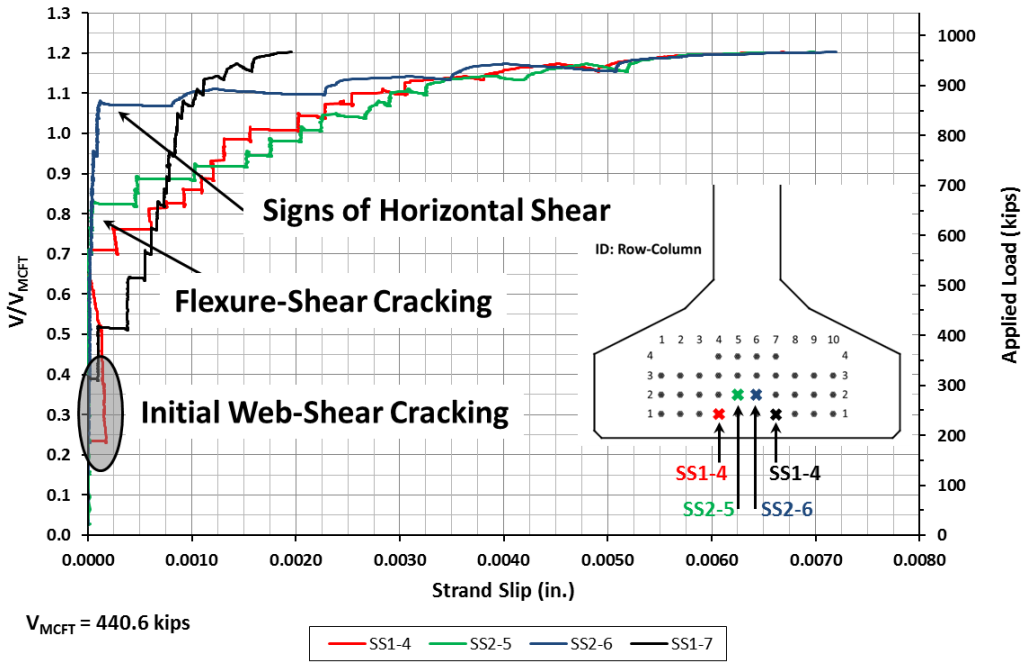

Figure 4-10: Strand Slip Plot for Test 1-0.6-S

Test 1-0.6-S failed in horizontal shear. As with the north end test, the strand slip measurements indicate that the demand on the strands was minimal, despite the applied load's greatly exceeding that which was expected to cause an anchorage failure. The results from specimen one indicate that the absence of flexure, shear, or flexure-shear cracks crossing the strands near the end of the beam precludes an anchorage failure. For Tx Girders, the critical crack is more likely to occur at the web-flange interface (horizontal shear). Such results were also expected in the second specimen, which differed only in the diameter of the prestressing strands used. The next subsection gives the results of the first test on that second specimen.

4.2.3 Test 2-0.5-N

Test 2-0.5-N had a shear span of 9.5 ft (a/d = 2.63). The first web-shear cracking in the end region occurred at an applied load of 325 kips (V = 178 kips). At an applied load of 700 kips (V = 383 kips), a flexure-shear crack formed on both sides of the girder 6 ft from the end of the beam. As loading continued, additional web-shear and flexure-shear cracks formed. At an applied load of 1100 kips (V = 602 kips), the flexure-shear cracks widened and the load-deflection curve flattened. At this point, more cracking was observed in the bottom flange than in previous tests (compare crack maps in Figure 4-2 with those in Figure 4-14). With hope of an anchorage failure being imminent, loading was continued. Finally, at an applied load of 1128 kips (V = 618 kips) the girder failed in web-crushing in the back span (Figure 4-11 and Figure 4-12). The load-deflection curve is plotted in Figure 4-13, and the shear span crack maps for test 2-0.5-N are located in Figure 4-14.

Figure 4-11: Back Span Web Crushing (Test 2-0.5-N)

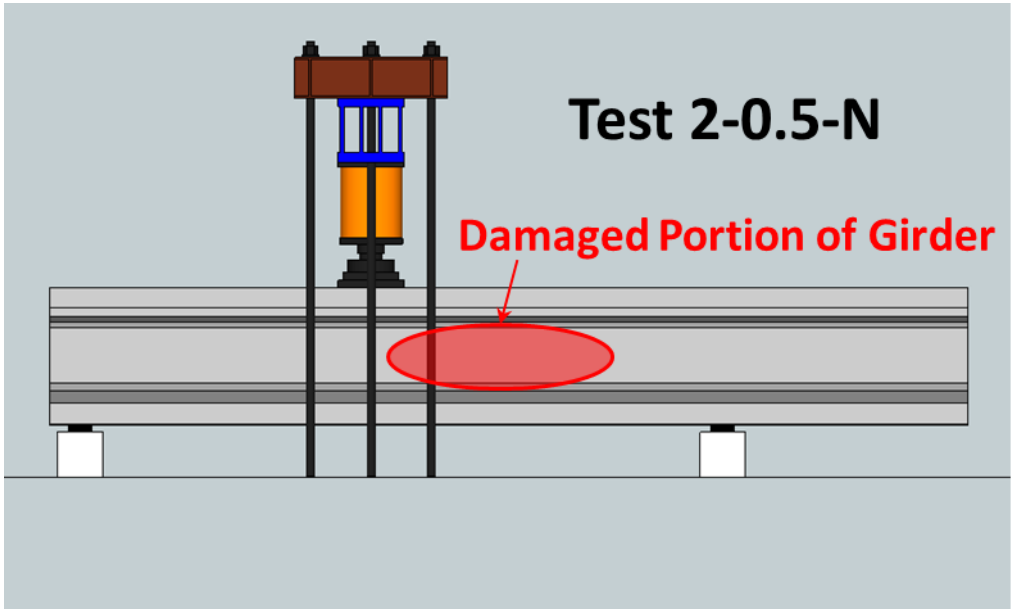

Figure 4-12: Illustration of Damaged Portion of Girder from Test 2-0.5-N

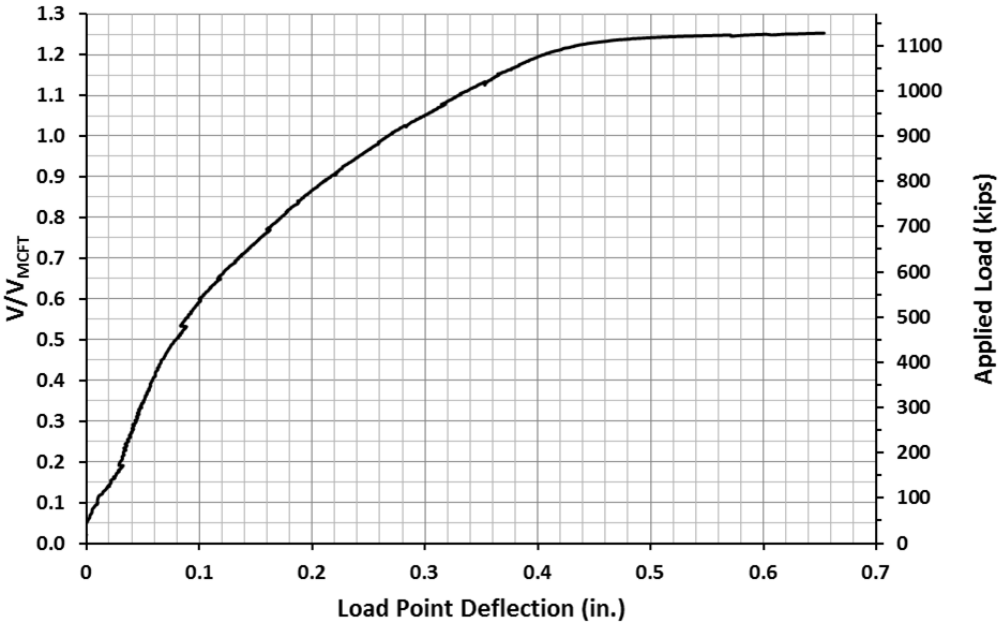

Figure 4-13: Load-Deflection Curve for Test 2-0.5-N

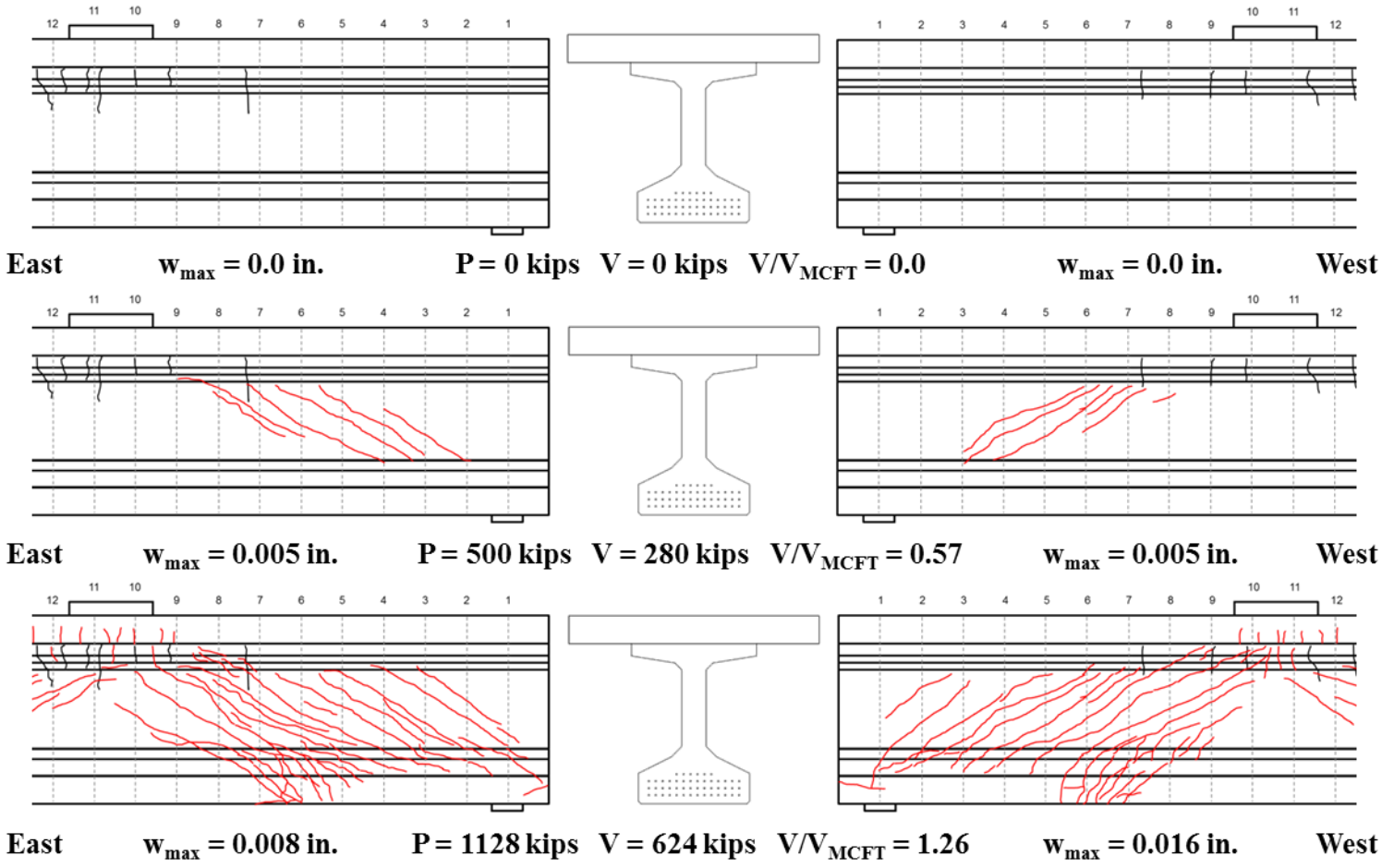

Figure 4-14: Crack Maps for Test 2-0.5-N

Strand slip for the fully-bonded strands in rows one and two is plotted in Figure 4-15, and again the values are quite small.

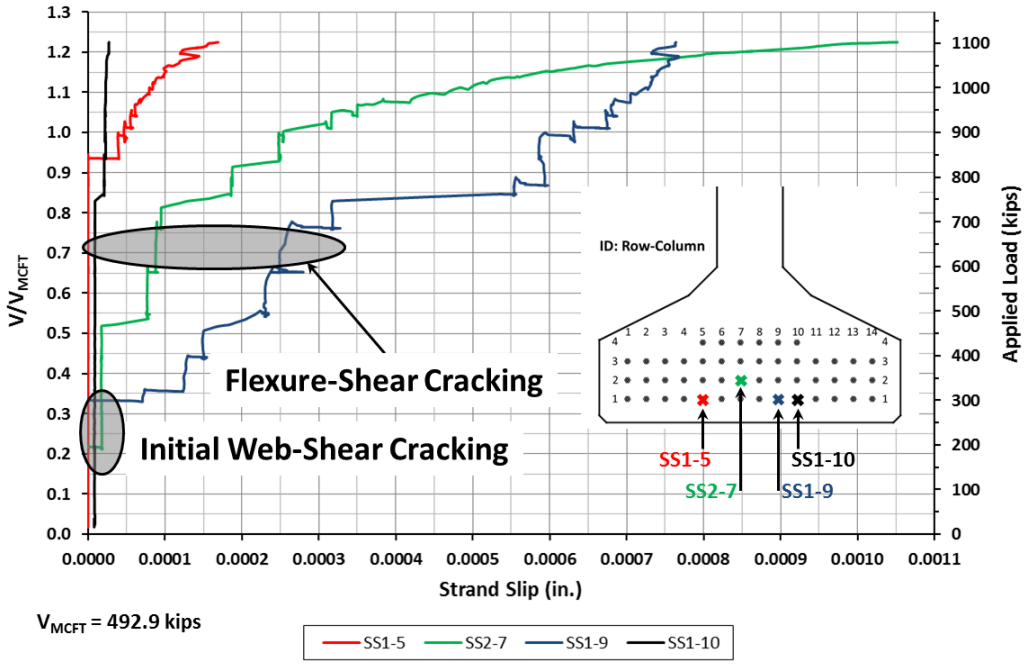

Figure 4-15: Strand Slip Plot for Test 2-0.5-N

The strain in the strand due to applied load was monitored during this test (as in test 1-0.6-N). Figure 4-16 and Figure 4-17 plot the strain in the fully-bonded strands at 31 in. and 49.5 in. from the end of the beam. The strain gauges at 19.5 in. from the end of the beam are in close proximity to the bearing pad. Complex states of stress exist near the bearing pad, and the strains in Figure 4-16 reflect this well. Initially, the measured strains were compressive, likely due to the compressive field over the bearing pad. As load increased, the strains became tensile, though very small. The strains measured further into the shear span were much smoother and larger.

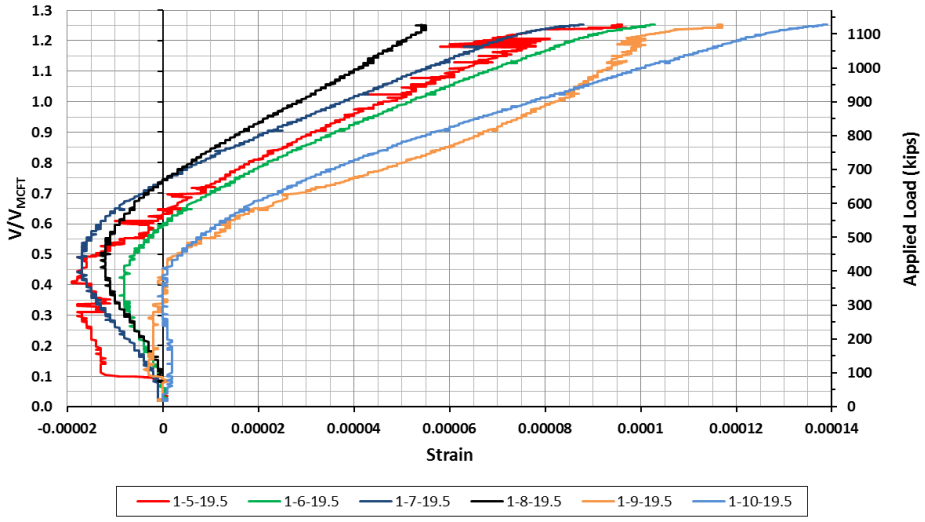

Figure 4-16: Strand Strain Due to Applied Load - 19.5 in. Series (Test 2-0.5-N)

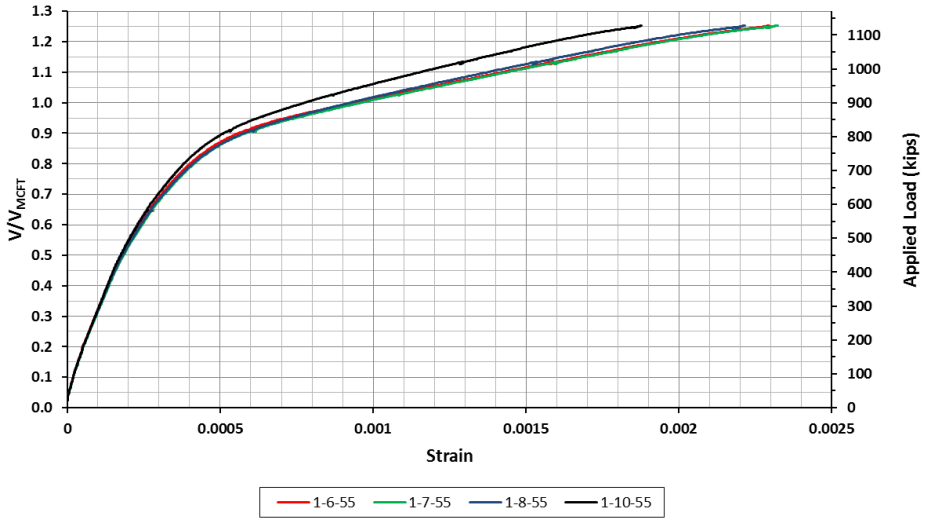

Figure 4-17: Strand Strain Due to Applied Load - 55 in. Series (Test 2-0.5-N)

In this specimen, three vibrating wire gauges were used to determine the effective prestressing before testing. Also, the vibrating wire gauge at $a/2$ (~ 5 ft from end of beam) was used to determine the demand (in stress) placed on the strands due to applied load. At the time of test 2-0.5-N, the effective stress in the strands was found to be 178 ksi. The stress was then recorded at various increments of load during testing. Next, the effective stress in the strands was subtracted to get the stress due to applied load.

Figure 4-18 contains a plot of stress in the strands for test 2-0.5-N. The maximum recorded stress due to applied loads was 34.7 ksi.

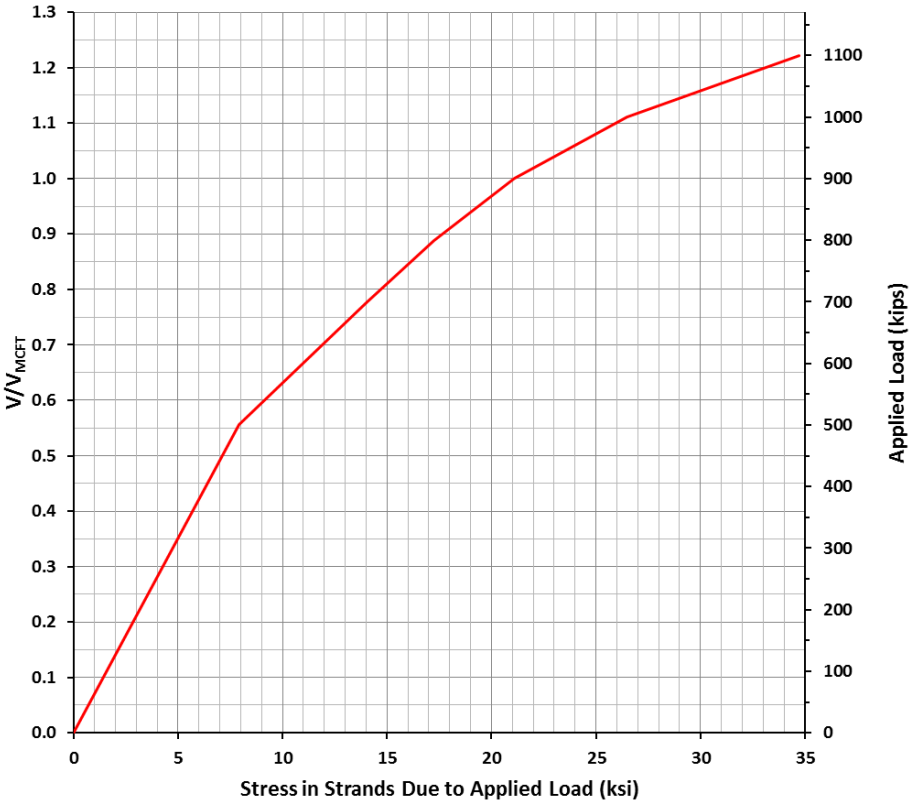

Figure 4-18: Stress in Strands Measured with Vibrating Wire Gauges (Test 2-0.5-N)

Test 2-0.5-N showed the most promise to fail in anchorage because more bottom flange cracking was observed than in prior Tx46 tests. Instead, the specimen failed in web-crushing. Similar to the tests before it, the strand slip and strand strain measurements indicated that the demand on the strands was minimal, despite the promising visual signs. This test also included the use of vibrating wire gauges to measure the demand on the strands. A comparison of the strand gauge data and vibrating wire gauge data is given in Section 4.3, in addition to the analysis of the strand strain measurements. Because the damage was done near the middle of the girder, it was not possible to isolate the damaged portion of the girder for the second test on that specimen. The results from that final test are summarized in the next subsection.

4.2.4 Test 2-0.5-S

Test 2-0.5-S had a shear span of 9.5 ft (a/d = 2.63). The first web-shear cracking in the end region occurred at an applied load of 200 kips (V = 110 kips). Additional web-shear cracking occurred as load was increased in increments of 100 kips. Eventually, at an applied load of 720 kips (V = 400 kips), the girder failed due to further web-crushing in the damaged portion of the girder. The load-deflection curve is plotted in Figure 4-19, and the shear span crack maps for test 2-0.5-S are located in Figure 4-20. Solid blue colored portions represent areas of concrete crushing and/or spalling. Strand slip for this test was negligible, so a plot is not shown.

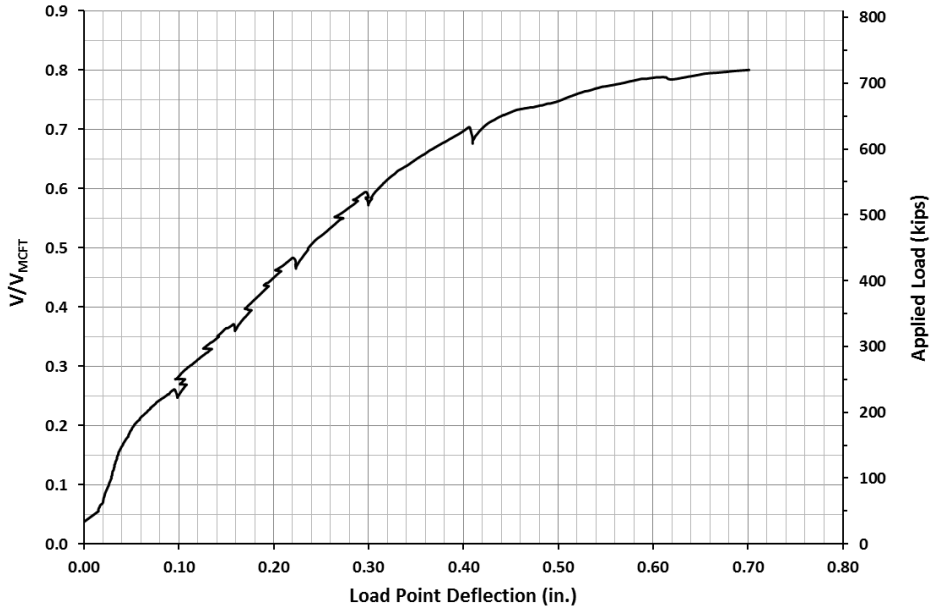

Figure 4-19: Load-Deflection Curve for Test 2-0.5-S

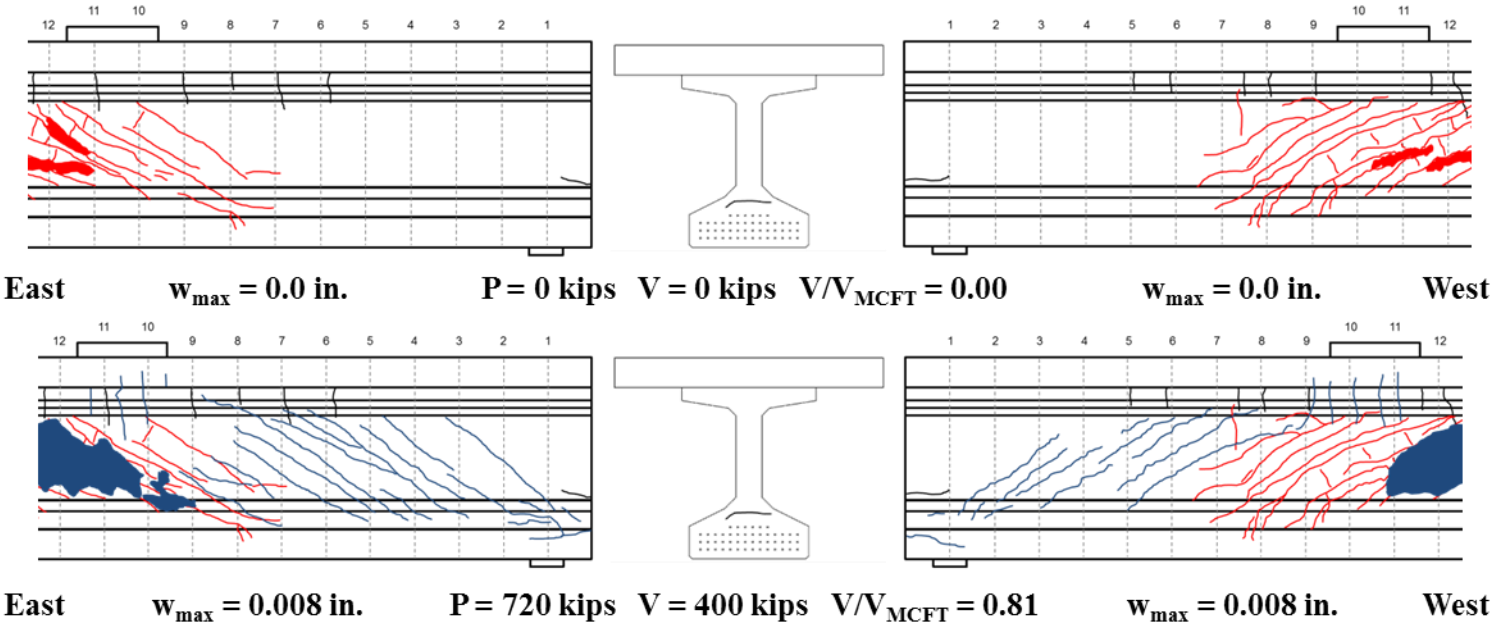

Figure 4-20: Crack Maps for Test 2-0.5-S

Despite the damage from the prior test, test 2-0.5-S was able to reach and exceed the applied load expected to cause an anchorage failure. This test did not experience measurable strand slip. In the next subsection, a final summary of all four tests is presented in tabular form, and the post-test ratio of demand-to-capacity is summarized, in order to provide a comparison with the preliminary analysis in Section 3.5.

4.2.5 Post-Test Demand

All four tests exceeded their anchorage capacities as calculated using AASHTO Equation 5.8.3.5-1. The summary of each test and its failure mode are located in Table 4-1.

Table 4-1: Summary of Test Outcome

Test ID	Maximum Applied Load	Maximum Applied Shear	V/V_{MCFT}	Failure Mode
1-0.6-N	865 kips	569 kips	1.29	Plastic Hinge Formation
1-0.6-S	967 kips	535 kips	1.22	Horizontal Shear
2-0.5-N	1128 kips	624 kips	1.26	Web-Crushing
2-0.5-S	720 kips	400 kips	0.81	Web-Crushing

In Section 3.5, the capacity of each failure mode (anchorage, shear, horizontal shear, and flexure) was calculated and presented in tabular form. In this subsection, the demand due to the maximum applied load was calculated for the four failure modes. These post-test demands are in Table 4-2. For each of those same failure modes at that same applied load, the ratio of demand-to-capacity was then found; the post-test ratios are in Table 4-3. After finding the ratios, a histogram, Figure 4-21, was made to illustrate the demand.

Table 4-2: Post-Test Demands at Expected Failure Load

Test ID	T_u kips	V_u kips	HS_u kips	M_u kip-ft	M_u kip-ft	P_{max} kips
1-0.6-N	904.7	568.6	903.2	3001.9	5123.1	865
1-0.6-S	846.0	535.4	786.9	2692.3	5042.2	967
1-0.5-N	1040.6	623.5	917.5	3133.2	5872.4	1128
1-0.5-S	553.6	400.1	585.6	2016.0	3768.5	720
	19.5 in.	$a/2$	UEP	6 ft	a	a

Table 4-3: Post-Test Ratio of Demand-to-Capacity at Failure Load

Test ID	T_u kips	V_u kips	HS_u kips	M_u kip-ft	M_u kip-ft	P_{max} kips
1-0.6-N	2.12	1.29	1.33	0.61	0.67	865
1-0.6-S	1.98	1.22	1.24	0.54	0.66	967
1-0.5-N	1.97	1.26	1.42	0.64	0.79	1128
1-0.5-S	1.05	0.81	0.91	0.41	0.50	720
	19.5 in.	$a/2$	UEP	6 ft	a	a

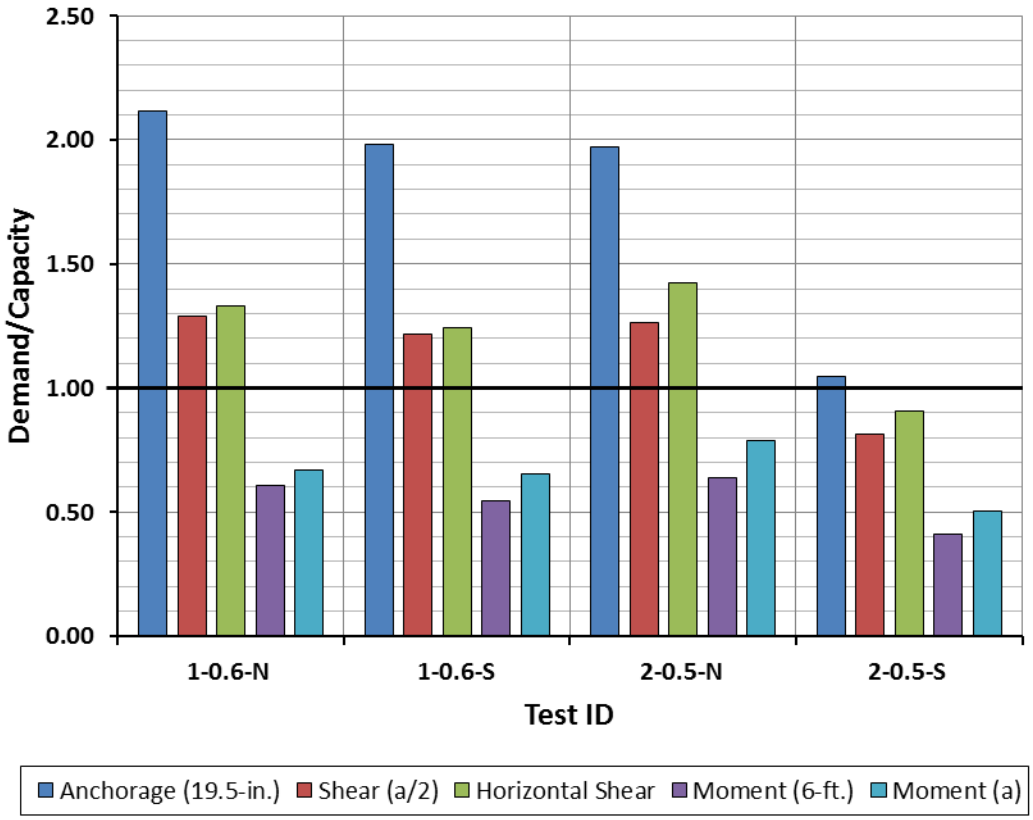

Figure 4-21: Post-Test Histogram

Table 4-3 and Figure 4-21 reiterate the fact that each test failed at an applied load greater than that expected to cause an anchorage failure, based on AASHTO Equation 5.8.3.5-1. The lack of anchorage failures demonstrates that for Tx Girders, the AASHTO anchorage provisions do not apply. (More information regarding the adequacy of the AASHTO anchorage provisions is given in the analytical program, discussed in Chapter 5.) Since all tests exceeded their 2010 AASHTO LRFD General Procedure shear capacity – with the exception of the final test, which was greatly impacted by the damage from the previous test – this testing also demonstrates that a reasonable percentage of debonding in Tx Girders does not have a marked impact on girder shear capacity. Now that the results of the experimental program are summarized, a more thorough analysis of certain aspects of the data is given in the following section.

4.3 EXPERIMENTAL PROGRAM: ANALYSIS OF RESULTS

With the outcome of each test and the data from the instrumentation summarized, further analysis of the results of the experimental program follows in this section. First, the anchorage prediction model from Russell, et al. (initially given in Section 2.4.2) is analyzed with respect to the results of this testing as an alternative to the AASHTO anchorage provisions. Second, the strain in the strands given by the strain gauges and the strain in the strands given by the vibrating wire gauges are compared to each other. Third, the strain in the strands due to applied load is analyzed and compared to that predicted by AASHTO Equation 5.8.3.5-1. The combination of this analysis begins to answers several questions regarding the current method for predicting anchorage failure.

4.3.1 Checking Russell, et al.'s Anchorage Failure Prediction Model with Results

In Chapter 2, anchorage-related research by Russell, et al. (1993) was summarized. Their research included an anchorage failure prediction model developed to predict anchorage failures based on an entirely different method than AASHTO Equation 5.8.3.5-1. In order to evaluate the validity of this method, it is applied to the results of the experimental program in this subsection. In order for this method to be accurate, it should predict the failure type based on the debonded length and embedment length.

The first step in generating the anchorage failure prediction model was to calculate and plot the beam's cracking moment resistance and web-shear cracking resistance (Figure 4-22 and Figure 4-23 show these for test 1-0.6-N). The cracking moment resistance and the web-shear cracking resistance were calculated at multiple points along the length of the beam as follows:

$$M_{cr} = \frac{I}{\bar{y}}\left(7.5\sqrt{f'_c} + \frac{F_{pe}}{A} + \frac{M_{pe}\bar{y}}{I} - \frac{M_D\bar{y}}{I}\right) \qquad \text{Equation 4-1}$$

$$V_{cw} = \left(3.5\sqrt{f'_c} + 0.3f_{pc}\right) b_v d \qquad \text{Equation 4-2}$$

where:

M_{cr} = cracking moment at the section (kip-in)

F_{pe} = effective prestressing force at the section (kips)

A = total area of girder and deck (in^2)

M_{pe} = moment due to eccentricity of the effective prestressing force at the section (kip-in)

$\bar{y}$ = distance from composite centroid to girder's bottom tensile fiber at the section (in.)

I = major composite moment of inertia (in^4)

M_D = moment due to dead load at the section (kip-in)

V_{cw} = web-shear cracking resistance at section (kips)

f_{pc} = effective compressive stress in concrete at centroid of composite cross section (ksi)

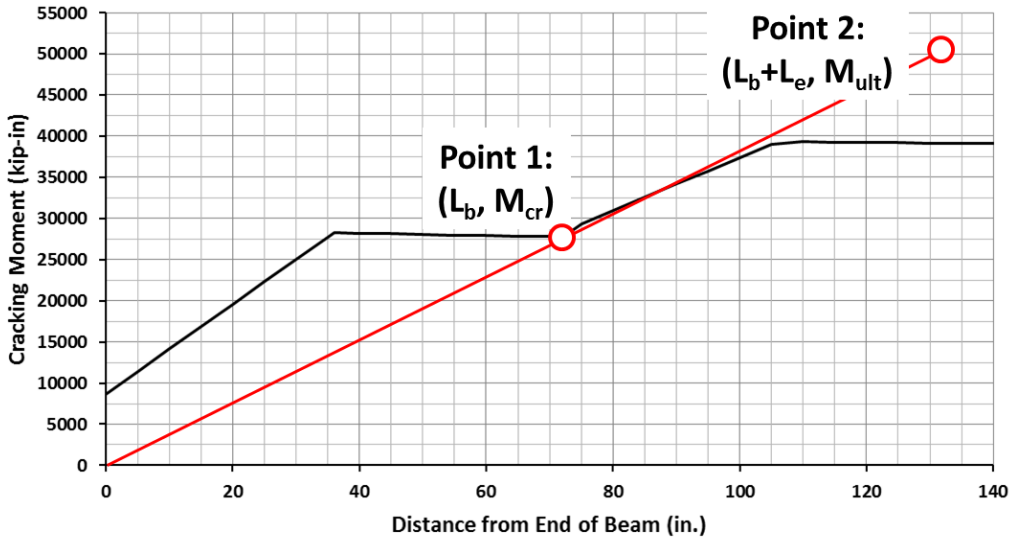

Figure 4-22: Beam's Moment Cracking Resistance & Model Equation (Test 1-0.6-N)

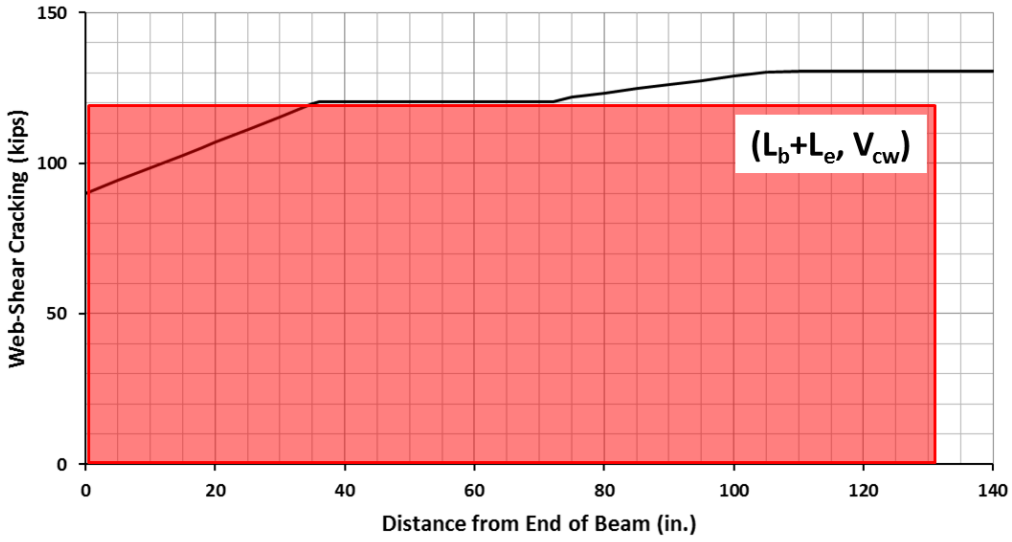

Figure 4-23: Beam's Shear Cracking Resistance & Model Equation (Test 1-0.6-N)

Once all the debonded lengths, embedment lengths, and cracking capacities were assembled (Table 4-4), the equation of two lines on the moment and shear plots were generated (Table 4-5) and plotted (Figure 4-24 through Figure 4-26). Each of the tests was then marked on the associated plot.

Table 4-4: Debonded Lengths, Embedment Lengths, & Cracking Capacities

Test ID	L_b	L_e	M_{cr}	M_{ult}	V_{cw}
	in.	in.	kip-in	kip-in	kips
1-0.6-N	72	60	27740.83	50858.19	120.43
1-0.6-S	72	54	28158.73	49277.78	120.43
2-0.5-N	72	54	32120.63	56211.10	156.30
2-0.5-S	72	54	32120.63	56211.10	156.30

Table 4-5: Associated Equations for Anchorage Failure Prediction Model

Test ID	Flexure Equation	Shear Equation
1-0.6-N	$L_b = 1.20L_e$	$L_b = 422.30 - L_e$
1-0.6-S	$L_b = 1.33L_e$	$L_b = 409.18 - L_e$
2-0.5-N	$L_b = 1.33L_e$	$L_b = 359.64 - L_e$
2-0.5-S	$L_b = 1.33L_e$	$L_b = 359.64 - L_e$

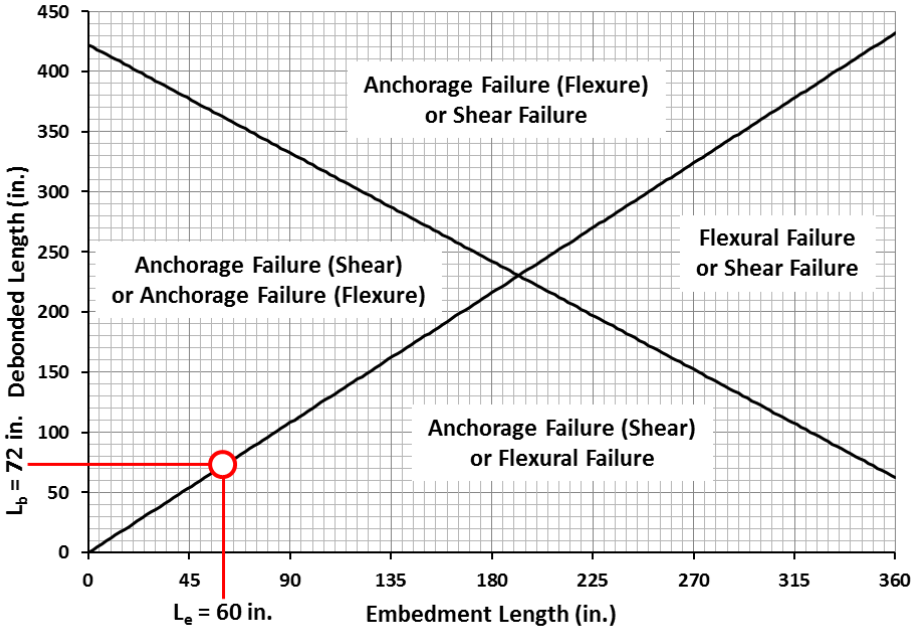

Figure 4-24: Anchorage Failure Prediction Model (Test 1-0.6-N)

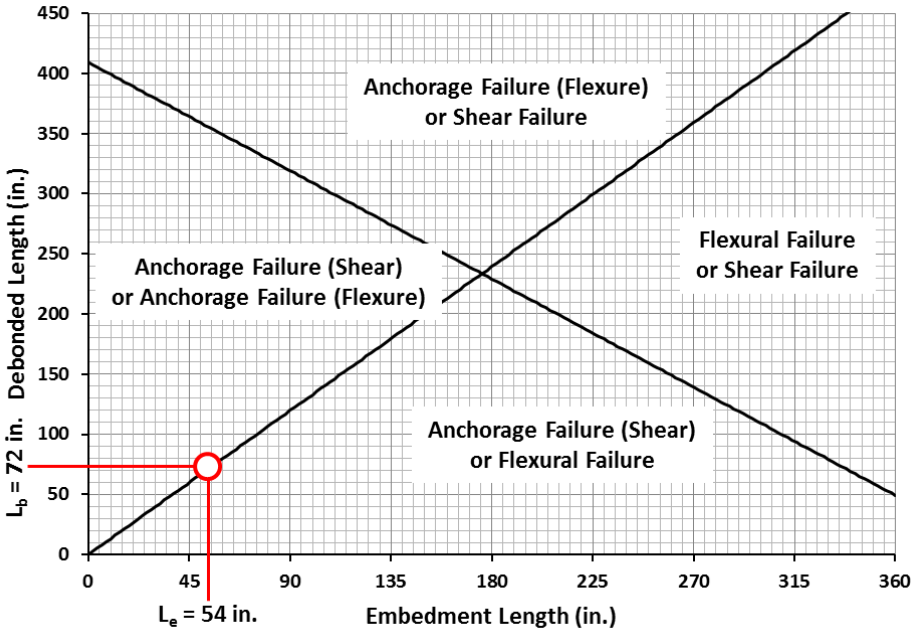

Figure 4-25: Anchorage Failure Prediction Model (Test 1-0.6-S)

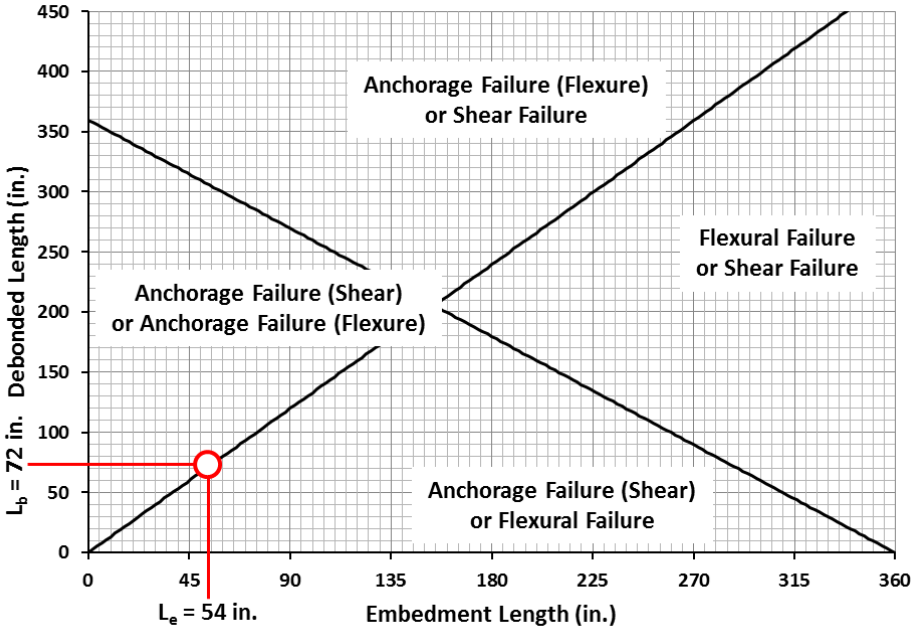

Figure 4-26: Anchorage Failure Prediction Model (Test 2-0.5-N and Test 2-0.5-S)

The plotted anchorage failure prediction model shows that for all four tests an anchorage failure was expected, or, at the very least, significant strand slip and strand strain measurements were expected. Neither occurred, so Russell, et al.'s anchorage prediction model is not accurate and, therefore, is not a better alternative to AASHTO Equation 5.8.3.5-1.

4.3.2 Results Comparison: Strain Gauges vs. Vibrating Wire Gauges

Whether the strain gauges installed on the strands gave similar results to the vibrating wire gauges is useful to know for future research. Using the results from test 2-0.5-N, presented in Section 4.2.3, the stress in the strands due to applied load given by the strain gauges and stress in the strands due to applied load given by the vibrating wire gauges were compared. This stress was checked at two points during testing. The first point occurred at the applied load expected to cause an anchorage failure, and the second point occurred at an applied load of 1100 kips (nearly the maximum applied load for this test).

For test 2-0.5-N, an anchorage failure was expected to occur at an applied load of 698.4 kips (V = 382.5 kips). The stress in the strands at around $a/2$ measured using the strain gauges was found first using the 55 in. series (Figure 4-17). At an applied load of 698.4 kips, the average strain in strands 1-6, 1-7, 1-8, and 1-10 was found to be 0.00037. Multiplying by the strand modulus given in Section 3.3.3 yielded a stress of 10.4 ksi. Next, the strain in the strands at an applied load of 1100 kips was found. The strain in strands 1-6, 1-7, 1-8, and 1-10 was found to be 0.00192, which corresponds to a stress of 53.8 ksi.

The stress in the strands due to applied load given by the vibrating wire gauge was also calculated using the strand modulus given in Section 3.3.3. At the applied load expected to cause an anchorage failure, the stress in the strands was measured at 14.0 ksi (Figure 4-18). The measured stress in the strands at an applied load of 1100 kips was 34.7 ksi. Table 4-6 contains a summary of the comparison.

Table 4-6: Summary - Strain Gauges and Vibrating Wire Gauges Comparison

Applied Load	Stress in Strands at $a/2$		
	Strain Gauges	Vibrating Wire Gauges	Difference
698.4 kips	10.4 ksi	14.0 ksi	3.6 ksi
1100 kips	53.8 ksi	34.7 ksi	19.1 ksi

The strain gauges were located on the bottom row of prestressing strands (2.5 in. from the bottom face of the beam) and the vibrating wire gauges are located at the centroid of the prestressing strands (2.75 in. higher than the bottom row of strands). This placement was expected to result in slightly higher stresses given by the strain gauges. Also, the strain gauges reflect local conditions (possibly stresses at a crack), and the vibrating wire gauges reflect average conditions (stresses over multiple cracks). This difference was expected to result in slightly higher stresses given by the strain gauges.

When compared, the results are mixed. At the applied load expected to cause an anchorage failure, the stress in the strands given by the strain gauges was lower than the stress in the strands given by the vibrating wire gauges; however, a difference of 3.6 ksi is insignificant due to the low measured stresses. If the measured stresses were higher and the difference between the gauges' measurements were constant, the difference would be even more significant. At an applied load of 1100 kips, the stress in the strands given by the strain gauges was much higher than the stress in the strands given by the vibrating wire gauge. This result was expected due to the variable distance from the tensile fiber and the presence of localized cracking. In short, the two types of gauges give reasonably similar results. For future research, the exclusive use of vibrating wire gauges is recommended due to their simple installation, excellent durability, and ease of data acquisition. The vibrating wire gauges should be placed at increments along the length of the beam to yield a more complete plot of the stress in the strands along the length of the beam, which would provide a more comprehensive look at the stress in the beam's strands as a whole instead of the stress in the strands at multiple disparate cross sections.

4.3.3 Stress in Strands: Experimental Method & Theoretical Method Comparison

One of the objectives of this research was to evaluate the adequacy of AASHTO Equation 5.8.3.5-1. This objective is primarily accomplished in the analytical program, but some evaluation can be done using the results of the experimental program on both the capacity and demand sides of AASHTO Equation 5.8.3.5-1. Because no anchorage failures occurred during testing, the precise anchorage capacity of the girder could not be determined and compared with the capacity given by AASHTO Equation 5.8.3.5-1. The results do show, however, that the girder's anchorage capacity is much greater than that calculated using AASHTO Equation 5.8.3.5-1.

The demand side of the anchorage equation is checked using experimental data and linear analysis. An anchorage failure was assumed to occur when T_u/T_n equaled 1.0. For tests 1-0.6-N and 2-0.5-N, strain gauges were placed near the front of the bearing pad (the expected location of the failure-critical crack according to the AASHTO anchorage resistance model). For tests 1-0.6-N and 2-0.5-N, the applied loads expected to cause an anchorage failure were 522.0 kips (V = 335.6 kips) and 698.4 kips (V = 382.5 kips), respectively. The strain in the strands at the front of the bearing pad corresponding to that applied load was found using Figure 4-4 and Figure 4-16. For tests 1-0.6-N and 2-0.5-N, the strains were found to be 0.000103 and 0.00002, respectively. After multiplying the strain by the strand modulus given in Section 3.3.3, the stress in the strands at the expected failure load was calculated to 3.00 ksi and 0.56 ksi, respectively, for the two tests.

The stress in the strands at the front of the bearing pad was also found using a linear analysis method (My/I). First, the moment corresponding to the applied load at which an anchorage failure is expected to occur needed to be found using statics (Figure 4-27 and Figure 4-28). These moments were 6375.9 kip-in and 2868.4 kip-in, respectively, for the two tests.

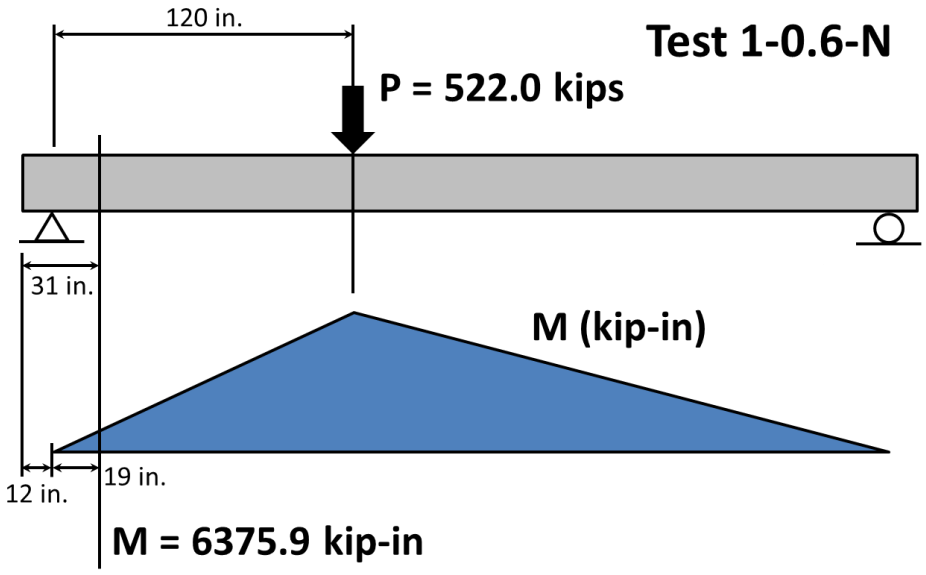

Figure 4-27: Moment at 31 in. for Expected Anchorage Failure (Test 1-0.6-N)

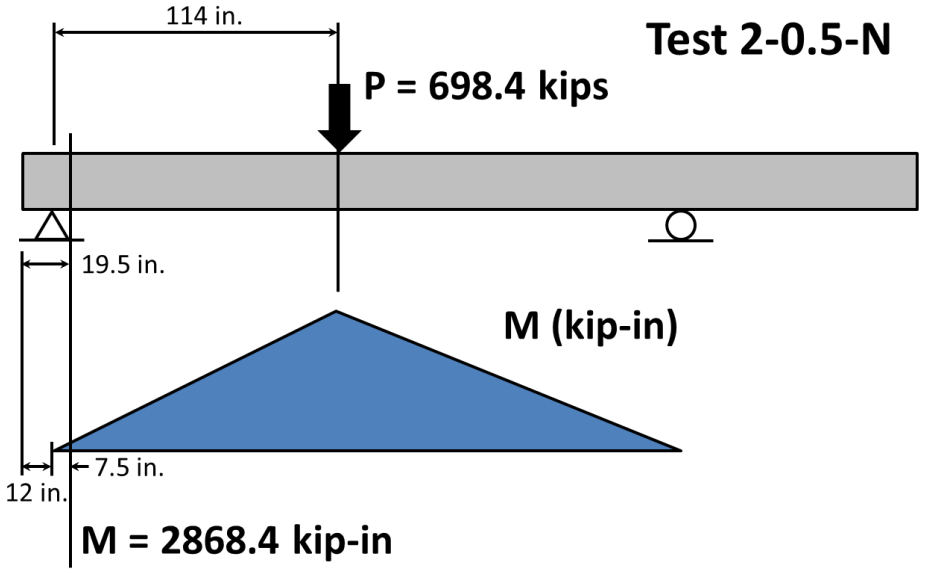

Figure 4-28: Moment at 19.5 in. for Expected Anchorage Failure (Test 2-0.5-N)

Next, the bending stress at the bottom row of strands was calculated. Figure 4-29 shows the distance from the centroid of the composite section to the bottom row of the prestressing strands.

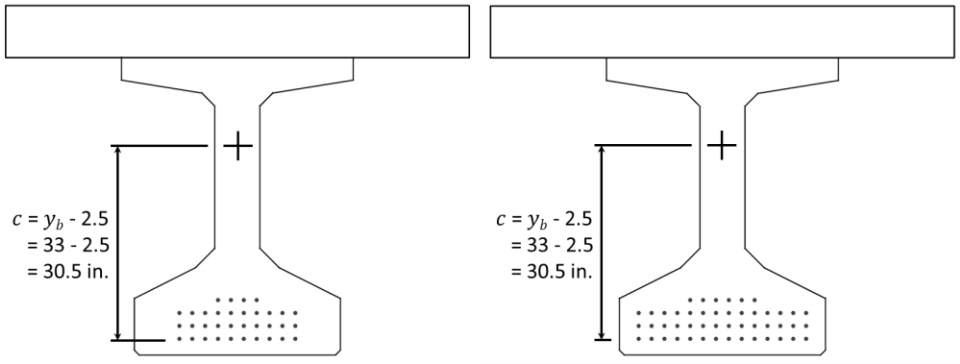

Figure 4-29: Distance from Girder Centroid to Bottom Row of Strands

The bending stress at the bottom row of the prestressing strands was calculated as follows:

$$\sigma_b = \frac{My}{I} = \frac{(6375.9)(30.5)}{494263} = 0.39\ ksi \qquad \text{Equation 4-3}$$

$$\sigma_b = \frac{My}{I} = \frac{(2868.4)(30.5)}{494263} = 0.18\ ksi \qquad \text{Equation 4-4}$$

Finally, the bending stress in the concrete needed to be transformed into the tensile stress in the prestressing strands. This transformation was done by multiplying the bending stress by the ratio of the prestressing strands' modulus to the concrete's modulus. The linear analysis method found the stress in the strands to be 2.61 ksi for test 1-0.6-N and 1.20 ksi for test 2-0.5-N.

$$f_{strand} = \sigma_b \frac{E_p}{E_c} = 0.39 \frac{29000}{4341} = 2.61\ ksi \qquad \text{Equation 4-5}$$

$$f_{strand} = \sigma_b \frac{E_p}{E_c} = 0.18 \frac{29000}{4341} = 1.20\ ksi \qquad \text{Equation 4-6}$$

where:

σ_b = linear bending stress (ksi)

M = moment due to applied load (kip-in)

y = distance from centroid to bottom row of prestressing strands (in.)

I = moment of inertia about major axis (in^4)

f_{strand} = Stress in bottom row of prestressing strands (ksi)

According to AASHTO Equation 5.8.3.5-1, at the applied load expected to cause an anchorage failure, the demand on the bottom row of the prestressing strands would be the maximum stress those strands are capable of developing at the section of consideration, which is in front of the bearing pad. At 19.5 in. from the end of the beam, the 0.6 in. diameter strands are capable of developing 89.9 ksi, and the 0.5 in. diameter strands are capable of developing 107.9 ksi. These stresses are much higher than the experimental method and theoretical method yielded. Table 4-7 contains a summary of the comparison between the experimental and theoretical methods and the AASHTO Equation 5.8.3.5-1 values. The explanation for the large discrepancy between the AASHTO Equation 5.8.3.5-1 values and the experimental and theoretical results may lie in the assumed anchorage resistance model (Section 2.3.2.1). This model assumes cracks cross the strands in front of the bearing pad. This type of cracking was not observed in this testing due to the larger bottom flange, so the demand on the strands was not as high as perhaps it would have been if significant cracking had been present due to a smaller bottom flange as found in AASHTO-type girders. Because this testing has shown the critical cracking in Tx Girders to be along the interface of the web and bottom flange, significant bottom flange cracking is not likely to occur. This observation should be considered in any revisions to a general anchorage design method.

Table 4-7: Summary - Experimental Method & Theoretical Method Comparison

Test ID	Stress in Bottom Row of Prestressing Strands			
	AASHTO Eqn. 5.8.3.5-1	Experimental	Linear Analysis	Difference (Exp. & Linear)
1-0.6-N	89.9 ksi	3.00 ksi	2.61 ksi	0.39 ksi
2-0.5-N	107.9 ksi	0.56 ksi	1.20 ksi	0.64 ksi

4.4 SUMMARY

In Chapter 4, the results and analysis of the experimental program answer several questions regarding the current method for predicting anchorage failures. The first answer

is that a reasonable percentage of debonding in Tx Girders does not have a marked impact on girder shear capacity. With the exception of the final test, which was greatly impacted by the damage from the previous test, all tests exceeded their 2010 AASHTO LRFD General Procedure shear capacity. The second answer applies to the applicability of the AASHTO anchorage provisions. Previous studies pertaining to this method of predicting anchorage failure suggest the resistance model is well founded, at least on AASHTO-type girders; however, this testing demonstrated that the 2010 AASHTO anchorage resistance model and its corresponding equation do not apply to modern I-girders, such as the Tx Girders. These tests indicate that the absence of flexure, shear, or flexure-shear cracks crossing the strands near the end of the beam precludes an anchorage failure. For Tx Girders, the failure-critical crack is more likely to occur at the web-flange interface (horizontal shear). The ratio of the width of the bottom flange to the width of the web appears to be an important factor. Answering these questions achieves several of this research's objectives, but all the objectives cannot be achieved until the results of the analytical program are concluded. Chapter 5 analyzes the AASHTO anchorage provisions in order to determine their adequacy and to recommend how they can be improved.

CHAPTER 5: ANALYTICAL RESULTS & ANALYSIS

The details and the results and analysis of the experimental program were presented in Chapters 3 and 4, respectively. This chapter, Chapter 5, discusses the results and analysis of the analytical program, in order to verify the conclusions drawn from the experimental analysis, determine additional behavioral differences between AASHTO-type girders and Tx Girders, determine what factors contribute to anchorage capacity, and determine the accuracy and conservativeness of the current anchorage design method.

Since the analytical program attempts to verify the conclusions drawn from the experimental analysis, those two conclusions from the previous chapter are briefly summarized here. The first conclusion was that a reasonable percentage of debonding in Tx Girders did not have a marked impact on girder shear capacity. With the exception of the final test, which was greatly impacted by the damage from the previous test, all tests exceeded their 2010 AASHTO General Procedure shear capacity. The second conclusion applied to the applicability of the AASHTO anchorage provisions. Previous studies pertaining to this method of predicting anchorage failure suggested that the resistance model was well founded, at least on AASHTO-type girders; however, this testing demonstrated that the 2010 AASHTO anchorage resistance model and its corresponding equation do not apply to modern I-girders, such as the Tx Girders. These tests indicated that the absence of flexure, shear, or flexure-shear cracks crossing the strands near the end of the beam precluded an anchorage failure. For Tx Girders, the failure-critical crack was more likely to occur at the web-flange interface (horizontal shear). The ratio of the width of the bottom flange to the width of the web appeared to be an important factor.

This chapter is divided into two sections. The first section details the development of a new Anchorage Evaluation Database (AEDB) for the analytical program and summarizes its contents. The second section presents the analysis of the analytical program using that database.

5.1 ANCHORAGE EVALUATION DATABASE DEVELOPMENT AND RESULTS

The development of the Anchorage Evaluation Database started with the Evaluation Database-Level I of the University of Texas Prestressed Concrete Shear Database (UTPCSDB), discussed in Section 2.2.1. Recall that these 223 tests met the following criteria:

- member depth greater than 12 in.
- made from conventional concrete with a 28-day strength greater than 4 ksi
- tested at a shear span-to-depth ratio greater than 2.0
- contained at least the minimum shear reinforcement for AASHTO (2010)
- simply supported beams (no segmental sections)
- prestressed or post-tensioned internally

The Evaluation Database-Level I was further filtered by removing tests that did not meet the following criteria:

- member web width greater than or equal to 6 in. (74 tests removed)
- effective prestressing greater than or equal to 125 ksi (3 tests removed)
- concentrated loading only (16 tests removed)
- pretensioned only (67 tests removed)

Nine tests recently found in literature that were not previously in the Evaluation Database-Level I were added, and, after filtering, the Anchorage Evaluation Database (AEDB) contained 72 shear tests, of which 25 were anchorage failures and 47 were shear failures. Table 5-1 summarizes the tests that compose the AEDB and their literature, and Figure 5-1 demonstrates the variety of beam types contained in the AEDB. Once the AEDB was developed, each test was examined and certain parameters were collected and calculated. These parameters are summarized in Table 5-2. Note that V_n is sometimes referred to as V_{MCFT}, and V_u is sometimes referred to as either V_{test} or just V. The tests highlighted in red are discussed below.

Table 5-1: Summary of Anchorage Evaluation Database

No.	Authors	Tests	Beam Type
1	Alshegeir & Ramirez (1992)	3	AASHTO Type I & Type II
2	Avendano & Bayrak (2008)	4	Texas Tx28
3	Hamilton, Llanos, & Ross (2009)	4	AASHTO Type III
4	Hanson & Hulsbos (1969)	2	PCI Box Beam & PCI BT-63
5	Heckmann & Bayrak (2008)	6	Texas Type C
6A	Avendano (2011)	9	Texas 4B28
6B	Hovell (2011)	7	Texas U54
7	Kaufman & Ramirez (1988)	4	AASHTO Type I & Type II
8	Labonte & Hamilton (2005)	1	AASHTO Type II
9	Langefeld & Bayrak (2012)	4	Texas Tx46
10	Naito, Parent, & Brunn (2005)	1	PCEF-45
11	Ramirez & Aguilar (2005)	2	AASHTO Type I
12	Runzell, Shield, & French (2007)	2	Minnesota MnType54
13	Shahawy & Batchelor (1996)	6	AASHTO Type II
14	Shahawy, Robinson, & Batchelor (1993)	5	AASHTO Type II
15	Tawfiq (1995)	12	AASHTO Type II
	Total	**72**	

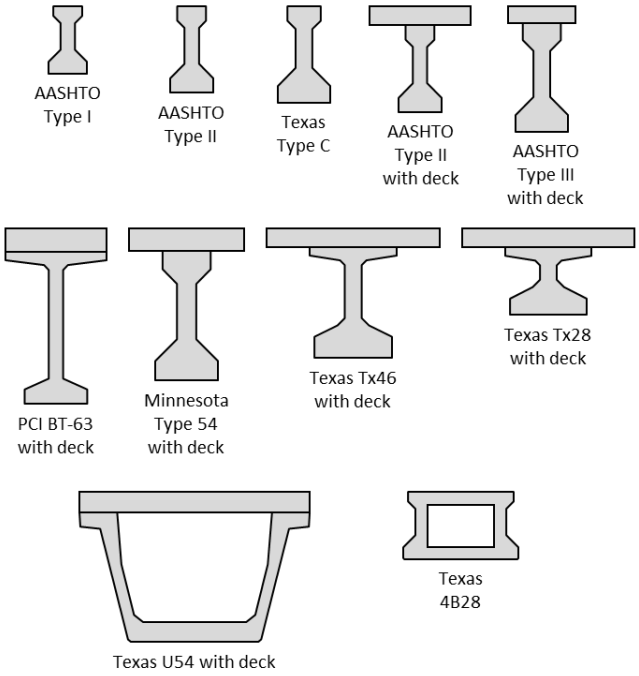

Figure 5-1: Summary of Beam Cross Sections in Anchorage Evaluation Database

Table 5-2: Results of Anchorage Evaluation Database

Authors	Test ID	a/d	V_n	T_n	V_u	T_u	V_u/V_n	T_u/T_n	% Debonding	b_f/b_w
Alshegeir & Ramirez	Type I (4A)	2.31	122.3	164.2	161.5	309.1	1.32	1.88	0.00	2.67
	Type II (1A)	2.16	150.0	240.4	222.0	425.8	1.48	1.77	0.00	3.00
	Type I (3A)	2.61	95.0	176.9	113.5	201.9	1.19	1.14	0.00	2.67
Avendano & Bayrak	Tx28 (I-L)	3.08	258.0	777.5	412.7	629.7	1.60	0.81	0.00	4.57
	Tx28 (I-D)	3.08	258.0	777.5	429.4	667.2	1.66	0.86	0.00	4.57
	Tx28 (II-L)	3.96	243.7	777.5	382.1	563.0	1.57	0.72	0.00	4.57
	Tx28 (II-D)	3.96	243.7	777.5	387.0	574.1	1.59	0.74	0.00	4.57
Hamilton, Llanos, & Ross	Type III (G2)	2.67	241.5	150.4	273.9	518.4	1.13	3.45	41.67	3.14
	Type III (G3)	3.96	223.9	150.4	224.2	403.0	1.00	2.68	41.67	3.14
	Type III (B1U4)	5.11	211.2	150.4	195.6	338.2	0.93	2.25	41.67	3.14
	Type III (B4U4)	5.11	211.2	150.4	213.6	381.4	1.01	2.54	41.67	3.14
Hanson & Hulsbos	Box (G1-1)	3.32	180.5	371.9	198.5	380.4	1.10	1.02	0.00	3.60
	Type II (G4-3)	2.76	99.3	232.3	136.0	260.9	1.37	1.12	0.00	3.00
Heckmann & Bayrak	Type C (B-C-70-1)	2.20	198.1	375.2	358.5	681.3	1.81	1.82	0.00	3.14
	Type C (B-C-70-4)	2.20	195.5	366.2	355.8	676.3	1.82	1.85	0.00	3.14
	Type C (B-C-70-5)	2.20	195.3	364.0	339.9	645.7	1.74	1.77	0.00	3.14
	Type C (B-C-70-6)	2.20	194.5	359.5	373.5	710.5	1.92	1.98	0.00	3.14
	Type C (B-C-60-1)	2.20	198.2	375.2	364.6	693.0	1.84	1.85	0.00	3.14
	Type C (B-C-60-2)	2.20	199.2	377.4	358.5	681.2	1.80	1.80	0.00	3.14

Table 5-2: Results of Anchorage Evaluation Database (continued)

Authors	Test ID	a/d	V_n	T_n	V_u	T_u	V_u/V_n	T_u/T_n	% Debonding	b_f/b_w
Hovell, Avendano, Dunkman, Moore, Bayrak, & Jirsa	Box (B-01-Q)	2.93	145.3	372.9	244.1	468.0	1.68	1.25	26.60	4.78
	Box (B-01-K)	3.42	145.1	372.9	246.7	473.0	1.70	1.27	26.60	4.78
	Box (B-02Q)	2.93	145.1	372.9	242.4	464.7	1.67	1.25	26.60	4.78
	Box (B-02K)	3.42	144.7	372.9	250.4	480.1	1.73	1.29	26.60	4.78
	Box (B-03Q)	2.93	145.3	372.9	290.5	557.3	2.00	1.49	26.60	4.78
	Box (B-03K)	3.42	144.7	372.9	296.7	569.2	2.05	1.53	26.60	4.78
	Box (B-04Q)	2.93	144.2	372.9	291.3	558.8	2.02	1.50	26.60	4.78
	Box (B-05Q)	2.93	144.5	372.9	300.6	576.7	2.08	1.55	26.60	4.78
	Box (B-05K)	3.42	145.1	372.9	284.4	545.5	1.96	1.46	26.60	4.78
	U (B-1N)	2.59	544.6	1248.7	659.0	1258.3	1.21	1.01	26.60	5.34
	U (B-1S)	2.62	357.9	1248.7	612.0	1167.9	1.71	0.94	26.60	5.34
	U (B-2N)	2.59	648.9	1248.7	610.0	1161.2	0.94	0.93	26.60	5.34
	U (B-3N)	2.63	565.8	673.0	628.0	1198.8	1.11	1.78	46.10	5.34
	U (B-3S)	2.63	574.6	673.0	655.0	1250.8	1.14	1.86	46.10	3.44
	U (B-4N)	2.62	808.5	1248.7	663.0	1263.3	0.82	1.01	26.60	5.34
	U (B-5N)	2.60	772.2	1057.1	973.0	1857.4	1.26	1.76	26.60	5.34
Kaufman & Ramirez	Type I (2)	2.20	97.3	156.3	145.0	278.0	1.49	1.78	0.00	2.67
	Type I (3)	2.20	104.2	161.7	100.0	191.2	0.96	1.18	0.00	2.67
	Type I (4)	2.20	99.1	164.4	110.0	210.6	1.11	1.28	0.00	2.67
	Type II (1)	2.40	147.4	238.7	140.0	268.0	0.95	1.12	0.00	2.67
Labonte & Hamilton	Type II (S1-STDS)	2.25	113.1	175.4	191.2	366.8	1.69	2.09	16.80	2.67
Langefeld & Bayrak	Tx46 (1-0.6-N)	2.76	440.6	427.3	568.6	904.7	1.29	2.12	35.30	4.57
	Tx46 (1-0.6-S)	2.63	440.6	427.3	535.4	846.0	1.22	1.98	35.30	4.57
	Tx46 (2-0.5-N)	2.62	492.9	528.3	623.5	1040.6	1.26	1.97	33.30	4.57
	Tx46 (2-0.5-S)	2.62	492.9	528.3	400.1	553.6	0.81	1.05	33.30	4.57
Naito, Parent, & Brunn	Bulb Tee (B1)	2.21	603.5	411.7	488.8	927.5	0.81	2.25	0.00	4.57

Table 5-2: Results of Anchorage Evaluation Database (continued)

Authors	Test ID	a/d	V_n	T_n	V_u	T_u	V_u/V_n	T_u/T_n	% Debonding	b_f/b_w
Ramirez & Aquilar	Type I (13.3-5.1-326P)	3.62	146.3	175.4	179.9	343.4	1.23	1.96	0.00	2.67
	Type I (16.2-5.1-326P)	3.66	146.2	175.4	214.9	410.7	1.47	2.34	0.00	2.67
Runzell, Shield, & French	MnDOT Type IV (I)	3.01	224.0	420.8	383.1	712.7	1.71	1.69	0.00	3.25
	MnDOT Type V (II)	3.57	299.3	420.8	320.3	591.8	1.07	1.41	0.00	3.50
Shahawy & Batchelor	Type II (A1-00-R/2-N)	2.72	150.1	245.0	177.7	306.2	1.18	1.25	0.00	3.00
	Type II (A1-00-R/2-S)	3.34	144.3	245.0	180.0	366.0	1.25	1.49	0.00	3.00
	Type II (A1-00-R-N)	2.72	183.6	245.0	221.7	412.5	1.21	1.68	0.00	3.00
	Type II (A1-00-3R/2-N)	2.72	211.6	245.0	218.7	363.2	1.03	1.48	0.00	3.00
	Type II (B0-00-R-N)	2.70	186.2	250.8	231.7	435.1	1.24	1.73	0.00	3.00
	Type II (B0-00-R-S)	3.06	91.2	236.1	206.0	394.2	2.26	1.67	0.00	3.00
Shahawy, Robinson, & Batchelor	Type II (A0-00-R-N)	2.04	246.2	245.0	325.3	616.7	1.32	2.52	0.00	3.00
	Type II (A0-25-R-N)	2.04	242.7	183.8	293.3	536.1	1.21	2.92	25.00	3.00
	Type II (A0-00-R-S)	2.04	246.3	245.0	281.1	507.4	1.14	2.07	0.00	3.00
	Type II (A0-25-R-S)	4.09	192.3	183.8	179.1	243.5	0.93	1.32	25.00	3.00
	Type II (C0-50-R-S)	5.25	173.1	108.1	135.9	177.5	0.79	1.64	45.00	3.00
Tawfiq	Type II (R8N)	2.82	234.8	273.7	282.4	497.6	1.20	1.82	0.00	3.00
	Type II (R10N)	2.82	160.6	280.9	281.0	536.3	1.75	1.91	0.00	3.00
	Type II (R12N)	2.82	237.8	273.7	288.6	507.5	1.21	1.85	0.00	3.00
	Type II (2R8N)	2.82	297.3	273.7	244.7	324.3	0.82	1.18	0.00	3.00
	Type II (2R10N)	2.82	298.6	273.7	249.7	331.2	0.84	1.21	0.00	3.00
	Type II (2R12N)	2.82	299.4	273.7	288.6	385.5	0.96	1.41	0.00	3.00
	Type II (R8S)	2.35	234.4	273.7	305.0	570.2	1.30	2.08	0.00	3.00
	Type II (R10S)	2.35	236.8	273.7	302.0	561.4	1.28	2.05	0.00	3.00
	Type II (R12S)	2.35	237.8	273.7	284.1	495.1	1.19	1.81	0.00	3.00
	Type II (2R8S)	2.35	297.4	273.7	259.0	353.5	0.87	1.29	0.00	3.00
	Type II (2R10S)	2.35	298.7	273.7	248.0	338.1	0.83	1.24	0.00	3.00
	Type II (2R12S)	2.35	299.4	273.7	295.0	396.5	0.99	1.45	0.00	3.00

5.2 ANALYTICAL PROGRAM ANALYSIS

Following the formation of the Anchorage Evaluation Database (AEDB), analysis first sought to find trends in the data and to differentiate between the AASHTO-type girders and the Tx Girders. When the ratio of shear demand-to-capacity was plotted versus the ratio of b_f/b_w (Figure 5-2), several important items were observed. First, the plot indicates that anchorage failures may lead to unconservative results with respect to the 2010 AASHTO LRFD General Procedure, as evidenced by nine of the twenty-five anchorage failures occurring at a ratio of less than 1.0. (There are also several unconservative shear failures, but most of these can be attributed to horizontal shear.) Second, when the plot considers beam cross section, as illustrated in Figure 5-3, the plot shows that for modern shapes (Tx Girders in particular, n = 8), the conservatism of the 2010 AASHTO LRFD General Procedure is not influenced by anchorage, because anchorage does not control for these sections. However, the plot also shows that anchorage failures in AASHTO-type girders may lead to unconservative results with respect to the 2010 AASHTO LRFD General Procedure.

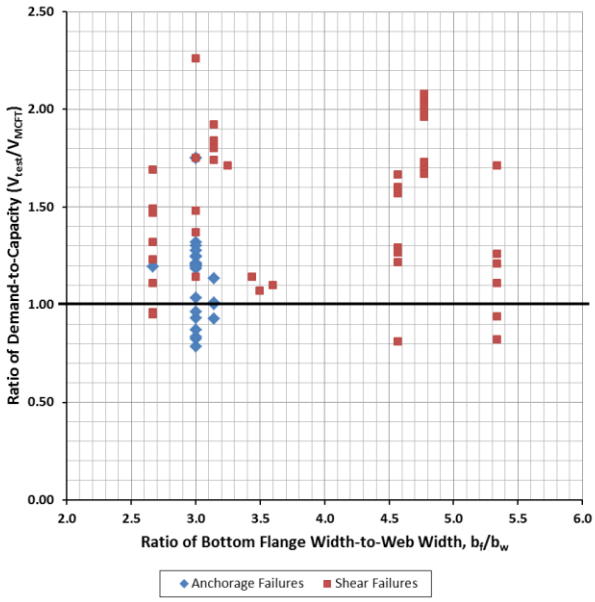

Figure 5-2: Ratio of Shear Demand to Capacity vs. Flange Width to Web Width

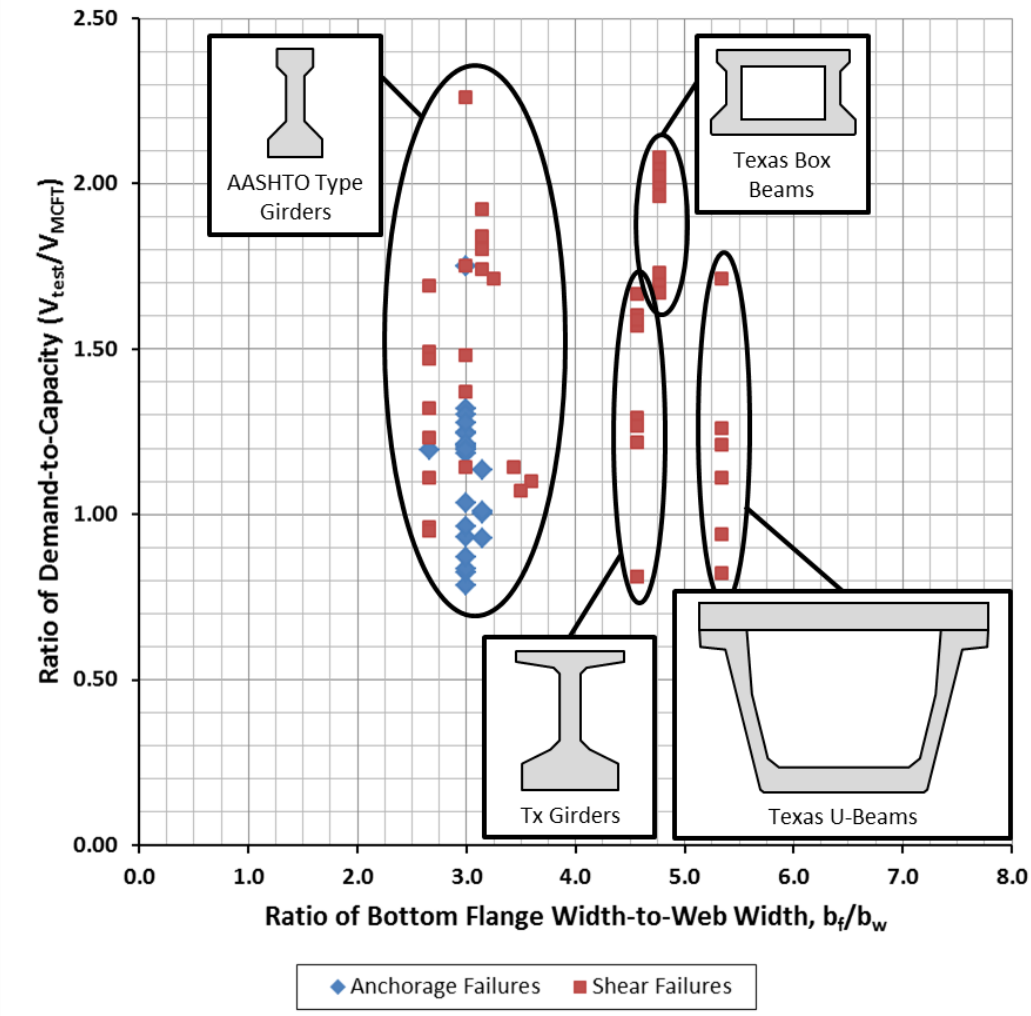

Figure 5-3: Shear Demand/Capacity vs. Flange/Web Width Based on Cross-Section

Trends were also sought in the nine unconservative anchorage failures, highlighted in red in Table 5-2. Commonalities that would explain the unconservative nature of these tests were elusive. All nine of these specimens were AASHTO-type girders, but some contained debonding and others did not. The two identical Hamilton, et al. specimens both contained harped strand and debonded strand under the web, yet one failed below its shear capacity, and one failed above it. Similarly, one of the two identical Shahawy, et al. specimens failed below its shear capacity at a much higher a/d ratio than the other that failed above its shear capacity at a lower a/d ratio. These two specimens,

along with a third unconservative test from the same study, were identical to the Tawfiq specimens, except the Shahawy, et al. specimens contained debonding under the web. Finally, of the Tawfiq specimens, only those with double the required shear reinforcement failed in anchorage, while the other variables remained mostly unchanged. Thus, this comparison discovered no commonalities that accounted for the unconservative nature of these tests. More full-scale experimental testing is needed in order to expand the Anchorage Evaluation Database and so increase the likelihood of discovering potential trends.

Finally, the performance of AASHTO Equation 5.8.3.5-1 was evaluated. The performance was assessed by plotting the ratio of shear demand-to-capacity on the horizontal axis and the ratio of anchorage demand-to-capacity on the vertical axis (Figure 5-4). For the method to be conservative and accurate, most anchorage failures should fall in the upper right quadrant, meaning that the tests exceeded both their shear capacity and their anchorage capacity. In addition, most shear failures should fall in the lower right quadrant, meaning that the tests exceeded their shear capacity but not their anchorage capacity. As indicated in the plot, nearly all of the anchorage failures fall in the upper right quadrant, but hardly any of the shear failures fall in the lower right quadrant. Instead, the shear failures fall in the upper right quadrant with the anchorage failures. The average, coefficient of variation, and accuracy for the tests in the plot are presented in Table 5-3. The average for anchorage failures is above 1.0 (conservative), but both averages are similar; an accurate method would yield an average less than 1.0 for shear failures. Therefore, the plot demonstrates that AASHTO Equation 5.8.3.5-1 is conservative but not accurate. A design using the anchorage equation would typically be conservative, but the designer would not be able to accurately predict between a shear failure and an anchorage failure.

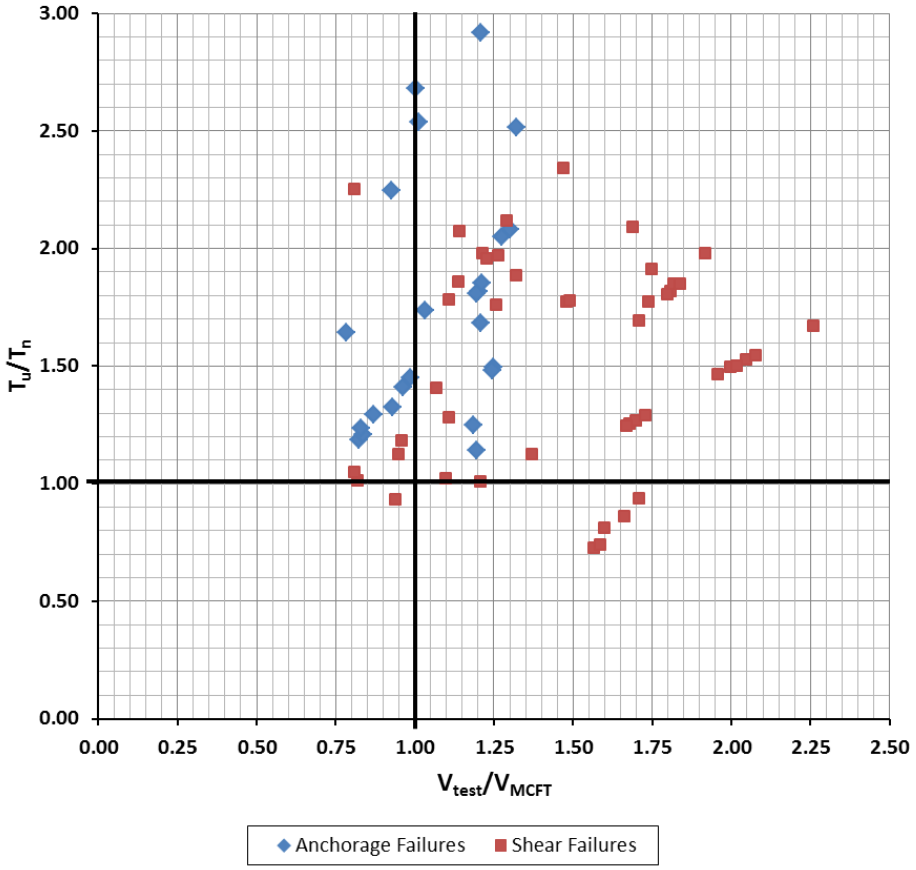

Figure 5-4: Ratios of Shear & Anchorage Demand to Capacity for AEDB

Table 5-3: Statistics for AASHTO Equation 5.8.3.5-1

Shear Failures		Anchorage Failures
1.53	**Mean**	1.82
0.28	**COV**	0.33
6/47	**Accuracy**	25/25

5.3 SUMMARY

Chapter 5 discusses the Anchorage Evaluation Database and its verification of the conclusions drawn from the experimental analysis, its behavioral differentiation between the AASHTO-type girders and the Tx Girders, and its evaluation of the accuracy and conservativeness of the current anchorage design method. Several important items are observed. The first observation is that for Tx Girders, the conservatism of the 2010

AASHTO LRFD General Procedure is not influenced by anchorage because anchorage does not control for these sections; this analytical finding supports Chapter 4's experimental finding that the larger bottom flange impedes the propagation of cracks across the strands. The second observation is that anchorage failures in AASHTO-type girders may lead to unconservative results with respect to the 2010 AASHTO LRFD General Procedure; however, more research is needed in order to find additional trends and commonalities between unconservative tests. The third and final observation is that AASHTO Equation 5.8.3.5-1 is conservative but not accurate; this equation does not accurately predict between a shear failure and an anchorage failure for the AEDB data.

CHAPTER 6: SUMMARY AND CONCLUSIONS

As part of the ongoing research on shear at the Phil M. Ferguson Structural Engineering Laboratory (FSEL), the anchorage-controlled shear capacity of prestressed concrete bridge girders was studied in two distinct ways, experimentally and analytically, in this research.

The three primary objectives of this research were (i) to investigate the impact of debonding on the anchorage of the prestressing strands, (ii) to investigate the impact of debonding on the girder's shear capacity, and (iii) to determine the accuracy and conservativeness of the current anchorage design method. In addition, the two secondary objectives were (iv) to determine whether or not the assumed anchorage resistance model applies to modern prestressed concrete bridge girders, such as the recently developed Tx Girder, and (v) to determine what factors contribute to anchorage capacity.

Available literature regarding anchorage-related issues and shear behavior of prestressed concrete bridge girders was reviewed. The review first included a summary of the University of Texas Prestressed Concrete Shear Database (UTPCSDB) that previously had been used to assess the accuracy and conservativeness of multiple shear design equations. The analysis of the data in the UTPCSDB indicated that, of the various shear design methods, the 2010 AASHTO LRFD General Procedure gives the best results for traditional modes of vertical shear failures but not for horizontal shear failures or anchorage failures. The review then included the results from recent research proposing a new method for predicting horizontal shear failures. Analysis of further data from the UTPCSDB showed that this proposed method, based on shear-friction, reliably predicts horizontal shear failures. Finally, the review included the 2010 AASHTO anchorage resistance model and its corresponding equation. Several previous studies pertaining to that method of predicting anchorage failures suggested that the resistance model was well founded, at least on AASHTO-type girders (these studies did not consider accuracy or conservatism).

Next, an experimental program was planned and carried out in order to determine the impact of debonding on the anchorage of the prestressing strands and the girder's shear capacity and to address whether the 2010 AASHTO anchorage resistance model and its corresponding equation apply to modern I-girders, such as the Tx Girder. Two such prestressed concrete bridge girders with about 35% debonding were designed, fabricated, and tested. The girders were instrumented for data collection, and these data were used to analyze the results of the shear testing that culminated the experimental program of this research.

Finally, an analytical program was carried out to determine the accuracy and conservativeness of the anchorage design procedures in the 2010 AASHTO LRFD Bridge Design Specifications and to determine what factors contribute to anchorage capacity. An Anchorage Evaluation Database (AEDB) was developed, by filtering and expanding the UTPCSDB, and then evaluated. The AEDB contained 72 shear tests, of which 25 were anchorage failures and 47 were shear failures.

The following section summarizes the findings and conclusions of the experimental and analytical programs, and a second section provides recommendations for future research of anchorage-related issues.

6.1 SUMMARY OF FINDINGS

The first two objectives, (i) and (ii), of this research were to investigate the impact of debonding on the anchorage of the prestressing strands and a girder's shear capacity. The results of the experimental testing show that a reasonable percentage of debonding in Tx Girders does not have a marked impact on girder shear capacity (and thus anchorage of the prestressing strands). With the exception of the final test, which was greatly impacted by the damage from the previous test, all tests exceeded their shear capacity calculated by using the 2010 AASHTO General Procedure.

The third objective, (iii), of this research was to determine the accuracy and conservativeness of the current anchorage design method. The results from the analytical program showed that AASHTO Equation 5.8.3.5-1 is conservative but not accurate. In

other words, this equation cannot be used to accurately differentiate between a shear failure and an anchorage failure. In regards to conservativeness, the analysis of the AEDB showed that anchorage failures in AASHTO-type girders may lead to unconservative results with respect to the 2010 AASHTO LRFD General Procedure.

The fourth objective, (iv), of this research was to determine whether or not the assumed AASHTO anchorage resistance model applies to modern prestressed concrete bridge girders, such as the recently developed Tx Girder. This testing demonstrates that the 2010 AASHTO anchorage resistance model and its corresponding equation do not apply to Tx Girders. Because of the Tx Girders' larger bottom flange, cracks do not propagate across the strands as they do in AASHTO-type girders. (Refer to Figure 6-1 for a scaled comparison of an AASHTO Type III and Tx46 prestressed concrete bridge girder.) This fact yields overly conservative results with respect to AASHTO Equation 5.8.3.5-1 for Tx Girders. The analytical findings support this conclusion.

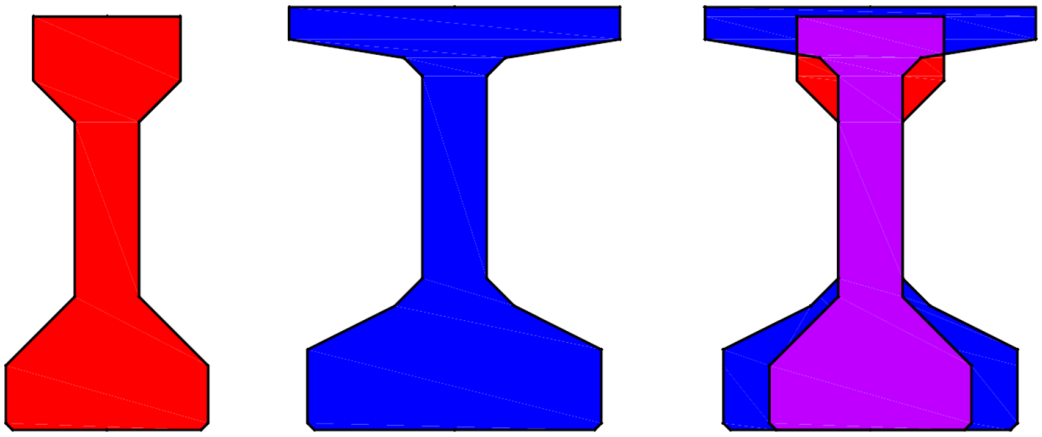

Figure 6-1: Comparison Between AASHTO Type III and Tx46 Cross Section

The fifth and final objective, (v), of this research was to determine the factors that contribute to anchorage capacity. Various factors were considered, but none of the considered factors reliably predicted anchorage failure or the lack thereof in the AEDB. More full-scale experimental testing is needed in order to expand the AEDB and so increase the likelihood of discovering potential factors and trends.

Meeting four of the five objectives of this research has produced two main conclusions with implications regarding the use of the AASHTO anchorage design method. First, this research established that Tx Girders are not prone to anchorage failures and the AASHTO anchorage equation does not reflect this observation. Second, this research uncovered the short-sided nature of the AASHTO anchorage design method; it is generally conservative, but not useful in a predictive manner and provides little generality. The completion of this research further underscores the need for additional research regarding anchorage-related issues.

6.2 RECOMMENDATIONS FOR FUTURE RESEARCH

Given the short-comings of the AASHTO anchorage design method as identified by this research, there is an obvious need for a validated, comprehensive, and rational approach to anchorage design that considers strength and serviceability. The method must cover a multitude of conditions, including but not limited to the following: presence of harped or debonded strands, variable debonding patterns and lengths, single-webbed or double-webbed members, and single or multiple bearing pads. To appropriately develop this method, additional full-scale experimental testing is needed to expand the Anchorage Evaluation Database, as currently there are not enough tests to distinguish major, general trends and variables. Any future additional research would be expected to further validate and expand the significant findings that this research has produced and so take the next step toward safer, more-efficient bridge designs.

APPENDIX A: DESIGN CALCULATIONS

Table 1A: Vertical Shear Capacity Calculations for 1-0.6-N

$f'_{c\,(Tx46)}$	5.8	ksi
E_c	4341	ksi
$f'_{c\,(deck)}$	10.0	ksi
D_{strand}	0.6	in²
A_{strand}	0.216	in²
E_{strand}	29000	ksi
f_{yv}	60	ksi
α	90	°
b_w	7	in.
h	54	in.
A_{Tx46}	761	in²
A_{deck}	576	in²
A_{total}	1337	in²
$A_{c,tension}$	490.38	in²
I_{Tx46}	198089	in⁴
I_{deck}	3072	in⁴
$I_{composite}$	494263	in⁴
f_{po}	189	ksi
f_{pe}	166	ksi
$\bar{y}_{b,Tx46}$	20.1	in.
$\bar{y}_{b,composite}$	33.0	in.
w_{Tx46}	793	plf
w_{deck}	600	plf
w_{total}	1393	plf

	A_{ps} Fully-Bonded in²	A_{ps} Debonded in²	y in.
Row 1	0.864	1.296	2.5
Row 2	0.864	1.296	4.5
Row 3	2.160	0	6.5
Row 4	0.864	0	8.5
	$A_{ps,total}$	7.344	in²

L	30	ft	
Span	28	ft	
Shear Span	10	ft	
Back Span	18	ft	
Overhang (S)	1	ft	
Overhang (N)	1	ft	

Dead	Near Rxn	20.90	kips
	Far Rxn	20.90	kips
Live	P	665.81	kips
	Near Rxn	428.02	kips
	Far Rxn	237.79	kips

Test ID: 1-0.6-N

F_{pe} kips	$\bar{y}_{strand}$ in.	d_v in.	s_{xe} in.	s in.	A_v in²	M_D kip-in	M_L kip-in	V_D kips	V_L kips	ε_s --	θ °	β --
788.8	5.77	43.40	43.40	6	0.4	953	25681	12.5	428.0	-0.000278	28.03	6.063

V_c	V_s	V_p	V_n	
140.18	326.14	0.00	440.56	kips

Table 2A: Horizontal Shear Capacity Calculations for 1-0.6-N

a	120	in.
Center of Bearing	12	in.
b_w	7	in.
h	54	in.
d_v	43.40	in.
l_{lp}	24	in.
y_{crit}	16.5	in.
k_d	1	--
c	0.4	ksi
μ	1.4	--
K_1	0.25	--
K_2	1.5	ksi
f_{pe}	166	ksi
$A_{ps,bonded}$	4.752	in^2
$A_{ps,debonded}$	2.592	in^2
A_v (#4)	0.2	in^2
A_v (#6)	0.44	in^2
f'_c	5.8	ksi

l_{UEP}	82.5	in.
l_{crit}	70.5	in.

x in.	A_{cv} kips	A_{vf} kips	P_{ps} kips	V_{ni} kips
0.0	0.0	0.0	0.00	0.00
36.0	252.0	15.4	788.83	365.40
82.5	325.5	2.8	914.33	314.20

HS_n 679.60 kips

Test ID: 1-0.6-N

Table 3A: Vertical Shear Capacity Calculations for 1-0.6-S

$f'_{c\,(Tx46)}$	5.8	ksi
E_c	4341	ksi
$f'_{c\,(deck)}$	10.0	ksi
D_{strand}	0.6	in²
A_{strand}	0.216	in²
E_{strand}	29000	ksi
f_{yv}	60	ksi
α	90	°
b_w	7	in.
h	54	in.
A_{Tx46}	761	in²
A_{deck}	576	in²
A_{total}	1337	in²
$A_{c,tension}$	490.38	in²
I_{Tx46}	198089	in⁴
I_{deck}	3072	in⁴
$I_{composite}$	494263	in⁴
f_{po}	189	ksi
f_{pe}	166	ksi
$\bar{y}_{b,Tx46}$	20.1	in.
$\bar{y}_{b,composite}$	33.0	in.
w_{Tx46}	793	plf
w_{deck}	600	plf
w_{total}	1393	plf

	A_{ps} Fully-Bonded in²	A_{ps} Debonded in²	y in.
Row 1	0.864	1.296	2.5
Row 2	0.864	1.296	4.5
Row 3	2.160	0	6.5
Row 4	0.864	0	8.5
	$A_{ps,total}$	7.344	in²

L	30	ft	
Span	21	ft	
Shear Span	9.5	ft	
Back Span	11.5	ft	
Overhang (S)	8	ft	
Overhang (N)	1	ft	

Dead	Near Rxn	13.93	kips
	Far Rxn	27.86	kips
Live	P	793.89	kips
	Near Rxn	434.75	kips
	Far Rxn	359.14	kips

Test ID: 1-0.6-S

F_{pe} kips	$\bar{y}_{strand}$ in.	d_v in.	s_{xe} in.	s in.	A_v in²	M_D kip-in	M_L kip-in	V_D kips	V_L kips	ε_s --	θ °	β --
788.8	5.77	43.40	43.40	6	0.4	524	25216	5.8	434.8	-0.000295	27.97	6.163

V_c	V_s	V_p	V_n	
142.50	326.97	0.00	440.56	kips

Table 4A: Horizontal Shear Capacity Calculations for 1-0.6-S

a	114	in.
Center of Bearing	12	in.
b_w	7	in.
h	54	in.
d_v	43.40	in.
l_{lp}	24	in.
y_{crit}	16.5	in.
k_d	1	--
c	0.4	ksi
μ	1.4	--
K_1	0.25	--
K_2	1.5	ksi
f_{pe}	166	ksi
$A_{ps,bonded}$	4.752	in²
$A_{ps,debonded}$	2.592	in²
A_v (#4)	0.2	in²
A_v (#6)	0.44	in²
f'_c	5.8	ksi

l_{UEP}	76.5	in.
l_{crit}	64.5	in.

x in.	A_{cv} kips	A_{vf} kips	P_{ps} kips	V_{ni} kips
0.0	0.0	0.0	0.00	0.00
36.0	252.0	15.4	788.83	365.40
76.5	283.5	2.4	842.62	267.81

HS_n 633.21 kips

Test ID: 1-0.6-S

Table 5A: Vertical Shear Capacity Calculations for 2-0.5-N

$f'_{c\,(Tx46)}$	11.2	ksi
E_c	6032	ksi
$f'_{c\,(deck)}$	12.3	ksi
D_{strand}	0.5	in²
A_{strand}	0.153	in²
E_{strand}	29000	ksi
f_{yv}	60	ksi
α	90	°
b_w	7	in.
h	54	in.
A_{Tx46}	761	in²
A_{deck}	576	in²
A_{total}	1337	in²
$A_{c,tension}$	490.38	in²
I_{Tx46}	198089	in⁴
I_{deck}	3072	in⁴
$I_{composite}$	494263	in⁴
f_{po}	189	ksi
f_{pe}	166	ksi
$\bar{y}_{b,Tx46}$	20.1	in.
$\bar{y}_{b,composite}$	33.0	in.
w_{Tx46}	793	plf
w_{deck}	600	plf
w_{total}	1393	plf

	A_{ps} Fully-Bonded in²	A_{ps} Debonded in²	y in.
Row 1	0.918	1.224	2.5
Row 2	0.918	1.224	4.5
Row 3	2.142	0	6.5
Row 4	0.918	0	8.5
	$A_{ps,total}$	7.344	in²

L	30	ft
Span	21	ft
Shear Span	9.5	ft
Back Span	11.5	ft
Overhang (S)	8	ft
Overhang (N)	1	ft

Dead	Near Rxn	13.93	kips
	Far Rxn	27.86	kips
Live	P	889.42	kips
	Near Rxn	487.06	kips
	Far Rxn	402.36	kips

Test ID: 2-0.5-N

F_{pe} kips	$\bar{y}_{strand}$ in.	d_v in.	s_{xe} in.	s in.	A_v in²	M_D kip-in	M_L kip-in	V_D kips	V_L kips	ε_s --	θ °	β --
812.7	5.75	43.43	43.43	6	0.4	524	28250	5.8	487.1	-0.000143	28.50	5.379

V_c	V_s	V_p	V_n	
172.91	319.94	0.00	492.85	kips

Table 6A: Horizontal Shear Capacity Calculations for 2-0.5-N

a	114	in.
Center of Bearing	12	in.
b_w	7	in.
h	54	in.
d_v	43.43	in.
l_{lp}	24	in.
y_{crit}	16.5	in.
k_d	1	--
c	0.4	ksi
μ	1.4	--
K_1	0.25	--
K_2	1.5	ksi
f_{pe}	166	ksi
$A_{ps,bonded}$	4.896	in²
$A_{ps,debonded}$	2.448	in²
A_v (#4)	0.2	in²
A_v (#6)	0.44	in²
f'_c	11.2	ksi

l_{UEP}	76.5	in.
l_{crit}	64.5	in.

x in.	A_{cv} kips	A_{vf} kips	P_{ps} kips	V_{ni} kips
0.0	0.0	0.0	0.00	0.00
36.0	252.0	15.4	812.74	378.00
76.5	283.5	2.4	873.69	266.07

HS_n	644.47	kips

Test ID: 2-0.5-N

Table 7A: Vertical Shear Capacity Calculations for 2-0.5-S

$f'_{c\,(Tx46)}$	11.2	ksi
E_c	6032	ksi
$f'_{c\,(deck)}$	12.3	ksi
D_{strand}	0.5	in²
A_{strand}	0.153	in²
E_{strand}	29000	ksi
f_{yv}	60	ksi
α	90	°
b_w	7	in.
h	54	in.
A_{Tx46}	761	in²
A_{deck}	576	in²
A_{total}	1337	in²
$A_{c,tension}$	490.38	in²
I_{Tx46}	198089	in⁴
I_{deck}	3072	in⁴
$I_{composite}$	494263	in⁴
f_{po}	189	ksi
f_{pe}	166	ksi
$\bar{y}_{b,Tx46}$	20.1	in.
$\bar{y}_{b,composite}$	33.0	in.
w_{Tx46}	793	plf
w_{deck}	600	plf
w_{total}	1393	plf

	A_{ps} Fully-Bonded in²	A_{ps} Debonded in²	y in.
Row 1	0.918	1.224	2.5
Row 2	0.918	1.224	4.5
Row 3	2.142	0	6.5
Row 4	0.918	0	8.5
	$A_{ps,total}$	7.344	in²

L	30	ft
Span	21	ft
Shear Span	9.5	ft
Back Span	11.5	ft
Overhang (S)	8	ft
Overhang (N)	1	ft

Dead	Near Rxn	13.93	kips
	Far Rxn	27.86	kips
Live	P	889.42	kips
	Near Rxn	487.06	kips
	Far Rxn	402.36	kips

Test ID: 2-0.5-S

F_{pe} kips	$\bar{y}_{strand}$ in.	d_v in.	s_{xe} in.	s in.	A_v in²	M_D kip-in	M_L kip-in	V_D kips	V_L kips	ε_s --	θ °	β --
812.7	5.75	43.43	43.43	6	0.4	524	28250	5.8	487.1	-0.000143	28.50	5.379

V_c	V_s	V_p	V_n	
172.91	319.94	0.00	492.85	kips

Table 8A: Horizontal Shear Capacity Calculations for 2-0.5-S

a	114	in.
Center of Bearing	12	in.
b_w	7	in.
h	54	in.
d_v	43.43	in.
l_{lp}	24	in.
y_{crit}	16.5	in.
k_d	1	--
c	0.4	ksi
μ	1.4	--
K_1	0.25	--
K_2	1.5	ksi
f_{pe}	166	ksi
$A_{ps,bonded}$	4.896	in²
$A_{ps,debonded}$	2.448	in²
A_v (#4)	0.2	in²
A_v (#6)	0.44	in²
f'_c	11.2	ksi

l_{UEP}	76.5	in.
l_{crit}	64.5	in.

x in.	A_{cv} kips	A_{vf} kips	P_{ps} kips	V_{ni} kips
0.0	0.0	0.0	0.00	0.00
36.0	252.0	15.4	812.74	378.00
76.5	283.5	2.4	873.69	266.07

HS_n 644.47 kips

Test ID: 2-0.5-S

APPENDIX B: TEXAS DEPARTMENT OF TRANSPORTATION STANDARD SHEAR REINFORCEMENT DETAILS FOR TX GIRDERS

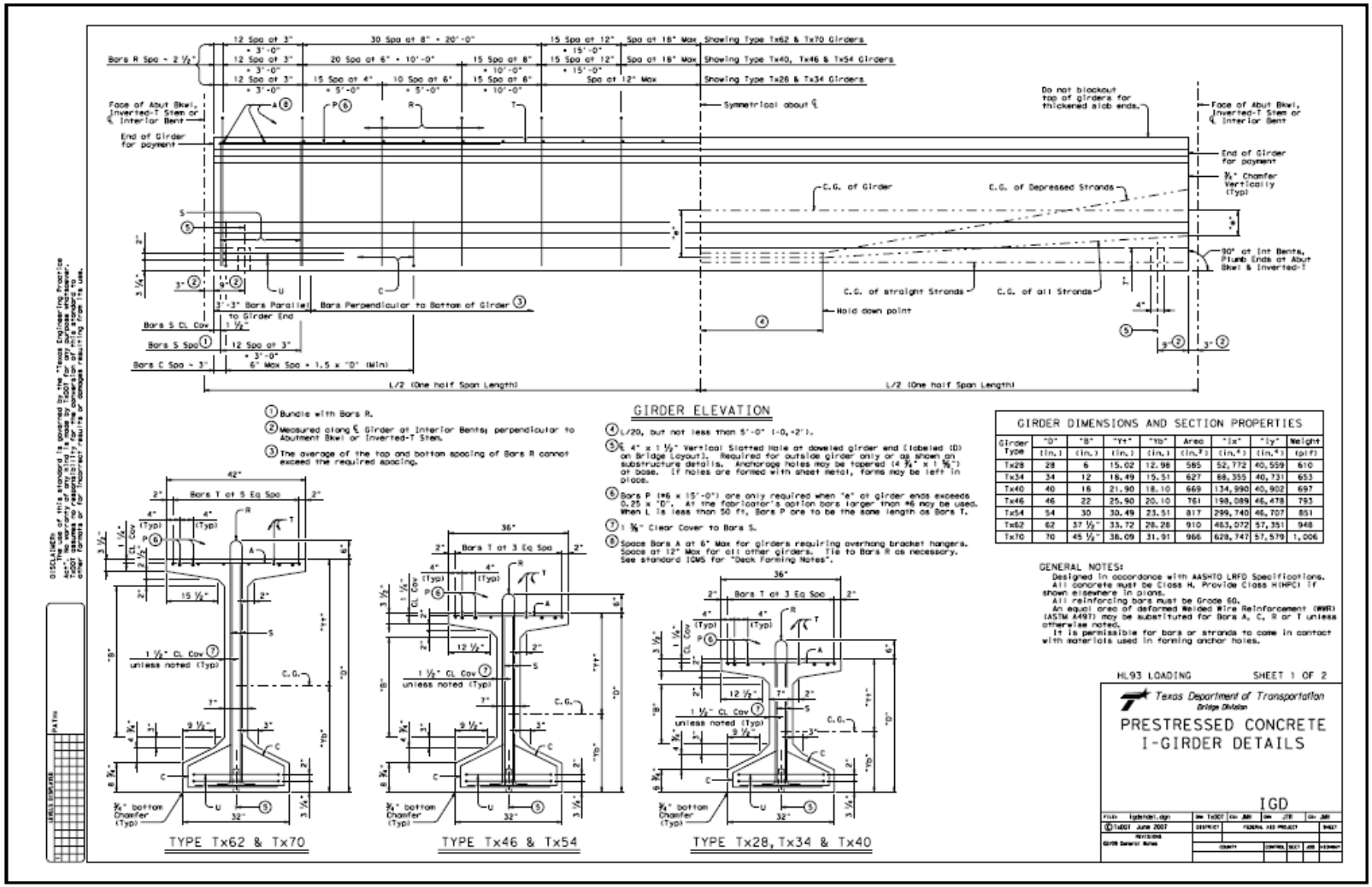

GIRDER ELEVATION

① Bundle with Bars R.

② Measured along ℄ Girder at Interior Bents; perpendicular to Abutment Bkwl or Inverted-T Stem.

③ The average of the top and bottom spacing of Bars R cannot exceed the required spacing.

④ L/20, but not less than 5'-0" (-0, +2").

⑤ ℄ 4" x 1 ½" Vertical Slotted Hole at doweled girder end (labeled (D) on Bridge Layout). Required for outside girder only or as shown on substructure details. Anchorage holes may be tapered (4 ½" x 1 ⅝") at base. If holes are formed with sheet metal, forms may be left in place.

⑥ Bars P (#6 x 15'-0") are only required when "e" at girder ends exceeds 0.25 x "D". At the fabricator's option bars larger than #6 may be used. When L is less than 50 ft, Bars P are to be the same length as Bars T.

⑦ 1 ⅜" Clear Cover to Bars S.

⑧ Space Bars A at 6" Max for girders requiring overhang bracket hangers. Space at 12" Max for all other girders. Tie to Bars R as necessary. See standard IGMS for "Deck Forming Notes".

GIRDER DIMENSIONS AND SECTION PROPERTIES

Girder Type	"D" (in.)	"B" (in.)	"Yt" (in.)	"Yb" (in.)	Area (in.²)	"Ix" (in.⁴)	"Iy" (in.⁴)	Weight (plf)
Tx28	28	6	15.02	12.98	585	52,772	40,559	610
Tx34	34	12	18.49	15.51	627	88,355	40,731	653
Tx40	40	18	21.90	18.10	669	134,990	40,902	697
Tx46	46	22	25.90	20.10	761	198,089	46,478	793
Tx54	54	30	30.49	23.51	817	299,740	46,707	851
Tx62	62	37 ½	33.72	28.28	910	463,072	57,351	948
Tx70	70	45 ½	38.09	31.91	966	628,747	57,579	1,006

GENERAL NOTES:

Designed in accordance with AASHTO LRFD Specifications.

All concrete must be Class H. Provide Class HIHPCI if shown elsewhere in plans.

All reinforcing bars must be Grade 60.

An equal area of deformed Welded Wire Reinforcement (WWR) (ASTM A497) may be substituted for Bars A, C, R or T unless otherwise noted.

It is permissible for bars or strands to come in contact with indentations used in forming anchor holes.

TYPE Tx62 & Tx70

TYPE Tx46 & Tx54

TYPE Tx28, Tx34 & Tx40

HL93 LOADING SHEET 1 OF 2

Texas Department of Transportation
Bridge Division

PRESTRESSED CONCRETE I-GIRDER DETAILS

IGD

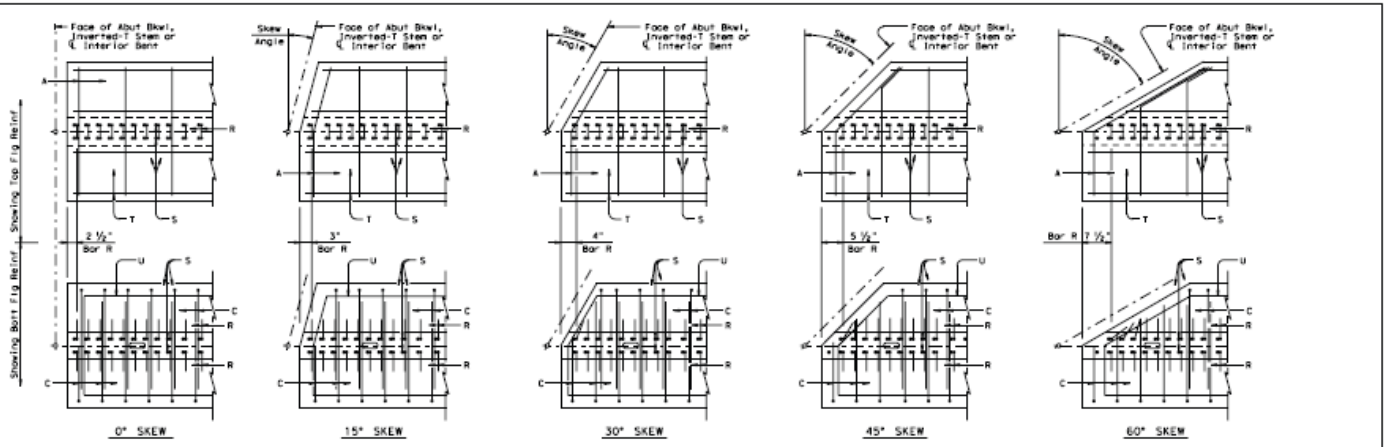

PLAN OF GIRDER ENDS⑨

⑨ Reinforcing patterns shown are provided as guides to determine reinforcement placement in skewed ends. Place Bars S as close to girder end as cover requirements permit, which may prevent them to be bundled with Bars R.

⑩ Bars may be cut or bent at skewed end as required.

⑪ Increase as necessary for bars at skewed end.

⑫ No portion of bar less than 10 ft.

⑬ For Welded Wire Reinforcement (WWR) option, area of Bars R may be reduced in proportion to the increase in reinforcement yield strength over 60 ksi. Yield strength of WWR is limited to 75 ksi.

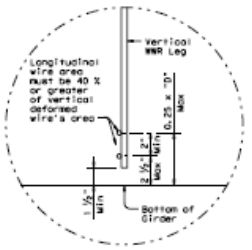

OPTIONAL WELDED WIRE REINFORCEMENT (WWR) DETAIL

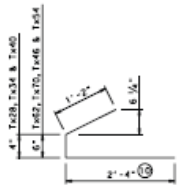

BARS C (#4)

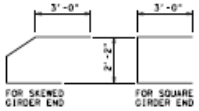

BARS U (#5)

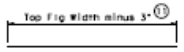

BARS A (#3)

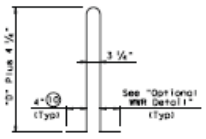

BARS R (#4)⑬

BARS S (#6)

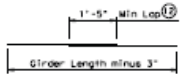

BARS T (#4)

HL93 LOADING SHEET 2 OF 2

Texas Department of Transportation
Bridge Division

PRESTRESSED CONCRETE I-GIRDER DETAILS

IGD

REFERENCES

1. Abdalla, O.A., J.A. Ramirez, and R.H. Lee (1993). "Debonding in Pretensioned Beams Precast Strands, Part 2: Simply Supported Tests." *Report No. FHWA/IN/JHRP-92/25*. Joint Highway Research Project, Indiana Department of Transportation and Purdue University, West Lafayette, Indiana.
2. Alshegeir, A., and Ramirez, J.A. (1992). "Strut-Tie Aapproach in Prestressed Deep Beams." *ACI Structural Journal*, Vol. 89, No. 3, pp. 296-304.
3. American Association of State Highway and Transportation Officials (AASHTO) (2007). "AASHTO LRFD Bridge Design Specifications: Customary Units." 4th Edition. Washington, DC.
4. American Association of State Highway and Transportation Officials (AASHTO) (2008). "2008 Interim Revisions: AASHTO LRFD Bridge Design Specifications: Customary Units." 4th Edition. Washington, DC.
5. American Association of State Highway and Transportation Officials (AASHTO) (2009). "2009 Interim Revisions: AASHTO LRFD Bridge Design Specifications: Customary Units." 4th Edition. Washington, DC.
6. American Association of State Highway and Transportation Officials (AASHTO) (2010). "2010 Interim Revisions: AASHTO LRFD Bridge Design Specifications: Customary Units." 4th Edition. Washington, DC.
7. American Concrete Institute (ACI) Committee 318 (2008). "Building Code Requirements for Structural Concrete (ACI 318-08) and Commentary." American Concrete Institute, Farmington Hills, MI.
8. Avendano, A.R. (2008). "Shear Strength and Behavior of Prestressed Concrete Beams." MSE Thesis, The University of Texas at Austin, Austin, TX.
9. Avendano, A.R. and Bayrak, O. (2008). "Shear Strength and Behavior of Prestressed Concrete Beams." *Technical Report IAC-88-5DD1A003-3*, Center for Transportation Research, The University of Texas at Austin, Austin, TX.

10. Hamilton III, H.R., G. Llanos, and B.E. Ross (2008). "Shear Performance of Existing Prestressed Concrete Bridge Girders." *Report No. BD 545-56*, University of Florida, Gainesville, FL.
11. Hanson, J.M. and Hulsbos, C.L. (1969). "Ultimate Shear Tests of Large Prestressed Concrete Bridge Beams." *American Concrete Institute SP-26, Concrete Bridge Design*, American Concrete Institute, Farmington Hills, MI, pp. 523-549.
12. Heckmann, C.P. (2008). "Effects of Increasing the Allowable Compressive Stress at Release on the Shear Strength of Prestressed Concrete Girders." MSE Thesis, The University of Texas at Austin, Austin, TX.
13. Hovell, C.G. (2011). "Structural Performance of Texas U-Beams at Prestress Transfer and Under Shear-Critical Loads." PhD Dissertation, The University of Texas at Austin, Austin, TX.
14. Hovell, C.G., A.R. Avendano, D. Dunkman, A. Moore, O. Bayrak, and J. Jirsa. (2010). "Behavior of Texas U-Beams and Box-Beams at Prestress Transfer and Under Shear Loads." *Report No. TX-10/0-5831-1*, Center of Transportation Research, The University of Texas at Austin, Austin, TX.
15. Hoyer, E. and Friedrich, E. (1939). "Beitrag zur Frage der Haftspannung in Eisenbetonbauteilen (Contribution towards the Question of Bond Strength in Reinforced Concrete Members)." *Beton und Eisen*, Vol. 38, No. 5, pp. 107-110.
16. Kaufman, M.K. and Ramirez, J.A. (1987). "Re-evaluation of the Ultimate Shear Behavior of High-Strength Concrete Prestressed I-Beams." *ACI Structural Journal*, Vol. 85, No. 3, pp. 295-303.
17. Labonte, T. and Hamilton III, H.R. (2005). "Self-Consolidating Concrete (SCC) Structural Investigation." *Report No. DB545, PRWO#21*, University of Florida, Gainesville, FL.
18. Naito, C., G. Brunn, G. Parent, and T. Tate. (2005). "Comparative Performance of High Early Strength and Self Consolidating Concrete for Use in Precast Bridge Beam Construction." *ATLSS Report No.05-03*, Lehigh University, Bethlehem, PA.

19. Nakamura, E. (2011). "Shear Database for Prestressed Concrete Members." MSE Thesis, The University of Texas at Austin, Austin, TX.
20. O'Callaghan, M. (2007). "Tensile Stresses in the End Regions of Pretensioned I-Beams at Release." MSE Thesis, The University of Texas at Austin, Austin, TX.
21. Ramirez, J.A. and Aguilar, G. (2005). "Shear Reinforcement Requirements for High-Strength Concrete Bridge Girders." *Report No. FHWA/IN/JTRP-2005/19*, Purdue University, West Lafayette, IN.
22. Ross, B.E., Ansley, M.H., and H.R. Hamilton III (2011). "Load Testing of 30-year-old AASHTO Type III Highway Bridge Girders." *PCI Journal*, Vol. 56, No. 4, pp. 152-163.
23. Runzell, B., C. Shield, and C. French. (2007). "Shear Capacity of Prestressed Concrete Beams." *Report No. MN/RC 2007-47*, University of Minnesota, Minneapolis, MN.
24. Russell, B.W. and Burns, N.H. (1993). "Design Guidelines for Transfer, Development, and Debonding of Large Diameter Seven Wire Strands in Pretensioned Concrete Girders." *Report No. FHWA/TX-93+1210-5F*, Center for Transportation Research, The University of Texas at Austin, Austin, TX.
25. Shahawy, M.A. (2001). "A Critical Evaluation of the AASHTO Provisions for Strand Development Length of Prestressed Concrete Members." *PCI Journal*, Vol. 46, No. 3, pp. 94-118.
26. Shahawy, M.A. and Batchelor, B. deV. (1996). "Shear Behavior of Full-Scale Prestressed Concrete Girders: Comparison between AASHTO Specifications and LRFD Code." *PCI Journal*, Vol. 41, No. 3, pp. 48-62.
27. Shahawy, M.A. and Cai, C.S. (2001). "Enhancement of the Performance of Prestressed Concrete Girders Using Strand Anchorage." *PCI Journal*, Vol. 46, No. 4, pp. 82-96.
28. Shahawy, M.A., B. Robinson, and B. deV. Batchelor. (1993). "An Investigation of Shear Strength of Prestressed Concrete AASHTO Type II Girders." Structures Research Center FDOT, Tallahassee, FL.

29. Tawfiq, K.S. (1995). “Cracking and Shear Capacity of High Strength Concrete Girders.” *Report No. FL/DOT/RMC/612(1)-4269*, FAMU/FSU College of Engineering, Tallahassee, FL.